

Studying the Effects of pH, Ion Concentration and Ion Valency on the Silica/Water Interface  
Using Nonlinear Optical Spectroscopy

by

Akemi M. Darlington

A thesis submitted in partial fulfillment of the requirements for the degree of

Doctor of Philosophy

Department of Chemistry  
University of Alberta

© Akemi M. Darlington, 2017

## Abstract

The silica/water interface is complex and depends on a multitude of properties like surface charge, ion concentration, ion identity, and surface structure. Yet because silica is an insulator, the interface it creates with water is often difficult to study. However, the nonlinear optical methods, such as second harmonic generation (SHG) and sum frequency generation (SFG) spectroscopy, are capable of probing the buried interfaces like the silica/water interface.

This thesis focuses on perturbing the silica/water interface through different actions and observing the response of the interfacial species using SHG and SFG. Firstly, the effect of experimental starting pH on the acid-base titration curves at the silica/water interface using SHG was explored. Depending on the starting pH, either two or three pK<sub>a</sub> sites were observed as the pH was varied. Vibrational SFG was then used to monitor the response of water molecules to changes in NaCl concentration and experimental starting pH. At high ionic strength, the pH dependent SFG of NaCl was different than that observed by SHG, indicating that they probed different aspects of the interface. Additionally, the experimental starting pH had little effect on the resultant SFG signal in contrast with the SHG results, which did depend on the experimental starting pH. This difference provided further support that SHG and *ssp* polarized SFG are sensitive to different features of the interface. We observed that the minimum intensity of the *ssp* polarized SFG depended on the salt concentration; specifically it shifted from ~ pH 6 to pH 8 upon increasing the salt from 0.1 M to 0.5 M. In contrast, the SHG minimum was always at pH 2 independent of salt concentration. The peak observed at 3200 cm<sup>-1</sup> that dominates the *ssp* polarized SFG has been proposed to be sensitive to water molecules farther from the surface. Consequently we theorized that this minimum in SFG intensity corresponded to a minimum in the zeta potential, which has been shown to shift to higher pH with higher salt concentration.

Next, the same polarization combinations of light were utilized in both SHG and SFG to do a direct comparison of the two techniques. Unlike the *ssp* SFG pH dependence, the *pss* polarized SFG pH dependence was similar to the *pss* polarized SHG. Despite the similarities in trend with pH, we observed that the magnitude of the intensity changes of the SHG signal could not be fully explained by the change in the intensity of the SFG of water molecules. This led us to conclude that there is another interfacial species that contributes directly to the SHG signal intensity, most likely the siloxides. Finally, the effect of calcium on both SHG and SFG was explored. The presence of CaCl<sub>2</sub> caused the SHG and both *ssp* and *pss* polarized SFG to behave differently compared to each other. Specifically, the SHG signal in the presence of calcium increased in response to increasing pH until a maximum intensity where upon it decreased with further increases in pH. In contrast SFG exhibited the opposite behavior where the signal intensity in the SFG decreased until a minimum was reached and then increased as the pH was further increased. To understand this unusual pH dependence of the *ssp* SFG, the SFG range was probed at higher wavenumbers. This expanded range allowed for the observation of a CaOH mode that grew in at high pH that interfered with SFG of the water molecules. Consequently, we attributed the increase in SFG intensity at higher pH to the appearance of this CaOH species. If these CaOH species were forming right at the surface, then it should disrupt the surface water molecules, which can be visualized using *pss* polarized SFG. Indeed, the *pss* polarized SFG decreased with increasing pH suggesting that the formation of CaOH at the interface disrupts the surface water. Moreover, the presence of a new mode in the SFG provides further support that there is another interfacial species that contributes to the SHG intensity, which explains the unusual pH dependence of the latter. Through this work, we have a better understanding of how

pH, ion concentration and ion identity affect the silica water interface. These results can be useful for modelling of geochemical phenomena and industrial processing of silica sands/soils.

## Preface

This thesis is an original work by Akemi Darlington. Some of the research that was collected for this thesis was part of collaboration projects with other group members in the Gibbs-Davis Group, and outside collaborations with Dr. Dennis Hore and Tasha Jarisz from University of Victoria, and Dr. Eric Tyrode and Adrien Sthoer from KTH Institute of Technology.

Chapter 2 of this thesis has been published as Darlington, A. M.; Gibbs-Davis, J. M., “Bimodal or Trimodal? The Influence of Starting pH on Site Identity and Distribution at the Low Salt Aqueous/Silica Interface.” *J. Phys. Chem. C* **2015**, *119* (29), 16560-16567. I was responsible for the data collection and analysis as well as the manuscript composition. Dr. Julianne Gibbs Davis was the supervisory author.

Chapter 3 of this thesis is an original work by me. No part of this chapter has been published. I collaborated with Dr. Shafiu Azam who performed the 0.5 M NaCl SFG studies in Figure 3.2. I performed the rest of the 0.1 M NaCl SFG titrations. I was responsible for all the data analysis. Dr. Hore and Tasha Jarisz performed the external verification of 0.1 and 0.5 M SFG (*ppp, ssp*).

Chapter 4 of this thesis is an original work by me. No part of this chapter has been published. I collaborated with Dr. Emma Kerian who performed the *pss* polarized SFG spectra titrations. Dr. Kerian also performed the nonlinear optical prediction calculations using NLOPredict, a program developed by Dr. Simpson. I was responsible for the *pss* polarized SHG titrations and all the *ssp* polarized SFG and p-in/all out SHG. I was also responsible for the

spectral fitting of the data, and the analysis of the data. External validations were completed by Dr. Hore and Tasha Jarisz (*sps* polarization)

Chapter 5 of this thesis was first initiated by Dr. Delwar Sikder and Dr. Shafiu Azam who first performed the SHG and SFG experiments that showed non monotonic behavior. Dr. Sikder's original 0.1 M CaCl<sub>2</sub> titration data is in Figure 5.1. I collected the remaining SHG data (all NaCl and 0.01 M CaCl<sub>2</sub> and 0.1 M CaCl<sub>2</sub> (Figure 5.8)). I also collected the SFG data of the 0.1 M CaCl<sub>2</sub> and 0.1 M NaCl. Dr. Azam collected the 0.5 M NaCl in Figure 5.3. The data in Figure 5.6 and Figure 5.7 was collected with the help of Dr. Tyrode and Adrien Sthoer at the KTH Institute of Technology in Stockholm, Sweden. I was responsible for all of the data analysis.

## **Acknowledgments**

First and foremost I would like to express my sincere gratitude to my supervisor Dr. Julianne Gibbs-Davis for all her help, encouragement, constructive criticism, and advice throughout my graduate career. I feel privileged to be a member Juli's group at the University of Alberta. Her steadfast support throughout the years has been an invaluable source of motivation for the completion of this degree.

I would like to acknowledge my defense committee members Dr. Lucy, Dr. Petersen, Dr. Cairo and Dr. Wang for their support, criticisms, and suggestions to improve my research.

I would also like to thank my colleagues in the Gibbs-Davis group, in particular Emma, Sun, Ben, Safeenaz, Eiman, Anyeld, Sarah and past group members Li, Azam, Delwar, and Kausar. You have all been amazing throughout this journey.

Most importantly, I must thank my friends and family that have supported me. I would like to express my heartfelt gratitude to my husband Brian Yeomans for his tireless emotional support and love. I would also like to thank my parents Joe and Brenda Darlington for their unending love, and support.

## Table of Contents

Abstract .....	ii
Preface.....	v
Acknowledgments.....	vii
Table of Contents.....	viii
List of Figures .....	xi
List of Tables .....	xviii
List of Schemes.....	xix
CHAPTER 1 .....	1
1.1 Importance of the Silica/Water Interface .....	2
1.2 Reflection and Refraction of Light at an Interface.....	3
1.3 Polarized Light .....	4
1.4 Probing Interfacial Structure .....	5
1.5 Second Harmonic Generation (SHG).....	6
1.5.1 Basic Theory.....	6
1.5.2 Non-Resonant SHG .....	8
1.5.3 Resonantly Enhanced SHG .....	10
1.6 Sum Frequency Generation (SFG) Theory .....	11
1.7 Electrical Double Layer .....	13
1.8 Nonlinear Optical Studies of the Silica/Water Interface .....	17
1.9 Perturbing the Silica/Water Interface with Ionic Strength, Ion Identity, and Flow Rates ..	25
1.10 Thesis Organization.....	35
CHAPTER 2 .....	38
2.1 Introduction .....	39
2.2 Experimental .....	41
2.2.1 Laser System and Assembly .....	41
2.2.2 Surface Preparation.....	42
2.2.3 Materials .....	43

2.2.4 SHG Titration Experiments .....	43
2.3 Results and Discussion.....	45
2.3.1 Theory of $\chi^{(3)}$ Technique.....	45
2.3.2 Two-Step SHG Titrations Initiated at Neutral pH.....	46
2.3.3 SHG Titrations from pH 12 to pH 2.....	49
2.3.4 SHG Titrations from pH 2 to pH 12.....	54
2.3.5 pH History and the Origin of the Three Surface Sites.....	56
2.4 Conclusions .....	62
CHAPTER 3 .....	64
3.1 Introduction .....	65
3.2 Experimental .....	67
3.2.1 Laser Assembly .....	67
3.2.2 Surface Preparation.....	68
3.2.3 Materials .....	69
3.2.4 SFG Experiments.....	69
3.3 Results and Discussion.....	70
3.3.1 Background Theory on SFG .....	70
3.3.2 Effect of 0.5 M and 0.1 M NaCl.....	71
3.3.3 pH History of 0.1 M NaCl.....	77
3.4 Conclusions .....	79
CHAPTER 4 .....	81
4.1 Introduction .....	82
4.2 Experimental .....	85
4.2.1 Laser Assembly .....	85
4.2.2 Materials .....	86
4.2.3 Surface Preparation.....	86
4.2.4 SHG Experiments .....	87
4.2.5 SFG Experiments.....	87
4.3 Results and Discussion.....	88

4.3.1 Theory of SHG .....	88
4.3.2 Typical Polarizations for SHG and SFG of the Silica/Water Interface .....	90
4.3.3 <i>pss</i> Polarized SHG and SFG .....	92
4.4 Conclusions .....	100
CHAPTER 5 .....	101
5.1 Introduction .....	102
5.2 Experimental .....	104
5.2.1 Laser Assembly .....	104
5.2.2 Materials .....	106
5.2.3 Second Harmonic Generation (SHG) .....	106
5.2.4 Sum Frequency Generation (SFG) .....	107
5.3 Results and Discussion.....	108
5.3.1 Background SHG and SFG.....	108
5.3.2 Effect of CaCl <sub>2</sub> on SHG.....	111
5.3.3 Effect of CaCl <sub>2</sub> on SFG .....	113
5.3.4 <i>pss</i> Polarized SFG.....	116
5.3.5 Probing the CaOH Vibrational Mode .....	119
5.4 Conclusions .....	126
CHAPTER 6 .....	128
6.1 General Conclusions .....	129
References.....	135

## List of Figures

**Figure 1.1** ..... 4

**Figure 1.2** Reflection and refraction of light: A) when the angle of incident light is  $\theta_1 < \theta_c$  B) when the angle incident light is  $\theta_1 = \theta_c$ ; and C) when the angle of the incident light is  $\theta_1 > \theta_c$ . This phenomena is dependent on the refractive index of medium 1 ( $n_1$ ) being larger than the refractive index of medium 2 ( $n_2$ ). ..... 4

**Figure 1.3** Depiction of A) *p*-polarized light parallel to the plane of incidence. B) *s*-polarized light perpendicular to the plane of incidence where the dots on the propagation beam indicate that the electric field is oscillating perpendicular to the XZ plane (in and out of the page). ..... 5

**Figure 1.4** Schematic of SHG at the silica/water interface. ..... 7

**Figure 1.5** Non-resonant SHG energy diagram. The dashed lined depict a virtual state, and the solid line depict a real state in the atom or molecule. ..... 9

**Figure 1.6** Resonantly enhanced SHG energy diagrams. A) When  $\omega$  is in resonance with the electronic transition. B) When  $2\omega$  is in resonance with the electronic transition. The dashed lines represent virtual states and the solid lines represent real states within the molecule or atom. ....11

**Figure 1.7** (A) Depiction of SFG at the silica/water interface and B) depiction of the energy diagram of SFG in resonance with an IR vibrational transition. ..... 12

**Figure 1.8** Schemes of the different electrical double layer models. A) The Gouy-Chapman model showing only the diffuse layer. B) The potential of the Gouy-Chapman model. C) The Stern model showing a compact layer of ions and a diffuse layer. D) The potential of the Stern model. E) The model of Esin and Markov, Grahame, and Devanathan showing ions penetrating

the Stern layer and F) The potential of the Esin and Markov, Grahame, and Devanathan model. The dotted gray line represents the Outer Helmholtz Plane (OHP), and the IHP is the inner Helmholtz plane. All figures are modified from reference 24. .... 15

**Figure 1.9** The Bockris, Devananthan and Muller (BDM) electrical double layer model. The blue spheres represent the water solvent molecules, while the arrow represents the direction of the dipole moment..... 16

**Figure 1.10** SHG electric field (in arbitrary units) as a function of pH in bulk solution. The dots are experimental points, while the solid line is the theoretical fit with the constant capacitance model. Reprinted with permission from reference 26. Copyright 1992 American Chemical Society..... 17

**Figure 1.11** A comparison of different *ssp* polarized water spectra from A) the Gibbs-Davis lab B) the Tyrode lab..... 21

**Figure 1.12** SFG intensity of water (0 M) (Grey) versus 0.1 M NaCl (black) in *ssp* polarization. The spectra were normalized to a gold reference. .... 27

**Figure 2.1** Schematic of the SHG laser assembly. A MaiTai and Empower lasers pump a regeneratively amplified Ti:Sapphire laser system. A portion of Ti:Sapphire laser light pumps an OPA-800C which is tuned to 550-580 nm. The OPA light is focused on the silica sample and the resulting SHG light (275-290 nm) is selected, amplified and counted using a monochromator, photomultiplier tube (PMT) and gated photon counter..... 42

**Figure 2.2** A representative titration composed of two separate experiments: one from pH 6 to pH 12 and the other from pH 7 to pH 2 with a background electrolyte of 10 mM NaCl. A)

Normalized  $E_{2\omega}$  (red circles) and concentration of  $\text{Na}^+$  (black triangles) as a function of solution pH for the silica/water interface. B) The corresponding surface charge density (open red circles) as a function of surface pH. .... 47

**Figure 2.3** A representative titration starting from pH 12 for the silica/water interface. A) Normalized  $E_{2\omega}$  as a function of solution pH (solid green squares). B) Surface charge density as a function of surface pH (open green squares). .... 51

**Figure 2.4** A) Representative titrations of surface charge density calculated via the Gouy-Chapman equation (closed red circles) or the Basic Stern model (closed grey triangles) versus solution pH. B) Calculated surface charge density versus surface pH using the Basic Stern model (grey triangles) or the Gouy-Chapman model (red circles). For the Basic Stern model the surface pH was determined from the potential at the 0-plane ( $\text{pH}_0$ , closed grey triangles) and the d-plane ( $\text{pH}_d$ , open grey triangles). .... 52

**Figure 2.5** A) Representative titrations from pH 12 to 2 with varying  $\text{Na}^+$  concentration as there was no background NaCl in the aqueous HCl used to decrease the pH (red circles) with comparison of pH 12 to 2 with a constant salt concentration (blue triangles). Based on the change in volume upon decreasing the pH, the  $\text{Na}^+$  concentration decreased by approximately 20%. B) Comparison between representative titrations performed on fused silica hemispheres from ISP Optics (green squares) (our standard supplier) and Almaz Optics (purple diamonds). .... 53

**Figure 2.6** A) Titration from pH 5.38 to pH 7.0 to 12.09, then 12.09 to 7.40 to 2.12 with 30 minute wait time at each pH point. The interval (a) between the bold lines represents where the pH was being changed and manually mixed. The interval (b) between the bold line and dotted line represents the typical wait time of 5 minutes used in all of the reported experiments, and the

interval (c) between the two dashed lines is where the data would have been collected in the all reported titrations. We note that during the course of the experiment the energy/pulse dropped from 450 nJ to 330 nJ per pulse. Incidents of ~0 intensity in A correspond to where the beam was blocked and the energy of the pulse was measured. B) The data from part (A) collected with 30-minute wait times (solid symbols) is overlaid on the data from 5-minute wait times from Figure 2.3A and Figure 2.2A (open symbols). These data were power normalized and then normalized to the values at pH 2 and pH 12..... 54

**Figure 2.7** A representative titration of the silica/water interface starting at pH 2. A) Normalized  $E_{2\omega}$  (blue diamonds) and  $\text{Na}^+$  concentration (black triangles) as a function of solution pH. B) The surface charge density as a function of surface pH (blue open diamonds)..... 55

**Figure 2.8** A) Titration from pH 6.4 to pH 3.7 to 2.1, then 2.1 to 3.7 to 12.0 with 30 minute wait times at each pH point. The interval (a) between the two bold lines represents where the pH was being changed and manually mixed. The interval (b) between the bold line and dotted line represents the typical wait time of 5 min used in all of the reported experiments, and the interval (c) between the two dashed lines is where the data would have been collected in the all reported titrations. For the final pH increase to 12, the average signal increased from 101 counts per second (cps) in the (c) interval to 108 cps in the last few minutes after 30 minutes wait time. B) The average  $E_{2\omega}$  values after 30 min wait time (closed symbols, the data from part (A)) are overlaid on the data from the paper (open symbols) and show the extent of hysteresis even with longer wait times. Owing to the stability of the laser, the open-symbol data was not power normalized and just normalized to the values at pH 2 and 12. C) An expanded version of pH 3.73 to pH 2.06, then back to pH 3.73 shows the lack of the response to the change in pH.

Incidents of ~ 0 intensity correspond to where the beam was blocked and the energy per pulse measured. .... 56

**Figure 2.9** Representative titrations of the silica/water interface with three different initial pH values: pH 2 (green diamonds), ~ pH 7 (red circle) and pH 12 (blue squares) at (A) 10 mM NaCl (closed symbols) and (B) 0.1 M NaCl (open symbols). .... 57

**Figure 2.10** Potential origins of the three surface sites with the three distinctive  $pK_a$  values. A) Three different hydrogen bonding environments of silanols. B) The three silanol sites that interact with water present at the amorphous silica surface according to *ab initio* calculations.<sup>27</sup>

..... 62

**Figure 3.1** Depiction of SFG laser assembly. IR light from the TOPAS-C and nDFG is focused on to the silica/water interface. Visible light at 800 nm is broadened in time and is overlapped with the IR light spatially and temporally at the interface. The sum of the light (Visible + IR) is filtered and collected on the spectrograph and CCD camera. HWP = half wave plate. .... 68

**Figure 3.2** Representative titrations of *ssp* polarized SFG of: A) 0.5 M NaCl pH 6.0 to 2.0; B) 0.5 M NaCl pH 6.0 to 12.0; C) 0.1 M NaCl pH 7.0 to 2.0; and D) 0.1 M NaCl pH 5.8 to 12.0. . 72

**Figure 3.3** Integrated area of 0.5 M NaCl (red) and 0.1 M NaCl (blue) representative titrations between 2950-3500  $\text{cm}^{-1}$  ..... 73

**Figure 3.4** Schematic of A) a more negatively charged surface that behaves as a negative surface B) a less negatively charged surface that is overcharged due to the ions at the interface and behaves as a positive surface. .... 75

**Figure 3.5** Representative titrations of *ssp* polarized SFG spectra of the silica/NaCl (0.1 M) interface A) from pH 2.0 to 12.0; B) from pH 6.0 to 12.0 and pH 7.0 to 2.0; and C) from pH 12.0 to 2.0..... 78

**Figure 3.6** Average integrated area of the SFG titrations from: pH 2.0 to 12.0 (red squares), pH 6.0 to 12.0 or pH 7.0 to 2.0 (black circles), and pH 12.0 to 2.0 (blue triangles). ..... 79

**Figure 4.1** A) SHG intensity (determined from previously published SH electric field vs pH data in supporting information of reference 107) vs pH from the silica/aqueous interface with 0.1 M NaCl SHG using *p*-in/all out polarization. The SHG plot is composed to two titrations, from pH 6 to 12 and from pH 7 to 2. B) Representative *ssp* polarized SFG from the silica/aqueous interface with 0.1 M NaCl, also composed of two titrations from pH 6 to 12 and from pH 7 to 2. .... 91

**Figure 4.2** A) Representative titrations of *pss* polarized SHG from the silica/aqueous interface with 0.1 M NaCl that is referenced to the SHG of pure water/silica (all SHG values were divided by the value of the SHG of water). Here two separate titrations were completed, pH 6.0 to 12.0. and pH 7.0 to 2.0. B) Representative titrations of *pss* polarized SFG of silica/aqueous interface with 0.1 M NaCl also collected via two separate titrations pH 6.0 to 12.0 and pH 7.0 to 2.0..... 93

**Figure 4.3** Representative 0.1 M NaCl titrations that have been fit using two Lorentzian peaks. A) Summed  $A/\Gamma$  values of the *pss* SFG high pH and low pH titrations. B) The separate  $A/\Gamma$  contributions of the  $3200\text{ cm}^{-1}$  (red) and  $3400\text{ cm}^{-1}$ (blue) centered modes from the *pss* polarization combination. C) The summed  $A/\Gamma$  values of the *ssp* SFG high pH and low pH titrations. D) The separate  $A/\Gamma$  contributions of the  $3200\text{ cm}^{-1}$  (red) and  $3400\text{ cm}^{-1}$  (blue) centered modes in *ssp* polarization combination..... 94

**Figure 4.4** Nonlinear optical predict of the magnitude of the  $\chi^{(2)}$  for resonant water molecules as a function of the tilt angle  $\theta$  between the surface normal and the principle axis. The solid line is the *ssp* polarization and the dashed line is *pss* polarization..... 98

**Figure 4.5** Averaged titrations that have been referenced to the intensity of the water for each experiment. A) Average *pss* polarized SHG intensity and B) Average *pss* polarized SFG intensity. .... 99

**Figure 5.1** Representative SHG titrations (*p*-in/all out polarization) on fused silica in the presence of 0.1 M NaCl and 0.1 M CaCl<sub>2</sub> with 10 mM NaCl. The spectra were divided by the highest intensity signal to normalize the spectra to 1.0 ..... 112

**Figure 5.2** Representative SHG titrations (*p*-in/all out polarization) of the silica interface in the presence of 0.1 M CaCl<sub>2</sub> (red circles) and 0.01 M CaCl<sub>2</sub> (black diamonds). The intensity at each pH point was divided by the maximum intensity in the titration. All titrations had a background electrolyte of 0.01 M NaCl to account for changes in sodium concentration with the addition of sodium hydroxide..... 113

**Figure 5.3** *ssp* polarized SFG of: A) Silica/CaCl<sub>2</sub> aqueous interface (0.1 M + 0.01 M NaCl) from pH 6.0 to pH 11.5. B) Silica/0.1 M NaCl interface from pH 6.0 to pH 12.0 C) Silica/0.5 M NaCl interface from pH 6.0 to 12.0..... 115

**Figure 5.4** Representative SFG titration of the silica interface with the *pss* polarization combination in the presence of 0.1 M CaCl<sub>2</sub> and 0.01 M NaCl. .... 117

**Figure 5.5** Average integrated area of *pss* polarized SFG of the silica/0.1 M CaCl<sub>2</sub> with 0.01 M NaCl background electrolyte. A) Integrated from 3000 – 3200 cm<sup>-1</sup> B) Integrated from 3200 –

3400 cm<sup>-1</sup>. The error bars represent the standard deviation of the three replicates of the titrations on cleaned silica samples.....118

**Figure 5.6** Representative SFG spectra of the OH vibrational region of the silica/ 0.01 M NaCl interface at A) *ppp* polarization and B) *ssp* polarization on Dr. Tyrode's laser assembly.....120

**Figure 5.7** Representative SFG of the silica/0.1 M CaCl<sub>2</sub> interface at A) *ppp* polarized SFG; and B) *ssp* polarized SFG collected on Dr. Tyrode's laser assembly.....121

**Figure 5.8** Representative titrations of water referenced data for the silica/CaCl<sub>2</sub> (0.1 M + 0.01 M NaCl) interface A) *p*-in/all out SHG intensity. Representative titrations SFG of the OH vibrational region for the silica/CaCl<sub>2</sub> (0.1 M + 0.01 M NaCl) interface: B) Integrated area (3000-3450 cm<sup>-1</sup>) of the *ssp* polarized SFG spectra measured on the Gibbs-Davis laser assembly; C) Integrated area (2800-3800 cm<sup>-1</sup>) of the *ssp* polarized SFG on the Tyrode laser assembly; and D) Integrated area (3000-3450 cm<sup>-1</sup>) of the *pss* polarized SFG on the Gibbs-Davis laser assembly.  
.....125

## List of Tables

**Table 2.1** Calculated pK<sub>a</sub> Values and Site Population for Different Starting pH. .....59

**Table 4.1** All unique, non-zero polarizations and the elements of  $\chi_{ijk}(2)$  that contribute to the spectrum for a C<sub>∞v</sub> interface.....92

## List of Schemes

<b>Scheme 2.1</b> SHG at the silica/aqueous electrolyte interface at low salt concentration. $\Phi_0$ is the surface potential at the 0 plane, $\Phi_d$ is the potential at the d-plane .....	<b>41</b>
<b>Scheme 5.1</b> Cartoon depiction of the contributions of different $\chi^{(2)}$ elements in second harmonic generation and sum frequency generation. SHG depends on the non-resonant response of all species at the interface; SiOH, SiO <sup>-</sup> , bulk water, aligned water, and ions. SFG depends on the resonant response of aligned water.....	<b>103</b>
<b>Scheme 5.2</b> Depiction of the silica/calcium interface as pH is increased. A) The pH where surface waters are being aligned by the surface siloxides. B) The pH where calcium disrupts the surface waters. C) The pH when a CaOH species forms and hydrogen bonds with the surface siloxides. ....	<b>122</b>
<b>Scheme 5.3</b> Alternative CaOH formation at high pH values where the OH vibrational mode is pointed with hydrogen towards the bulk.....	<b>124</b>

## **CHAPTER 1**

### **Introduction**

## **1.1 Importance of the Silica/Water Interface**

Understanding the complexity of the solid/liquid interface is crucial to understanding many geochemical, environmental and industrial processes.<sup>1-4</sup> One of the major sources of such complexity is the difference in behavior of molecules at the interface compared to their counterparts in the bulk. For example, in bulk water the hydrogen bonding between adjacent water molecules gives water its unique properties like a high boiling point. In bulk water, each water molecule is on average hydrogen bonded to 3 to 4 water molecules.<sup>5</sup> When a solid surface is introduced into the system, it disrupts the hydrogen bonding network of the water molecules that are directly adjacent to the interface. These water molecules will consequently rearrange into the lowest energy configuration and attempt to reestablish the maximum amount of hydrogen bonds between the surface and bulk water molecules. This will in turn cause the next layer of water molecules to reorient. The amount of reorientation depends on the nature of the solid surface and the solution conditions.<sup>6</sup>

Silica is one of the most common mineral oxides found in the Earth's crust and, as such, the silica/water interface is prevalent in both the environment and in industry. For example, the interactions between the silica and the aqueous phase can dramatically affect the chemical separations in the processing of the Athabasca Oil Sands. One of the major challenges to studying this interface is the difficulty of studying a buried interface, i.e. between the bulk silica and bulk water, as it is often difficult to distinguish processes that happen at the interface versus those that are occurring in the bulk. Therefore, to study the silica/water interface, techniques like second harmonic generation (SHG) and vibrational sum frequency generation (SFG) spectroscopy have been utilized because of their surface specificity.

This chapter first focuses on some important components of optics that are utilized in nonlinear spectroscopy. Next, there will be an overview of how light interacts with an interface; an explanation on the second-order nonlinear techniques SHG and SFG; a brief description on electrical double layers that form at the silica/water interface; and lastly a discussion of how SHG and SFG have been utilized to study perturbations of the silica/water interface and the information this provides.

## 1.2 Reflection and Refraction of Light at an Interface

An interface is present when two different materials or phases are in contact; in both cases the two components of the interface will have different refractive indices. When light comes in contact with an interface it can be absorbed, scattered, refracted or reflected depending on the properties of the interface. When light is reflected, the angle of incidence of the incoming light is equal to the angle of incidence of the reflected light (Figure 1.1). When light is refracted, it is governed by Snell's Law, where the angle of refraction is dependent on the angle of incidence of the incoming light and the refractive indices of the two media. Specifically, when light travels through a medium with a higher index of refraction ( $n_1$ ) to a medium with a lower index of refraction ( $n_2$ ) the angle of refraction ( $\theta_2$ ) is larger than the original angle of incidence ( $\theta_1$ ) as seen in Figure 1.1. As the angle of incidence ( $\theta_1$ ) increases, the angle of refraction ( $\theta_2$ ) will also increase until it is  $90^\circ$  from surface normal. The angle where this occurs is called the critical angle ( $\theta_C$ ). At angles of incidence above the critical angle, the light wave cannot be refracted through the medium and is entirely reflected in a process known as total internal reflection (TIR). The TIR process is often taken advantage of in nonlinear optical setups because it minimizes loss from signal refraction.

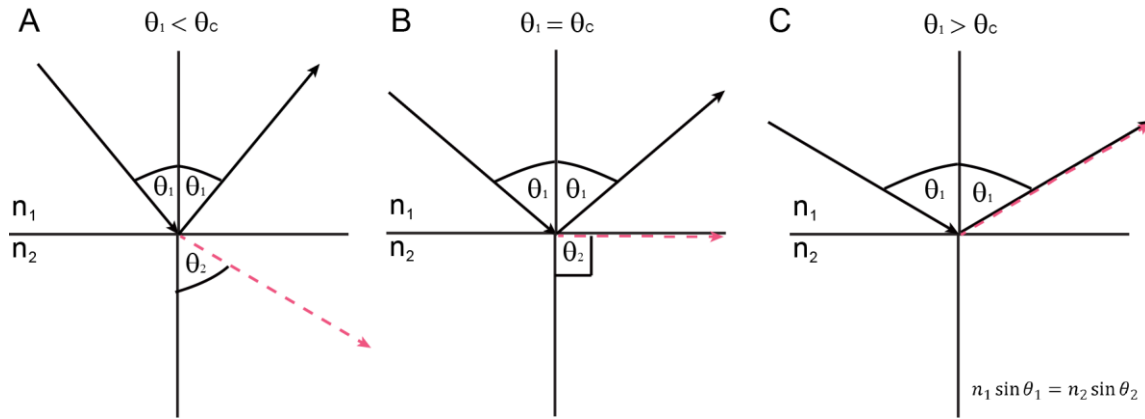
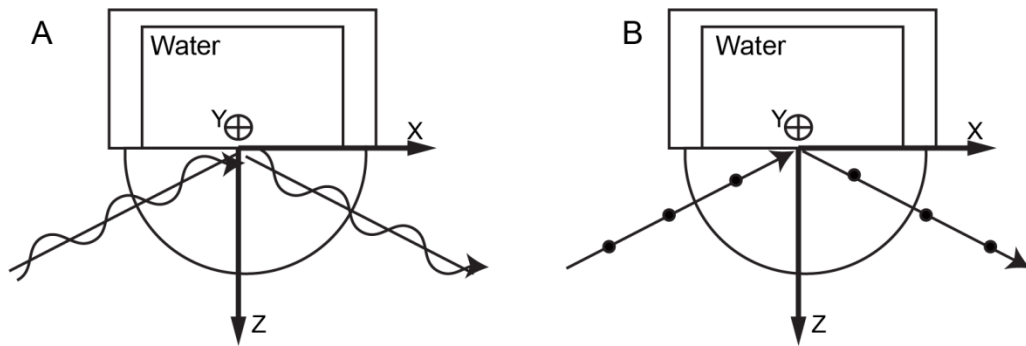


Figure 1.1

**Figure 1.2** Reflection and refraction of light: A) when the angle of incident light is  $\theta_1 < \theta_c$ ; B) when the angle of incident light is  $\theta_1 = \theta_c$ ; and C) when the angle of the incident light is  $\theta_1 > \theta_c$ . This phenomena is dependent on the refractive index of medium 1 ( $n_1$ ) being larger than the refractive index of medium 2 ( $n_2$ ).

### 1.3 Polarized Light

In nonlinear optical processes like second harmonic generation (SHG) and sum frequency generation (SFG), it is typical to use linearly polarized light as seen in Figure 1.3. Linearly polarized light is defined by the direction of its oscillating electric field in relation to the plane of incidence. The plane of incidence is the plane that contains the surface normal, defined as the Z axis in this case, and the direction of the light propagation (XZ plane) in Figure 1.3. Figure 1.3A depicts *p*-polarized light, which is light that has its electric field component oscillating parallel to the XZ plane. Consequently, *p*-polarized light has X and Z components of its electric field. Figure 1.3B shows *s*-polarized light, which is light that has its electric field component oscillating perpendicular to the XZ plane. Accordingly, *s*-polarized light only has Y components of the electric field.



**Figure 1.3** Depiction of A) *p*-polarized light parallel to the plane of incidence. B) *s*-polarized light perpendicular to the plane of incidence where the dots on the propagation beam indicate that the electric field is oscillating perpendicular to the XZ plane (in and out of the page).

#### 1.4 Probing Interfacial Structure

In first-order spectroscopy, also known as linear spectroscopy, the presence of an applied electric field ( $E$ ), induces a polarization at the interface ( $P$ ) given by:<sup>7-9</sup>

$$P = \epsilon_0 \chi^{(1)} E \quad (\text{Equation 1.1})$$

The magnitude and phase of the induced polarization is dependent on the electric susceptibility of the material ( $\chi^{(1)}$ ), the applied incident electric field ( $E$ ) and the vacuum permittivity ( $\epsilon_0$ ). There are many techniques that allow us to study surface and interfacial properties. In linear spectroscopy, techniques such as attenuated total reflectance infrared (ATR-IR) spectroscopy reduce contributions from the bulk media. The surface selectivity of ATR-IR is based on having a narrow penetration depth of the produced evanescent wave at the interface. The penetration depth of the evanescent field is determined by the wavelength of light, angle of incidence, and refractive indices of the media. If the sample being studied is a mineral oxide/water interface the penetration depth of the evanescent wave can probe 1-2  $\mu\text{m}$  distance from the interface depending on the wavelength of light.<sup>10</sup> Although this penetration depth is relatively small, the interfacial region can be on the order of a few nanometers. Consequently, in TIR experiments

like ATR-FTIR the bulk solution is still being probed, which can interfere with interpreting molecular behavior at the interface.

In contrast to linear optical methods, the surface specificity in second order nonlinear optical methods is governed by symmetry constraints rather than solely by the penetration depth of the evanescent wave. Specifically, second order nonlinear optical techniques are forbidden in centrosymmetric media, i.e. media that possess inversion symmetry. In the case of the fused silica/water interface, only at the interface between the two centrosymmetric media is the centrosymmetry broken. However, the nonlinear responses are only observed with high electric field strengths such as those achieved by pulsed laser systems or powerful continuous wave lasers because the nonlinear response is intrinsically much, much smaller than the linear response.<sup>11</sup> Thus at high electric field strengths contributions from the second order and third order nonlinear susceptibilities,  $\chi^{(2)}$  and  $\chi^{(3)}$ , respectively are no longer negligible and the induced polarization can be written as

$$\mathbf{P} = \epsilon_0(\chi^{(1)}\mathbf{E} + \chi^{(2)}\mathbf{E}^2 + \chi^{(3)}\mathbf{E}^3 + \dots) \quad (\text{Equation 1.2})$$

Two techniques that probe the second order nonlinear susceptibility  $\chi^{(2)}$  are SHG and SFG.

## 1.5 Second Harmonic Generation (SHG)

### 1.5.1 Basic Theory

Within the electric dipole approximation, SHG is forbidden in centrosymmetric media. When light with a frequency  $\omega$  interacts with a non-centrosymmetric crystal or an interface, it induces a polarization that oscillates at twice the frequency of  $\omega$  ( $P_{2\omega}$ )

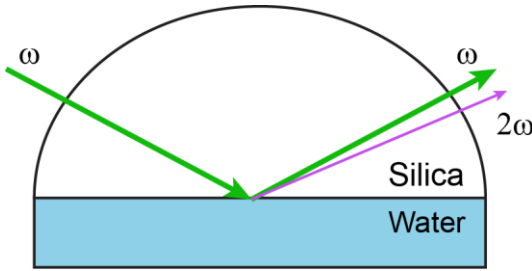


**Figure 1.4** Schematic of SHG at the silica/water interface.

This oscillation generates an electric field that also oscillates at  $2\omega$  ( $E_{2\omega}$ ), which emanates from the interface and can be detected (Figure 1.3). The square root of the intensity ( $I_{2\omega}$ ) of the SHG response is proportional to the induced second order polarization ( $P_{2\omega}^{(2)}$ ).

$$\sqrt{I_{2\omega}} = E_{2\omega} \propto P_{2\omega}^{(2)} = \chi^{(2)} E_\omega E_\omega \quad (\text{Equation 1.3})$$

The second-order susceptibility,  $\chi^{(2)}$ , is a third-order tensor which contains 27 tensor elements. It can be represented using Cartesian coordinates in the laboratory frame, where  $P_I^{(2)}$  represents the induced polarization vector component in the I direction,  $E_J$  represents the incident electric field vector component in the J direction, and  $E_K$  represents the incident electric field vector component along the K direction, and  $\chi_{IJK}^{(2)}$  represents one of the tensor elements of the second-order susceptibility. For SHG, the  $\chi_{IJK}^{(2)}$  (IJK=XYZ) describes the efficiency of generating I polarized SHG using J and K polarized incident electric fields.

$$P_I^{(2)} = \sum_{J,K} \chi_{IJK}^{(2)} E_J E_K \quad (\text{Equation 1.4})$$

For an interface like the silica/water interface, which possesses  $C_{\infty v}$  symmetry, only 7 of the 27 tensor elements are non-zero. The non-zero tensor elements for the silica/water interface are  $\chi_{ZZZ}^{(2)}$ ,  $\chi_{XXZ}^{(2)}$ ,  $\chi_{YYZ}^{(2)}$ ,  $\chi_{XZX}^{(2)}$ ,  $\chi_{YZY}^{(2)}$ ,  $\chi_{ZXX}^{(2)}$ , and  $\chi_{ZYY}^{(2)}$ . Because the X and Y axes are indistinguishable, some of the tensor elements are equal and it simplifies down to four unique

non-zero tensor elements  $\chi_{zzz}^{(2)}$ ,  $\chi_{xxz}^{(2)} = \chi_{yyz}^{(2)}$ ,  $\chi_{xzx}^{(2)} = \chi_{yzy}^{(2)}$ , and  $\chi_{zxx}^{(2)} = \chi_{zyy}^{(2)}$ . Different combinations of the polarized light described in Section 1.3 can be used to access the different tensor elements. For example *ssp* polarized light (*s*-polarized SFG, *s*-polarized visible, and *p*-polarized IR) can be used to access the  $\chi_{yyz}^{(2)}$  tensor element. Accordingly, for analysis of the water structure at an interface, *ssp* polarized SFG is the most common polarization combination.

One advantage of SHG is the  $\chi^{(2)}$  can be related to the number of interfacial species in a simple way. Specifically, the  $\chi^{(2)}$  second-order susceptibility can be defined as:

$$\chi^{(2)} = N\langle\beta\rangle \quad (\text{Equation 1.5})$$

where the  $N$  is the number density of interfacial molecules,  $\beta$  is the molecular hyperpolarizability of the corresponding molecules, and the brackets represent the orientationally averaged value. Furthermore, the  $\chi^{(2)}$  can be split up into two different contributing terms:  $\chi_{NR}^{(2)}$  and the  $\chi_R^{(2)}$ . These parameters describe the non-resonant second order susceptibility and the resonant second order susceptibility, respectively.

$$\chi^{(2)} = \chi_R^{(2)} + \chi_{NR}^{(2)} \quad (\text{Equation 1.6})$$

### 1.5.2 Non-Resonant SHG

In non-resonant SHG, two photons of frequency  $\omega$  combine at a non-centrosymmetric interface or crystal and generate a photon of  $2\omega$ . This is depicted in Figure 1.4, where the solid line depicts a real state, in this case the ground state of the interfacial atom or molecule, and the dashed lines represent a virtual level. These virtual levels correspond to the combined energy of the two photons.

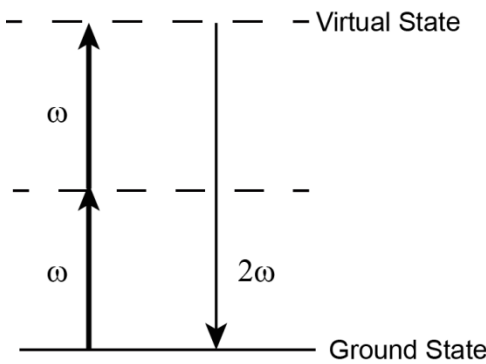


**Figure 1.5** Non-resonant SHG energy diagram. The dashed lines depict a virtual state, and the solid line depict a real state in the atom or molecule.

In the case of non-resonant SHG, none of the frequencies of incident or emitted light are in resonance with any of the electronic signatures of specific molecules or ions. Therefore  $\chi^{(2)}_{NR}$  encompasses any of the interfacial species. In the case of the silica/water interface, this will include any interfacial water molecules, silica (particularly non-centrosymmetric species such as silanols, silanoliums and siloxides), and any ions:

$$\chi_{NR}^{(2)} = \chi_{H_2O}^{(2)} + \chi_{Silica}^{(2)} + \chi_{ions}^{(2)} \quad (\text{Equation 1.7})$$

Non-resonant SHG is a popular technique to study how charged interfaces like silica behave. In 1992, Eisenthal and coworkers showed that the presence of a static electric field, which is set up by charged sites on mineral oxide interfaces like silica, can enhance the signal intensity of the SHG. This static electric field and the corresponding interfacial potential ( $\Phi$ ), lead to the contribution of a third-order susceptibility term ( $\chi^{(3)}$ ) to the second harmonic response:

$$E_{2\omega} \propto P_{2\omega}^{(2)} = \chi^{(2)} E_\omega E_\omega + \chi^{(3)} E_\omega E_\omega \Phi \quad (\text{Equation 1.8})$$

The contributions of  $\chi^{(3)}\Phi$  can be further broken down into two terms. The first term describes the alignment of the dipole moment of water molecules ( $\mu_{H_2O}$ ) due to the interfacial potential,

where  $kT$  is the thermal energy and  $b$  is a constant. The second term contains the third-order molecular hyper polarizability of water ( $\gamma_{H_2O}$ ) and the interfacial potential.

$$\chi^{(3)}\Phi = N_{H_2O} \frac{\mu_{H_2O}\Phi}{bkT} \beta_{H_2O} + N_{H_2O} \gamma_{H_2O} \Phi \quad (\text{Equation 1.9})$$

Any interfacial dependent signal observed is attributed to the interfacial potential aligning the dipoles of water. This thesis will focus on the use of pH to modify the interfacial potential of the silica surface. As silica contains surface silanol sites, altering the pH results in the formation of negatively charged siloxides or positively charged silanoliums through acid-base chemistry. As will be discussed later in section 1.7, the surface charge density resulting from these processes can be related to the interfacial potential using models of the electric double layer.

### 1.5.3 Resonantly Enhanced SHG

In the case of resonantly enhanced SHG, either the input frequency of light  $\omega$ , or the output light at  $2\omega$  is in resonance with an electronic signature of the molecule or atom at the interface as shown in Figure 1.5. To understand the resonance enhancement of the molecular hyperpolarizability,  $\beta$  can be expressed as the summation over the electronic states.<sup>11</sup>

$$\langle \beta \rangle = \frac{-4\pi^2 e^3}{h^2} \sum_{b,c} \frac{\langle m | \vec{\mu}_i | n \rangle \langle n | \vec{\mu}_j | o \rangle \langle o | \vec{\mu}_k | m \rangle}{(\omega - \omega_{ba} + i\Gamma_{ba})(2\omega - \omega_{ca} + i\Gamma_{ca})} \quad (\text{Equation 1.10})$$

Where  $m$ ,  $n$  and  $o$  represent the ground, intermediate, and excited state respectively,  $\omega_{ba}$  and  $\omega_{ca}$  are the frequencies of the corresponding electronic transitions,  $\omega$  is the incident frequency,  $\vec{\mu}$  is the electric dipole moment operator,  $\Gamma_{ba}$  and  $\Gamma_{ca}$  are the damping coefficients for the transitions,  $h$  is Planck's constant, and  $e$  is the elementary charge. As shown in Equation 1.10 and Equation 1.5 when either the incident light at  $\omega$  or the second harmonic light at  $2\omega$  is close to an electronic resonance frequency within the surface species ( $\omega_{ba}$  and  $\omega_{ca}$ , respectively), there is an increase in

the  $\beta$  value. Consequently, the SHG signal is dominated by the contribution from  $\chi^{(2)}_R$ , and the contribution from  $\chi^{(2)}_{NR}$  is assumed to be small and to undergo negligible changes.

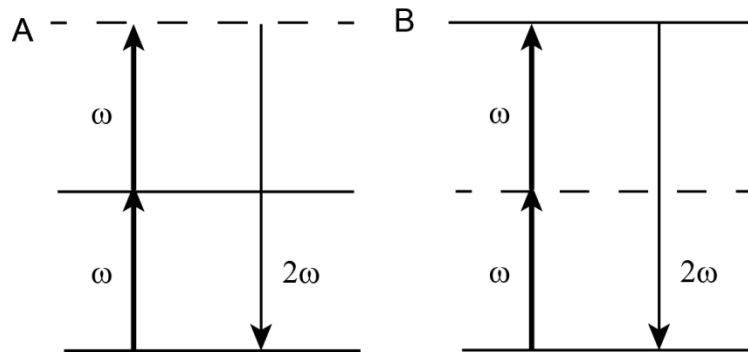


**Figure 1.6** Resonantly enhanced SHG energy diagrams. A) When  $\omega$  is in resonance with the electronic transition. B) When  $2\omega$  is in resonance with the electronic transition. The dashed lines represent virtual states and the solid lines represent real states within the molecule or atom.

Resonantly enhanced SHG can be utilized to study how different ions, molecules, and compounds bind to different interfaces by tuning the incident light or second harmonic light to an electronic signature of the molecule of interest.

## 1.6 Sum Frequency Generation (SFG) Theory

Sum frequency generation (SFG) is a nonlinear optical technique that has the same underlying principles as resonant SHG. The main difference is that SFG uses two different incident beams, one a visible beam ( $E_{VIS}$ ) and the other an IR beam ( $E_{IR}$ ). The IR light is tuned so that it is in resonance with a vibrational transition of a molecule at the interface.

$$\sqrt{I_{SFG}} = E_{SFG} \propto P_{SFG} = \chi^{(2)} E_{VIS} E_{IR} + \chi^{(3)} E_{VIS} E_{IR} \phi \quad (\text{Equation 1.11})$$

The same breakdown of  $\chi^{(2)}$  and  $\chi^{(3)}$  can be applied as in Equations 1.6 and 1.8. However, because IR light that is in resonance with a vibrational transition is utilized, only the molecules that contain that vibrational mode will be detected. In the case of the silica/water interface, if an IR laser light is in resonance with the O-H vibrational mode, then only those molecules like

water that have an O-H vibration and assemble into a non-centrosymmetric arrangement at the interface will be observed.

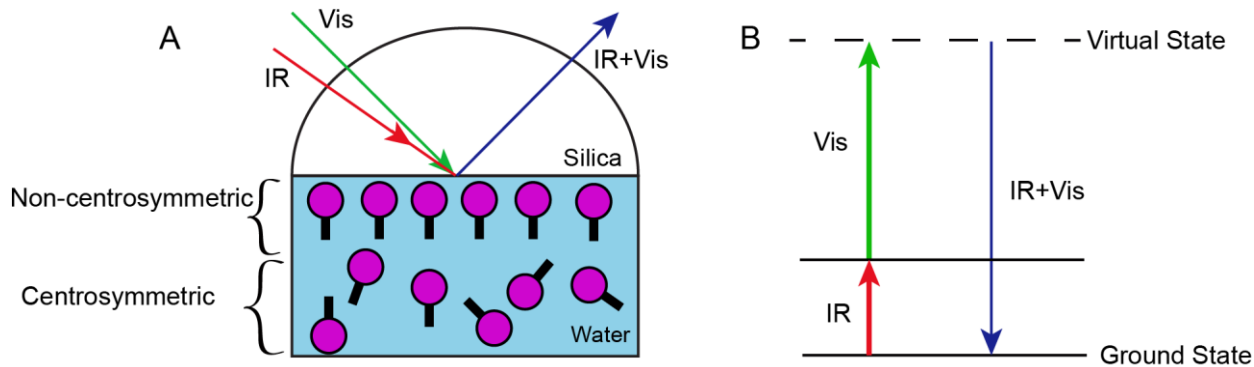


**Figure 1.7** (A) Depiction of SFG at the silica/water interface and B) depiction of the energy diagram of SFG in resonance with an IR vibrational transition.

Three parameters that can be ascertained by fitting the SFG spectra are the intensity, position and phase of the oscillator. These parameters provide information about the interfacial molecules. The second-order nonlinear susceptibility can be further expressed as:<sup>9-10, 12</sup>

$$\chi^{(2)} = \chi_{NR}^{(2)} + \chi_R^{(2)} = \chi_{NR}^{(2)} + \sum_q \frac{A_q}{\omega_{IR} - \omega_q + i\Gamma_q} \quad (\text{Equation 1.12})$$

In Equation 1.12,  $\omega_{IR}$  is the frequency of the IR beam,  $A_q$  is the amplitude of the resonant vibrational mode,  $\omega_q$  is the resonant frequency of the vibrational mode and  $\Gamma_q$  is the damping constant of the resonant vibrational mode. According to Equation 1.12 the magnitude of  $A_q/\Gamma_q$  is proportional to the ordering of the molecules and the number density of the molecules. The phase of the  $q$  mode, related to the sign of  $A_q$ , provides information about which direction the specific molecular assembly is facing and can be determined using either phase-sensitive SFG methods<sup>13-15</sup> or mathematical models.<sup>16-17</sup>

There are two typical setups for SFG with respect to the bandwidth of the IR light in the frequency domain. The first is scanning SFG, where the frequency of both the IR and visible

beams are narrow ( $<10\text{ cm}^{-1}$ ) and the IR light is tuned and scanned point by point over a wide range of wavenumbers while the visible beam remains fixed. This technique can be slow depending on the wavenumber range that needs to be collected, but typically offers high spectral resolution.<sup>18-19</sup> The second method of SFG, broadband SFG, uses a fixed visible beam that is narrow ( $<10\text{ cm}^{-1}$ ) in frequency and a broad IR pulse ( $>120\text{ cm}^{-1}$ ). Broadband SFG provides the ability to collect a large portion of the spectrum at once. By changing the central frequency of the IR band, the entire SFG spectrum of water can be acquired in 5-6 acquisitions. In addition, broadband SFG offers greater signal to noise ratio than scanning measurements.<sup>18-19</sup> Most of the experiments performed in this thesis were collected using a broadband SFG setup with the exception of those performed by the Hore lab at the University of Victoria.

## 1.7 Electrical Double Layer

The silica/water interface is often described in terms of an electrical double layer. This is an electrical phenomenon, first described by Helmholtz,<sup>20-21</sup> which takes place at a charged surface in the presence of electrolytes. A “double layer” is believed to form at the interface between a charged surface (0-plane) and aqueous solution, where ions are attracted to the surface charge essentially creating a layer of charge (d-plane).<sup>21-25</sup> A variety of models have been further developed in order to better understand the behavior of these double layers.

At low concentrations of ions (up to 0.1 M) the double layer is often modeled as a diffuse layer of charge. This model is often referred to as the Gouy-Chapman model.<sup>21, 25</sup> In this model the electrical potential exponentially drops as the distance from the surface increases. The magnitude of the interfacial potential can be calculated as a function of the counter ion concentration ( $C$ ) and the surface charge density ( $\sigma_0$ ) according to:<sup>21, 26</sup>

$$\Phi_0 = \frac{2kT}{e} \sinh^{-1} \left( \sigma_0 \sqrt{\frac{\pi}{2C\epsilon kT}} \right) \quad (\text{Equation 1.13})$$

where  $\epsilon$  is the bulk dielectric constant,  $e$  is the elementary charge,  $k$  is the Boltzmann constant and  $T$  is the temperature in Kelvin. The theory of the electrical double layer was further developed by Stern, who suggested that at the surface there was both a compact layer of charge and a diffuse layer like the Gouy-Chapman layer (Figure 1.7C). In the compact layer the potential drops linearly until it reaches the diffuse layer where it changes to an exponential drop in potential (Figure 1.7D).<sup>20</sup> Although Stern did not distinguish between the outer and inner Helmholtz plane, in his original paper he proposed that counter ions could become dehydrated and specifically adsorb to the surface to form this compact layer.<sup>20</sup> Grahame extended the Stern model and proposed that ions could also form a compact layer without specific adsorption by remaining hydrated and approaching the surface only as close as the outer Helmholtz layer.<sup>20</sup> Three groups: Esin and Markov, Grahame, and Devanathan proposed variations of the idea that some ions can penetrate the Stern layer and adsorb to the charged surface while others are only present at the outer Helmholtz layer (Figure 1.7E and Figure 1.7F). These latter models are typically referred to as triple layer models.<sup>20, 24</sup> Such surface models often consider that potential-determining ions like hydroxide are present at the inner Helmholtz layer and changes in surface charge density with pH arise from the binding of these potential-determining ions, although this is counterintuitive from a chemical sense as it involves negatively charged ions binding to a negative surface (Figure 1.7E). The same triple layer model can also be used to describe specific adsorption of oppositely charged ions like cations with a negative surface. In this case the potential would become less negative moving from the surface to the inner Helmholtz plane.

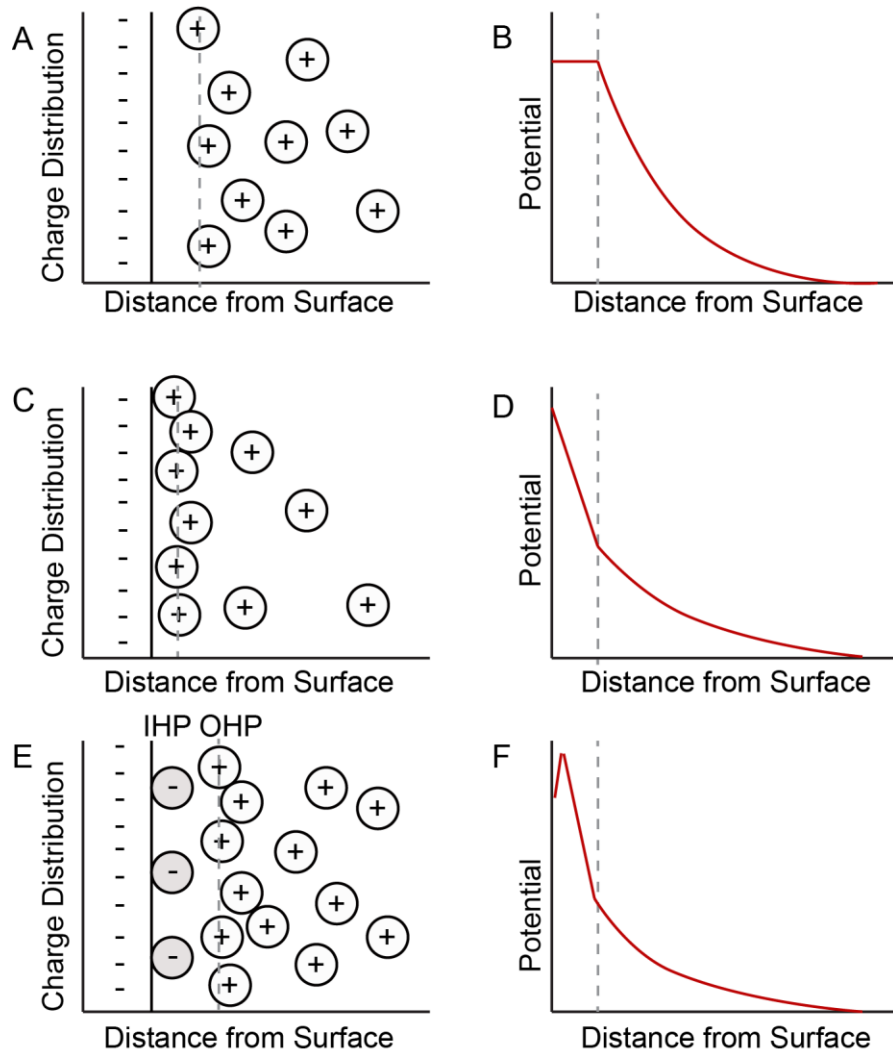


**Figure 1.8** Schemes of the different electrical double layer models. A) The Gouy-Chapman model showing only the diffuse layer. B) The potential of the Gouy-Chapman model. C) The Stern model showing a compact layer of ions and a diffuse layer. D) The potential of the Stern model. E) The model of Esin and Markov, Grahame, and Devanathan showing ions penetrating the Stern layer and F) The potential of the Esin and Markov, Grahame, and Devanathan model. The dotted gray line represents the Outer Helmholtz Plane (OHP), and the IHP is the inner Helmholtz plane.

Bockris, Devanathan and Muller included the effects of polar solvents like water at the surface of charged surfaces in their electrical double layer model (BDM model).<sup>24, 27</sup> The solvents contribute to the potential drop across the surface/electrolyte interface (Figure 1.8). One of the main features of this model is the orientated water molecules at the charged surface. In

this layer of water, specifically adsorbed ions can also be present at the surface. Next to the layer of specifically adsorbed ions is a layer of hydrated cations followed by the diffuse layer.

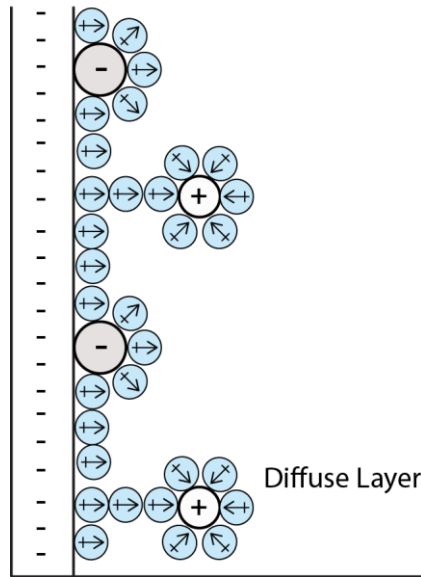


**Figure 1.9** The Bockris, Devananthan and Muller (BDM) electrical double layer model. The blue spheres represent the water solvent molecules, while the arrow represents the direction of the dipole moment.

One often confusing convention is that the “Stern layer” is often referred to in the literature when describing parts of the electric double layer. This “Stern layer” often encompasses solvent molecules and ions (both solvated and dehydrated) rather than just the specifically adsorbed ions originally proposed by Stern. In addition, the zeta potential, which is technically measured at the plane of shear, is assumed to originate close to the start of the diffuse layer. In the case of the models here, this would correspond to the near the edge of the outer Helmholtz plane.<sup>28</sup> Consequently zeta potential measurements are often utilized to determine the interfacial potential right outside the “Stern layer”.

## 1.8 Nonlinear Optical Studies of the Silica/Water Interface

In 1992, Eisenthal and coworkers showed that the intensity of the non-resonant SHG signal was dependent on the surface charge of silica through the deprotonation of the silica sites.<sup>26</sup> According to this work, SHG could be used to determine the interfacial potential of mineral oxides like silica. Specifically, Eisenthal and co-workers reported that, in the presence of 0.5 M NaCl, as the pH was increased the SHG signal intensity generally increased, which was attributed to deprotonation of the surface (Figure 1.10). The interesting feature of these results was that the pH dependent SHG data resembled the acid-base dissociation curves of diprotic acids, which led to the conclusion that the silica/water interface has two different acidic silanol sites with  $pK_a$  values around 4.5 and 8.5.<sup>26</sup>

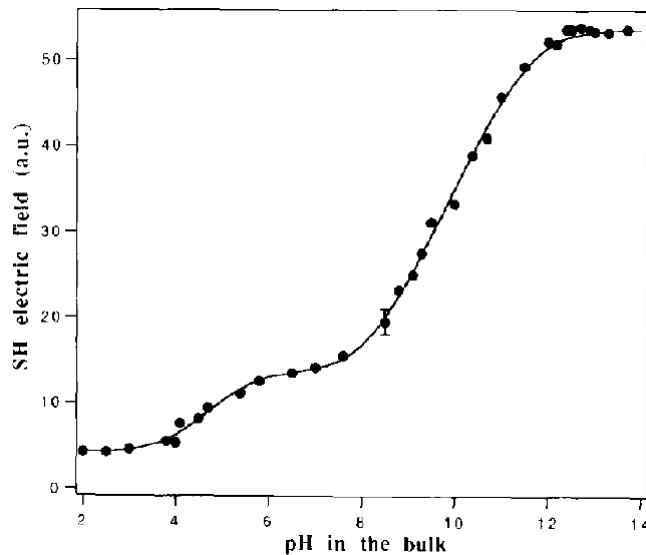


**Figure 1.10** SHG electric field (in arbitrary units) as a function of pH in bulk solution. The dots are experimental points, while the solid line is the theoretical fit with the constant capacitance model. Reprinted with permission from reference 26. Copyright 1992 American Chemical Society.

The work done by Eisenthal and coworkers was the first demonstration using SHG to probe the acid-base behavior of the silica/aqueous electrolyte surface. Prompted by the need to

explain the increase in the SHG signal intensity as a function of pH, Eisenthal and coworkers also performed studies on the dependence of the SHG signal intensity on temperature.<sup>26</sup> They found that the SHG signal intensity increased with increasing temperature at high pH, when the surface was thought to be completely deprotonated. Calculating the SHG E-field difference measured at high pH and low pH for different temperatures and multiplying this difference by the temperature-dependent dielectric constant of water yielded a 1/T dependence. This 1/T dependence supported the authors proposed mechanism that the static electric field set-up by negative charges on silica polarized and/or oriented water molecules near the interface in a Boltzmann distribution, leading to the observed temperature dependence (Equation 1.9). Integrating the response of the water to this static electric field set-up by the charged interface yielded the interfacial potential dependent  $\chi^{(3)}$  term. Therefore, with this new  $\chi^{(3)}$  method, non-resonant SHG could be used to determine the interfacial potential at insulator/water interfaces.

Using this  $\chi^{(3)}$  method, the acid-base behavior of charged monolayers at the air/water interface was next studied.<sup>29-30</sup> Interestingly, the magnitude of the second harmonic field changed only by approximately 2.5 times the initial  $E_{2\omega}$  value when the pH was varied for a docosylamine monolayer with a maximum surface charge density of one charged molecule per 22 Å<sup>2</sup>. This change in  $E_{2\omega}$  was much lower compared to the 10 times increase in  $E_{2\omega}$  observed at the silica/water interface, for a much smaller maximum surface charge density of one siloxide per 4.5 nm<sup>2</sup>.<sup>26, 30</sup> Comparing these results leads to the question: why does the silica/water interface exhibit a higher magnitude change of the SHG signal intensity as a response to pH compared to that of a charged monolayer Langmuir-Blodgett film? As will be shown, we will address this question in Chapter 4 by comparing nonlinear optical methods including non-resonant SHG in pH variation experiments at the silica/aqueous interface.

Another question that was prompted by Ong *et al.*'s work was the origin of the bimodal acid-base titration curve at the silica/water interface. A bimodal titration curve typically signifies that there are two deprotonatable sites at the silica/water interface. There have been many researchers who have tried to determine the origin of the two different acidic sites present at the silica/water interface in the range of pH 2 to 12.<sup>31-34</sup> Most of this work has been done through different computer simulations of a quartz surface<sup>31</sup> or an amorphous silica<sup>32</sup> surface. In one simulation, density functional theory based molecular dynamics (DFTMD) was used to calculate the acidity of the surface.<sup>31, 34</sup> The simulations indicated that the acidity of the surface was due to different hydrogen bonding patterns at the interface, where a pK<sub>a</sub> of 5.6 was calculated for silanols that were donating a hydrogen bond to the oxygen of a water molecule, and another pK<sub>a</sub> of 8.5 was calculated for silanols that were donating a hydrogen bond to a neighboring silanol.<sup>31</sup> However, this simulation failed to observe the experimental pK<sub>a</sub> value of the silica/water interface of 4.5.<sup>31</sup> Another study observed the pK<sub>a</sub> of 4.5 but only for sites that were on or in close proximity to strained silica trimer rings (Si-O-Si bridges).<sup>33</sup> More recently, simulations have also been performed on the amorphous silica/water interface.<sup>32</sup> Although no pK<sub>a</sub> values have been determined, the authors did observe three different types of silanols on the surface of amorphous silica that could hydrogen bond with water molecules: isolated, germinal, and vicinal silanol sites. Although simulations can help explain physical phenomena, they also have their limitations. For example, the mentioned simulations have mostly been performed on a fully hydroxylated surface (neutral) and not a charged silica surface. The charged surface may significantly alter the results of the simulations because the water molecules will behave differently due to the static field that is set up by a charged surface. Thus, simulations often need to be verified by experimental methods to test the validity of the models on real samples.

Another complimentary technique that allows for experimental verification of interface simulations is vibrational SFG.

Indeed, the orientation and amount of ordered water can be measured even more directly than SHG using the complementary vibrational technique SFG. Consequently, soon after Eisenthal's work, Shen and coworkers studied the silica/water interface using SFG to study the aligned water molecules at the interface as a function of pH.<sup>35-36</sup> In the SFG spectra of the silica/pure water interface, there are two distinguishable resonant modes observed: one peak at 3200 cm<sup>-1</sup> and the other peak at 3400 cm<sup>-1</sup> (Figure 1.10A). Based on the Raman spectra of pure ice and water, these peaks in the SFG spectra were assigned to a more hydrogen bonded peak or "ice-like" peak at 3200 cm<sup>-1</sup>, and a less hydrogen bonded or "water-like" peak at 3400 cm<sup>-1</sup>.<sup>35</sup> Interestingly, the 3200 and 3400 cm<sup>-1</sup> peaks have been observed at many different water interfaces, which include other mineral interfaces like Al<sub>2</sub>O<sub>3</sub>,<sup>37-38</sup> TiO<sub>2</sub>,<sup>39-40</sup> and CaF<sub>2</sub>.<sup>41</sup> The double peaked water feature along with a narrow band around 3700 cm<sup>-1</sup> is also observed at the air/water interface<sup>4, 42</sup> and at hydrophobic/water interfaces;<sup>43</sup> this latter peak is attributed to a dangling (non-hydrogen bonded) OH.

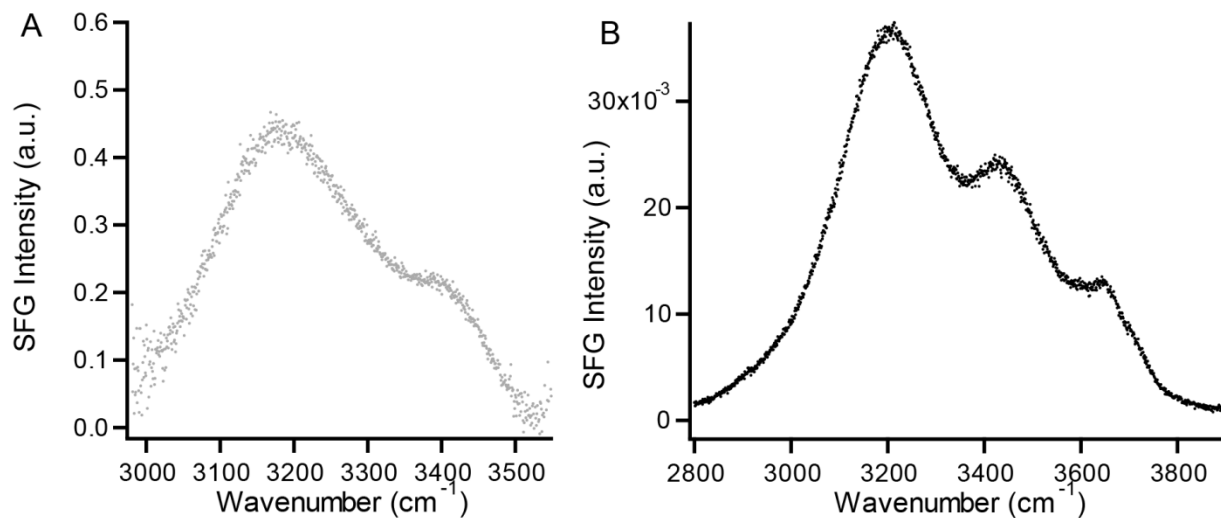


**Figure 1.11** A comparison of different *ssp* polarized water spectra from A) the Gibbs-Davis lab B) the Tyrode lab.

As mentioned, Shen and coworkers also studied the effect of pH on the alignment of water molecules at the silica/water interface.<sup>35-36</sup> When no salt was present in the experiment, the SFG signal intensity increased with pH at both the  $\alpha$ -quartz/water and fused silica/water interfaces.<sup>36</sup> This pH dependence of the signal intensity agreed well with Eisenthal's assumption that the aligned water was mostly responsible for the increase in the SHG signal intensity with increasing pH. However, when salt was present (albeit at unspecified concentrations), then the SFG signal did not behave in the expected way.<sup>35, 39</sup> For example, Shen and coworkers found that there was more SFG signal at pH 1.5 than at pH 3.8 or 5.3.<sup>35</sup> The authors reasoned that pH 1.5 was near the point of zero charge of silica, which is  $\sim$  pH 2-3,<sup>23</sup> and was consequently dominated by neutral silanol sites. Because of these neutral silanols, any water molecules that were hydrogen bonded to the surface were theorized to be oriented with the hydrogens of the water facing away from the surface. Although the authors did not comment directly on the origin of the decrease going from pH 1.5 to pH 3.8 and 5.3, they did propose that when the surface is strongly negatively charged at high pH, water molecules flipped orientation so that the

hydrogens were pointed towards the silica surface. Therefore from these statements we reason that one could rationalize the decrease in intensity at pH 3.8 and 5.3 to the competition between the water molecules accepting hydrogen bonds from neutral sites and water molecules donating hydrogen bonds to siloxide sites leading to more aligned water at the neutral surface of pH 1.5 than at the negatively charged surface at pH 3.8 or 5.3. In another example, Cremer and co-workers also showed that there was more SFG intensity at pH 2 compared to pH 4 at 30 mM NaCl,<sup>39</sup> which is generally consistent with Shen and co-workers' previous data. Once again the authors did not comment specifically on the increase in signal intensity upon decreasing the pH from 4 to 2.

The absolute orientations of the water molecules can be determined using phase sensitive SFG, which allows for the measurement of the both the real and imaginary (Im) part of the complex  $\chi^{(2)}$ .<sup>13, 44</sup> For water, a positive Im( $\chi^{(2)}$ ) value denotes water molecules that are pointed with their hydrogens pointing toward the silica surface, while a negative Im( $\chi^{(2)}$ ) value denotes water molecules that are pointed with their hydrogens directed away from the surface towards the bulk water.<sup>13</sup> Shen and co-workers found that at low pH, the low wavenumber region of the Im( $\chi^{(2)}$ ) spectrum has a negative peak centered around 3050 cm<sup>-1</sup>. As the pH increased the low wavenumber mode (~ 3200 cm<sup>-1</sup>) changed sign from negative to positive. The 3400 cm<sup>-1</sup> peak on the other hand only had a positive Im( $\chi^{(2)}$ ) from pH 2 to 11.<sup>13</sup> These results show that at least one population of water molecules at the silica/water interface flip orientation upon changing pH, which helped support Shen and coworkers previous hypothesis that at pH 1.5 water molecules were orientated with the hydrogens pointed away from the surface.

Furthermore, phase sensitive measurements have also been useful at reconciling unusual observations in isotopic dilution experiments regarding the origin of both the 3200 and 3400 cm<sup>-1</sup>

peaks. The confusion in the origin of these peaks was identified in a recent study done by Bonn and coworkers.<sup>45</sup> According to the “ice-like” and “liquid-like” origin of the two peaks, upon isotopic dilution (*i.e.*, diluting D<sub>2</sub>O with H<sub>2</sub>O) the peaks would still be present but decrease in intensity.<sup>45</sup> However, instead of observing two OD peaks (2400 and 2515 cm<sup>-1</sup>) with lower intensity for the D<sub>2</sub>O/H<sub>2</sub>O mixture, only one broad peak was observed centered around 2510 cm<sup>-1</sup>. Because there was only the double-peaked OD SFG spectrum in the pure D<sub>2</sub>O solution, but not in the HDO (mixture) spectrum, the authors concluded that the symmetric mode of water was split by an anharmonic intramolecular interaction.<sup>45</sup> Specifically, they theorized that the double peak feature present for both the silica/water and silica/D<sub>2</sub>O interfaces was the result of a Fermi resonance between the symmetric stretch of water and the overtone of the water bending mode. To expand on Bonn’s work at the air/water interface, Tahara and coworkers performed phase sensitive SFG with isotopic dilution at the silica/water interface.<sup>14</sup> They also found that upon isotopic dilution the 3200 and 3400 cm<sup>-1</sup> peaks merged into one peak centered around 3400 cm<sup>-1</sup> in the regular SFG spectra ( $[\chi^{(2)}]^2$ ). However, the phase sensitive measurements showed the presence of at least two distinct peaks with opposite orientation.<sup>14</sup> In the phase sensitive measurements at pH 12 the HOD molecules only have a positive  $\text{Im}(\chi^{(2)})$  centered around 3400 cm<sup>-1</sup> with a broad shoulder at the lower wavenumbers (3000-3200 cm<sup>-1</sup>). As the surface is protonated, thereby decreasing the static electric field, the 3400 cm<sup>-1</sup> peak still had a positive  $\text{Im}(\chi^{(2)})$ , which indicated that weakly hydrogen-bonded water molecules were still present with their hydrogens pointed towards the surface. The shoulder peak (3000-3200 cm<sup>-1</sup>), however, changed from a positive  $\text{Im}(\chi^{(2)})$  to a negative  $\text{Im}(\chi^{(2)})$ , which is consistent with strongly hydrogen-bonded water molecules transitioning from having their hydrogens pointed towards the surface to having their hydrogens pointed away from the surface. Furthermore, Tahara and

coworkers results suggested that there were potentially 2 or 3 different OH-oscillating modes at the interface, based on the presence of modes at 3000, 3200 and 3400 cm<sup>-1</sup>,<sup>44</sup> which is similar to Shen and coworkers' earlier work with phase-sensitive measurements. We note the presence of these distinct modes in the isotopic dilution experiments calls into question the interpretation of the 3200 and 3400 cm<sup>-1</sup> modes in the pure water spectra as Fermi resonances as opposed to modes originating from different water populations. As for why only one mode was apparent in the intensity SFG spectrum from HOD while two modes were present in the intensity spectrum of H<sub>2</sub>O remains unclear.

In addition to 3000, 3200 and 3400 cm<sup>-1</sup> peaks, a peak present around 3600 cm<sup>-1</sup> has also been observed (Figure 1.10B).<sup>43, 46-49</sup> This peak was sensitive to the angle of incidence of both the incoming IR and the visible laser beams.<sup>48</sup> The angular dependence of the SFG response was due to the changes in the Fresnel factors, which are dependent on the refractive indices of the materials.<sup>48</sup> Because this peak appears to be sensitive to alignment of the laser system, the presence of this peak has not been observed in all experimental set-ups. Although the molecular origin of this peak remains unclear, it is a solvent exposed OH vibrational mode because it can be exchanged with D<sub>2</sub>O.<sup>43</sup> Moreover, the high frequency of this peak is characteristic of a freely vibrating OH bond, or a weakly hydrogen bonded OH bond.<sup>4, 42-43</sup> The documented existence of the 3600 cm<sup>-1</sup> peak is important to note for Section 5.3.3 where experiments performed on Dr. Tyrode's laser assembly also revealed its presence.

To conclude, at the silica/water interface there are many different OH modes of water present. As will be discussed next, the behavior of the water molecules at the interface, manifested in these different OH vibrational modes, are greatly affected by both the surface structure and composition of the aqueous phase.

## **1.9 Perturbing the Silica/Water Interface with Ionic Strength, Ion Identity, and Flow Rates**

One of the easiest ways to perturb the interface is to add aqueous ions to the system and vary the ionic strength. In 1992, Eisenthal and coworkers showed that as ions are added to the system at a particular pH, the intensity of the non-resonant SHG decreases.<sup>26</sup> This result was contrary to previously known work done on silica colloids that showed as ions were added to the system, it increased the deprotonation of silanol sites to siloxides, thus would cause an increase in the static electric field.<sup>50-52</sup> Eisenthal and coworkers concluded that the effect of electrolyte concentration on the SHG signal intensity was a result of the formation of the electric double layer. As the electrolyte concentration was increased, it caused a steep decay of the static electric field with distance from the interface because the ions were screening the interfacial charge. This resulted in fewer water molecules being oriented by the electric field and therefore less signal observed experimentally.

The intensity of the SFG signal also decreases in response to varying the ionic strength in a similar manner to the SHG signal. Adding electrolytes to the silica/water interface had a dramatic effect on the shape and intensity of the SFG spectra.<sup>47, 49-50, 53</sup> Although both the 3200 and 3400 cm<sup>-1</sup> peaks decreased in the presence of electrolyte, the 3200 cm<sup>-1</sup> peak decreased more as the salt concentration of the solution increased.<sup>47</sup> As the static electric field was screened by the ions, the depth of penetration of the electric field decreased, resulting in less water molecules aligned by the electric field. Therefore, the water molecules that were furthest from the surface contributed less to the overall SFG intensity. This suggested that the 3200 cm<sup>-1</sup> peak represented water molecules that were further from the surface.<sup>47</sup> In addition, when orientational analysis was performed by Hore and coworkers on the water spectra as the salt concentration was varied,

it was concluded that the  $3400\text{ cm}^{-1}$  peak corresponded to water molecules that were closest to the surface.<sup>47</sup> By studying a wide range of ionic strengths, Hore and coworkers were also able to comment on how the different contributions of  $\chi^{(2)}$  and  $\chi^{(3)}$  were changing as a result of the increasing ionic strength using sodium chloride as the electrolyte.<sup>50</sup> What Hore and coworkers observed was that there were four distinct regions observed in the behavior of the water molecules in response to the addition of salt. Intensity SFG spectra that were obtained in the presence of very dilute salt solutions (0 - 0.7 mM) had a flat region that was attributed to a convolution of increased static electric field from the deprotonation of surface sites by the addition of ions, and the decreasing SFG intensity from the screening of the interfacial potential.<sup>51-52</sup> This was followed by a region (0.7 mM – 0.1 M) where screening of the electric field dominated the spectral response and thus the overall SFG decreased. This decrease was thought to be from changes in the  $\chi^{(3)}$  contribution. Following this was a region (0.1 M – 1.1 M) where the SFG signal intensity plateaued. In this region (0.1 M – 1.1 M) it was theorized that the contributions to the  $\chi^{(2)}$  and  $\chi^{(3)}$  were both constant, which causes the SFG signal to plateau. The last region (1.7 - 4.1 M) showed significant disruption of the ordering of the water molecules. In the last region it was theorized that the contributions to both the  $\chi^{(2)}$  and  $\chi^{(3)}$  would decrease because the high concentration of ions disrupted the hydrogen bonding of the water molecules close to the surface. Although knowing how the contributions of both the  $\chi^{(2)}$  and  $\chi^{(3)}$  are changing in response to variations in the ionic strength is important for understanding the properties that govern SFG, it is unclear in the paper how the authors detangled the different contributions from the SFG spectra alone. In addition, knowledge of how the formation of the Stern layer affects the contribution of the  $\chi^{(2)}$  and  $\chi^{(3)}$  also needs to be further explored. Changing the ionic strength of the aqueous solution will have a significant impact on the behavior of the

silica/water interface. As described in section 1.7, an electrical double layer of positively charged cations will form at a negatively charged silica surface. However, at concentrations of ions below 0.1 M, the distribution is typically modeled as a diffuse double layer. Higher concentrations of ions (greater than 0.1 M) are modeled with ions in a compact layer, called the Stern layer, in addition to an adjacent diffuse layer. Thus the models would predict that different concentrations of ions should behave differently at the silica/water interface. However, besides the salt concentration there are many factors like the hydrophilic/hydrophobic nature of the interface that also influences the structure of the Stern layer.

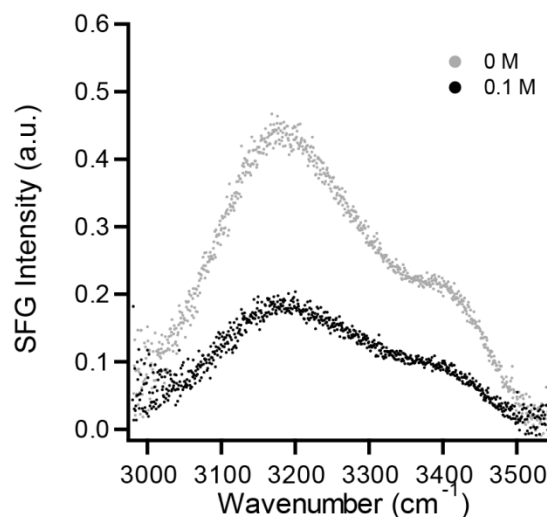


**Figure 1.12** SFG intensity of water (0 M) (Grey) versus 0.1 M NaCl (black) in *ssp* polarization. The spectra were normalized to a gold reference.

The nature of the interface also plays a role in the behavior of water molecules. Covert et al. showed how a variety of aqueous interfaces (fused silica, calcium fluoride, polystyrene, and poly(methyl methacrylate)) behaved when the concentration of electrolyte was varied.<sup>54</sup> They analyzed the data in two different ways. First the data was normalized to the overall highest intensity in the spectrum. This showed the relative change in the signal intensity in response to the change in ionic strength. Secondly, the data was analyzed by normalizing the spectra to the

highest intensity at each ionic strength. This showed how the shape of the SFG intensity changed with ionic strength. For example, water exhibits a strong peak at  $3200\text{ cm}^{-1}$ , when the spectra are normalized to the highest intensity at each salt concentration, it shows that the  $3200\text{ cm}^{-1}$  is the dominant peak in the spectra. This could mean that there are more water molecules further from the surface compared to water molecules close to the surface. When the same spectra are normalized to the highest intensity spectra, pure water in the case of silica, then it shows that the increase of ions to solution, causes less water molecules to be aligned overall. The different behavior of the various surfaces revealed that the response of the water orientation to the electrolyte in solution depended highly on many different factors like surface charge, ion adsorption and hydrophobicity of the surface. The nature of the surface is an important characteristic to study because interfaces can exhibit multiple behaviors. For example, silica is known as a hydrophilic surface because of the silanol functional groups, but there have been reports of silica exhibiting hydrophobic character as well. Allen and coworkers showed that less water vapor is adsorbed to the silica surface compared to the  $\text{Al}_2\text{O}_3$  surface, which suggests that the silica surface is more hydrophobic than the  $\text{Al}_2\text{O}_3$  surface.<sup>55</sup> In addition, Allen and coworkers also showed that ethylene glycol vapor adsorbed to the silica surface.<sup>55</sup> This led to the conclusion that silica has some hydrophobic character that allows organic molecules to adsorb to the surface. The hydrophobic character of the silica/water vapor interface has been theorized to be due to the presence of siloxane bridges on the silica surface.<sup>56</sup> The number of siloxane bridges present on the silica surface will modulate the extent of hydrophobicity of the silica surface. Although the nature of the interface is an important characteristic, the composition of the aqueous phase also modulates the behavior of the silica/water interface.

As various ions are one of the major components of water in the natural environment, determining the influence of ion identity is important to understanding the silica/water interface. In particular, ions can differ in their charge, size, amount of hydration, and valency. All of these factors are expected to impact how the ions will behave at the silica/water interface. In colloidal silica experiments, ion identity can also modulate the surface charge density of silica. For example for the alkali chloride group,  $\text{Cs}^+$  promotes more negative surface charge density than  $\text{Na}^+$  and  $\text{Li}^+$ .<sup>52, 57-61</sup> Some divalent ions like  $\text{Ca}^{2+}$  and  $\text{Mg}^{2+}$  are able to increase the surface charge of silica more effectively than monovalent ions like  $\text{Na}^+$ ,  $\text{K}^+$ ,  $\text{Cs}^+$ .<sup>52, 57</sup> Other colloidal silica studies have focused on how different ions can increase the dissolution rate of solid silica.<sup>51, 62-63</sup> One challenge in monitoring the influence of ions and pH on colloidal silica is that the silica colloids coagulate at high ionic strength and extreme pH values.<sup>51-52, 62-63</sup> One reason for this instability can be attributed a phenomena called charge reversal, which can occur at high salt concentration.<sup>64-67</sup> In the case of silica, the negative surface attracts more positively charged cation than is necessary to neutralize the surface charge. This means that there is an excess of charge at the outer Helmholtz plane and the effective surface charge appears to be positive. The phenomenon of charge inversion is more commonly observed when higher valent ions are present (+3 or +4 valency) at the silica surface,<sup>64, 68</sup> however charge reversal has also been observed for divalent ions (+2),<sup>65, 69</sup> and in some cases on monovalent ions (+1).<sup>70-71</sup> In addition, high concentrations of ions can cause the coagulation of the silica colloids due to bridging interactions between colloids and dewatering of the surface by ions. Because of these challenges when using colloidal silica, planar silica is used most commonly in both SHG and SFG to study the effects of ions on the silica/water interface.

SHG can be used to study how ions modulate the interface in different ways. First, SHG can be used to understand how strongly ions adsorb to the silica/water interface. For example, Geiger and coworkers have done numerous non-resonant SHG studies to investigate how different trivalent ions ( $\text{Al}^{3+}$ ,  $\text{La}^{3+}$ ,  $\text{Gd}^{3+}$  and  $\text{Lu}^{3+}$ ) change the binding behavior to silica at pH 4.<sup>72</sup> By observing how the SHG signal intensity changes based on the addition of the electrolyte of interest they can determine the binding constants of the ions to the interface.<sup>72</sup> Geiger and coworker have also studied the binding behavior of the divalent ions ( $\text{Mg}^{2+}$ ,  $\text{Ca}^{2+}$ ,  $\text{Ba}^{2+}$  and  $\text{Sr}^{2+}$ ). These data are consistent with silica colloid data, which showed that the smaller divalent ions ( $\text{Mg}^{2+}$  and  $\text{Ca}^{2+}$ ) are more attracted to the negative silica surface compared to  $\text{Sr}^{2+}$  and  $\text{Ba}^{2+}$ .<sup>52</sup> The Geiger group has also used resonantly enhanced SHG to study how ions like chromate bind to the silica/water as chromate displays a resonance centered around a  $\lambda$  value of 290 nm allowing for resonantly enhanced SHG with incident light wavelength of 580 nm.<sup>73</sup> Real time kinetics of chromate absorption and desorption showed reversible binding that was consistent with the high mobility of Cr(VI) in the environment.<sup>73</sup> In addition, studies were also performed on methyl ester and carboxylic acid functionalized silica, which were used to mimic soil surface active compounds like humic and fulvic acids, and how these functionalized surfaces affected chromate absorption and desorption.<sup>74</sup> The results of these different binding studies were useful in understanding how pollutants adsorb to silica in nature.

The second way SHG can be used to study the silica/water interface is by monitoring how the identity of the ion affects the acid-base chemistry of the interface. Our group used Eisenthal's  $\chi^{(3)}$  method to study how the identity of alkali chloride ions affected the bimodal behavior ( $\text{pK}_a$  4.5 and 8.5) of the silica/water interface. In our work, we proposed a simple model

to describe the affinity of the metal ion for the deprotonated silanol.<sup>75-77</sup> The deprotonation of the silanol firsts leads to the formation of the surface siloxides through:



where the acid dissociation constant ( $K_a$ ) described this process. The surface siloxide then coordinated with a metal ion through surface complexation:



This process is described by a surface complexation constant ( $K_{sc}$ ). The final overall equilibrium expression can be expressed as:



where the effective acid dissociation constant ( $K_a^{eff}$ ), is the product of the  $K_a$  and the  $K_{sc}$ , can be used to calculate the effective  $pK_a$  ( $pK_a^{eff}$ ) of the silanol sites. The identity of the ions changed these effective  $pK_a$  values in the order of  $\text{NaCl} < \text{LiCl} < \text{KCl} < \text{CsCl}$  for both the more acidic ( $pK_a^{eff} 4.5$ ) and less acidic ( $pK_a^{eff} 8.5$ ), with differences in effective  $pK_a$  being more pronounced for the less acidic silianols.<sup>75</sup> Upon lowering the concentration of the aqueous solution to 0.1 M of the alkali chlorides the effective  $pK_a$  of the less acidic site in the presence of less NaCl was observed to be more acidic, whereas the effective  $pK_a$  value became more basic in the presence of lower LiCl, KCl and CsCl concentrations.<sup>77</sup> In contrast, the more acidic  $pK_a^{eff}$  did not shift much upon decreasing the salt concentration.<sup>77</sup> From these results, it was shown that the alkali ions, with the exception of NaCl, stabilized the protonated silanol form as opposed to stabilizing the deprotonated siloxide form for these less acidic sites. This unusual influence was attributed to a combination of interactions between the water, electrolytes and surface sites. This deviated

behavior of NaCl from the other alkali chloride ions was theorized to be due to different hydration of NaCl at the interfacial region compared with KCl, LiCl and CsCl. This hypothesis was supported by molecular dynamics simulations done by Klein, Borguet and coworkers, where NaCl was found to be dehydrated at the negatively charged silica interface, unlike CsCl which remained hydrated at the same interface.<sup>78</sup> Overall, these SHG experiments have shown that the identity of the ion has a profound effect on the acid-base behavior at the silica/water interface.

With ions having different sizes, charges and varying degrees of hydration, they should impact the hydrogen bonding network of water molecules at the silica/water interface differently. To explore the influence of ion size and hydration energy, Chou and coworkers studied how the identity of monovalent alkali chlorides perturbed the water molecules at the buried silica interface from 0 to 0.1 M.<sup>53</sup> The magnitude of the signal decrease at pH 5.7 as the concentration of the electrolyte was increased showed that K<sup>+</sup> most perturbed the water molecules, followed by Li<sup>+</sup>, and then Na<sup>+</sup>.<sup>53</sup> This trend was explained by balancing two different properties; the first was the equilibrium of the complexation of the cation with the surface, and the second component was the hydrated ionic radii of the ions.<sup>53</sup> These results contrasted with another study done by Cremer and coworkers who studied the effect of low concentration monovalent, divalent and polyatomic ions on the silica/water interface at pH 10.<sup>79</sup> They found that the series was Li<sup>+</sup>>Cs<sup>+</sup>>Rb<sup>+</sup>>NH<sub>4</sub><sup>+</sup>>K<sup>+</sup>>Na<sup>+</sup>>Ca<sup>2+</sup>>Mg<sup>2+</sup>>Zn<sup>2+</sup>, where Li<sup>+</sup> attenuated the signal the least and Zn<sup>2+</sup> attenuated the signal the most.<sup>79</sup> In addition, all the divalent ions that were studied decreased the signal intensity more than the monovalent ions, which suggested that the divalent ions had a higher affinity for the silica surface at pH 10. Cremer and coworkers also found that at pH 6.5 any ionic specific differences were close to the limit of experimental error at these low salt concentrations.<sup>79</sup> Although these examples show very different behavior of the SFG in

response to the same cations, they had very different experimental conditions with regards to the pH of the experiment and concentrations of ions that were studied. These factors may explain the differences in the results.

Most studies have focused on the effects of cations at the silica/water interface because silica is negatively charged and cations would be attracted to the surface. However anions can also perturb the silica/water interface. In SHG measurements, Azam *et al.* found the pH-dependent SHG changed drastically upon varying the halide. This was attributed to changes in the surface charge density of silica. However, Brown and co-workers found no evidence of specific anion effects on surface charge density of colloidal silica, which could suggest that the anions directly influenced the SHG rather than indirectly contributing by influencing the amount of oriented water.<sup>80</sup> Cremer and coworkers also studied the effect of anions on the organization of the water molecules at the silica interface at pH 10. They found that the sodium salts SCN<sup>-</sup> and ClO<sup>-</sup>, which are weakly hydrated, led to the least amount of attenuation of the SFG signal, while the signal decreased the most in the presence of Cl<sup>-</sup> and Br<sup>-</sup>. The NO<sub>3</sub><sup>-</sup> anion attenuated the signal an intermediate amount.<sup>81</sup> These results show that even anions can affect the behavior of the silica/water interface. One consideration when setting up an experiment is whether the experiment will be using a flow cell or not. Recently, there has been evidence that shows the flow rate of experimental system can impact the results of the experiment.

Water in the environment is not stationary and thus may also impact the surface properties of interfaces. In SHG studies, Geiger and coworkers showed that the response of the SHG signal was dependent on pH, ion identity, and ionic strength when using a flow cell.<sup>82</sup> They found, using a flow cell, that the SHG signal intensity tracked the bulk pH changes well if low electrolyte concentrations are used upon transitioning the pH from pH 11 to pH 3 and back

again. However, if higher concentrations of electrolytes were used, the SHG signal would be “jammed” for hours.<sup>82</sup> The time delay of the SHG response to changes in pH, increased with increasing electrolyte concentration until 0.1 M where it levels off and was also sensitive to ion identity. Specifically, the more polarizable the anion the greater the time delay, as well as the more hydrated the cation the longer the delay time in the SHG response to pH. However, these long delay times decreased when the flow rate was increased from lamellar to turbulent flow. Moreover, as lamellar flow is likely in certain environments, these results suggested the silica surface will respond more readily to pH changes in freshwater systems, where there are low ionic strengths, compared to the silica surfaces in estuaries and ocean currents.

An interesting study by Bonn and coworkers showed that the SFG intensity is also affected by the flow of water over the surface.<sup>83</sup> They found that on both CaF<sub>2</sub> and SiO<sub>2</sub> surfaces that were immersed in 10 mM NaCl, flow lead to a reversible modification of the surface, and thus a realignment of water.<sup>83</sup> On the silica water interface, if the flow was turned on at pH 6.5, then there was a decrease in signal intensity. The difference in the SFG intensity in the presence and absence of flow illustrated that the molecular arrangement of water molecules was changing at the interface. Upon turning the flow off, the SFG signal required 30 minutes to recover back to the original intensity. Bonn and coworkers suggested that the long recovery time was due to the dissolution of silica into silicic acid at the interface. When the flow was turned on; it introduced fresh water to the system, which lowered the concentration of the silicic acid at the surface. This in turn caused a shift in the equilibrium to the dissolution of the silica surface. The increased dissolution around neutral pH values has been previously confirmed.<sup>49</sup> Interestingly, if the flow rate was turned on at either pH 3 or pH 11 there was next to no change in the SFG signal intensity. The authors theorized that the pH dependence of the flow rate was a result of the

kinetic of the deprotonation versus the kinetics of dissolution. Because the flow greatly affects the SFG signal intensity at pH 6.5, it was concluded that the kinetics of the dissolution overwhelms the kinetics of deprotonation of the silica surface at pH 6.5. Finally, similar experiments were performed on CaF<sub>2</sub> which has a point of zero charge at pH 6.2<sup>41</sup> unlike silica which is negatively charged above pH 2.<sup>84</sup> Due to the differently charged nature of CaF<sub>2</sub> immersed in water, it had very different behavior to flow. When CaF<sub>2</sub> was positively charged (at pH 3), turning the flow on caused the SFG signal to increase. Whereas when the surface of CaF<sub>2</sub> was negatively charged (pH 12) then turning the flow on caused the SFG signal to decrease.<sup>83</sup> These flow dependent studies of the behavior of the water molecules at immersed surfaces will have an impact on modelling and dissolution studies of these environmental interfaces. Although the work completed in this thesis was not under flow, many of the researchers in nonlinear optics do use flow cells. Based on the data above, the flow of the experiments impacts the results widely in both SHG and SFG, thus the effect of the flow rate on previous experiments in the literature needs to be considered.

## 1.10 Thesis Organization

Understanding the behavior of the acid-base chemistry of the silica water interface is important in many industrial and geochemical applications. By utilizing the surface specificity of nonlinear optical techniques like SHG and SFG, we can obtain molecular level insights into how ions and pH changes affect the silica/water interface. In particular there are very few SHG pH titrations that are performed at low salt concentrations. In this scenario the diffuse layer should be contributing most to the electrical double layer. As the pH of the bulk solution is increased, more ions will be attracted to the silica surface, which may influence the shape of the SHG signal intensity. In contrast to SHG, most of the pH variation studies performed with SFG were done at

lower salt concentrations. The higher salt concentrations (0.1 to 0.5 M) would form a compact Stern layer and a diffuse layer in the electrical double layer. The formation of the compact Stern layer is expected to change the behavior of the resultant SFG.

Chapter 2 describes the investigation of starting pH and how it affects the bimodal acid-base behavior of the silica/water interface using non-resonant SHG. It was found the experimental starting pH has a significant impact on the shape of the acid-base titration curves of the silica/water interface. The changes in the behavior are quantified based on the changes of the  $pK_a$  values of the acid-base titrations. The relative populations of the different acidic sites were also determined from the titration curves. The observed changes are then rationalized based on reported simulations of acidic sites at the silica/water interface.

Chapter 3 describes using resonant enhanced SFG to study how the concentration of NaCl and experimental starting pH changes the alignment of water molecules at the silica/water interface. The response of the OH vibrational stretching region was probed in SFG using *ssp* polarization, the most common polarization combination for probing interfacial water. By systematically varying the pH at high concentrations we showed that the resultant *ssp* polarized spectra do not show the same trends as originally published by Shen and coworkers. We believe that the presence of the high concentration of ions is causing the interface to overcharge in the low pH region. The effect of experimental starting pH was also probed in *ssp* polarized SFG, but did not exhibit the hysteresis observed in the SHG measurements in Chapter 2.

SHG and SFG often utilize different polarization combinations to compare results between these techniques. Thus, Chapter 4 describes the use of *pss* polarized SHG and SFG of 0.1M NaCl to perform a direct comparison of the silica/water interface. We found that although

*pss* polarized SFG signal intensity exhibits the same trend that is observed in SHG signal intensity, it cannot fully account for the entire SHG intensity that is observed at the silica/water interface. In this chapter we theorize that the extra SHG intensity includes a contribution of the deprotonated silica surface in addition to the amount of ordered water.

In Chapter 5 the focus of the thesis changes from monovalent ions to the divalent ion calcium because of its history in causing low extraction efficiencies in oil sands water processing. Both non-resonant SHG and resonantly enhanced SFG are used to try to understand how the presence of 0.1 M CaCl<sub>2</sub> changes the silica/water interface. The presence of CaCl<sub>2</sub> causes drastically different behavior compared to NaCl in the intensity of both SHG and SFG. Using both *ssp* and *pss* polarized SFG, we determined how the water molecules are behaving at the interface. In addition, the SFG spectra exhibit a prominent peak that was attributed to CaOH. The CaOH mode appeared at high pH and caused spectral interference in the SFG signal. In the case of the behavior of the SHG intensity, it cannot be explained by the behavior of the water molecules in the presence of calcium, indicating once again that the silica surface is directly contributing to the SHG signal.

In the final chapter of this thesis, the general conclusions from the results of all the research projects are summarized.

## **CHAPTER 2**

### **Bimodal or Trimodal?: The Influence of Starting pH on Site Identity and Distribution at the Low Salt Aqueous/Silica Interface**

Portions of this chapter are reproduced in part with

Permission from the American Chemical Society

Darlington, A. M.; Gibbs-Davis, J. M., Bimodal or Trimodal? The Influence of Starting pH on Site Identity and Distribution at the Low Salt Aqueous/Silica Interface. *J. Phys. Chem. C* **2015**, *119* (29), 16560-16567.

## 2.1 Introduction

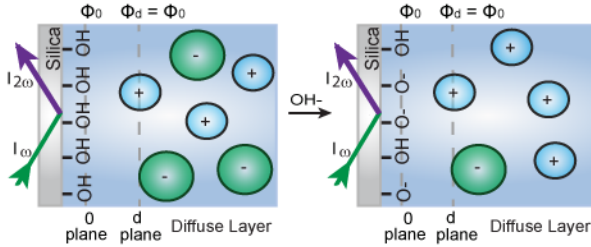
The silica/water interface is one of the most environmentally and technologically relevant interfaces. The charged nature of this interface above pH 2, results in most processes at this interface involving electrostatic interactions.<sup>85</sup> These electrostatic interactions, which largely depend on the acid-base chemistry of silica, are critical to many geochemical, environmental and industrial processes. Consequently, to accurately predict both pollutant adsorption and transport<sup>1, 3</sup> and interactions between analytes and glass substrates in biodiagnostics<sup>86</sup> a complete picture of the silica interface is required. Furthermore, numerous geochemical studies on silicates have found that a layer of amorphous silica forms at the quartz/water<sup>46</sup> and silicate/water<sup>87</sup> interfaces, indicating that the reactivity of amorphous silica is profoundly relevant to a variety of geochemical systems.<sup>46, 87-88</sup>

Despite its importance, measuring the interfacial acid-base chemistry of silica over a wide pH range is challenging. Because silica is an insulator, techniques that measure the surface charge density through the conductivity of the material cannot be used. Potentiometric methods are amenable to silica, and consequently, there have been many studies that have looked at how the acid-base chemistry of silica colloids is perturbed by the addition of aqueous electrolytes.<sup>52, 63</sup> More recently, X-ray photoelectron spectroscopy measurements have yielded the interfacial potential of colloidal silica.<sup>89</sup> However, one of the many difficulties in measuring colloidal silica is that it is unstable over a large pH range.<sup>52</sup> An alternative strategy involves utilizing planar silica and directly determining its acid-base chemistry with surface specific methods. Nonlinear optical techniques like second harmonic generation (SHG) and sum frequency generation (SFG) present unique advantages that include the ability to identify interfacial molecules based on their

spectroscopic signatures, differentiate between molecules ordered at the interface versus those in the bulk solution, and study interfaces for a variety of materials including insulators.<sup>26, 36</sup>

In 1992, Eisenthal and coworkers demonstrated that non-resonant SHG is a surface sensitive and label-free way to monitor the acid-base behavior of the silica/water interface. In this first study the authors revealed that the planar silica/water interface had two distinct types of silanol surface groups ( $\text{SiOH}$ ) with  $\text{pK}_a$  values of 4.5 and 8.5.<sup>26</sup> This bimodal behavior of silica, which is characteristic of a diprotic acid, has been associated with two different solvation<sup>36</sup> or hydrogen-bonding<sup>31, 33</sup> environments of the silanol sites. Using SHG, our group has recently demonstrated that the identity and concentration of both cations and anions in the aqueous phase affects the  $\text{pK}_a$  values as well as the relative distribution of the two acidic sites at the silica/water interface.<sup>75-77</sup> We attributed this salt influence to both the varying affinity of the ions for the siloxide sites ( $\text{SiO}^-$ ), which has been supported by density functional theory (DFT) calculations,<sup>78</sup> and the varying influence of the ions on the hydrogen-bonded structure of interfacial water, which is implicated in the surface acidity.

Although the nonlinear optical method vibrational SFG has shown that small quantities of salt alter the interfacial structure of water at the interface,<sup>47, 49, 53</sup> with the exception of one study performed on colloidal silica<sup>90</sup> non-resonant SHG studies for determining the  $\text{pK}_a$  values of the silica/water interface were done at high salt concentrations (at least 0.1 M).<sup>26, 75-77, 82</sup> Thus there is a gap in knowledge regarding the interfacial acid-base chemistry in the presence of low salt concentrations. Herein we report the SHG acid-base titrations of the silica/water interface with 10 mM  $\text{Na}^+$  (Scheme 2.1). We also explore how the pH history of the silica/water interface influences the distribution of types of acidic sites present at the surface.



**Scheme 2.1** SHG at the silica/aqueous electrolyte interface at low salt concentration.  $\Phi_0$  is the surface potential at the 0 plane,  $\Phi_d$  is the potential at the d-plane.

## 2.2 Experimental

### 2.2.1 Laser System and Assembly

A portion of light ( $\sim 1.1$  W) from our regeneratively amplified Ti:Sapphire laser assembly (Spectra Physics, Spitfire Pro, 3.3 W,  $<120$  fs, 1 kHz rep rate) was used to pump an optical parametric amplifier (Spectra Physics OPA-800CF) to produce laser light of  $550 \pm 2$  nm. The output 550 nm light from the optical parametric amplifier (OPA 800C) was then attenuated to  $0.4 \pm 0.1$   $\mu$ J per pulse by a neutral-density filter (New Focus, cat. # 5215) and directed through a half wave plate and polarizer for *p*-polarized light selection. The polarized light was focused through a fused silica hemisphere (ISP Optics, 1 in. diameter, QU-HS-25, UV-grade  $\text{SiO}_2$ ) onto the silica/water interface at an angle of  $62^\circ$  from surface normal. A custom-built Teflon cell positioned the silica/water interface perpendicular to the laser table with the aqueous phase exposed so that the pH could be routinely changed and monitored from the top opening. The second harmonic light was passed through a colored glass filter (Thorlabs) to remove the reflected fundamental light, and focused through a monochromator set at the second harmonic wavelength of 275 nm (Optometrics Corp., Mini-Chrom MC1-02) and onto a photomultiplier tube (PMT) (Hamamatsu Photonics). The electrical response from the PMT was amplified and counted with a gated photon counter (Stanford Research Systems) (Figure 2.1). Finally, to

determine if the trimodal behavior of the pH 12-2 trace was not specific to our fused silica sample, we also purchased hemispheres from Almaz Optics (UV Grade fused silica hemisphere diameter 25.4 ( $\pm$  0.1) mm). We note multiple samples from ISP Optics were used in the measurements shown in all of the figures to ensure that no behavior was sample specific.

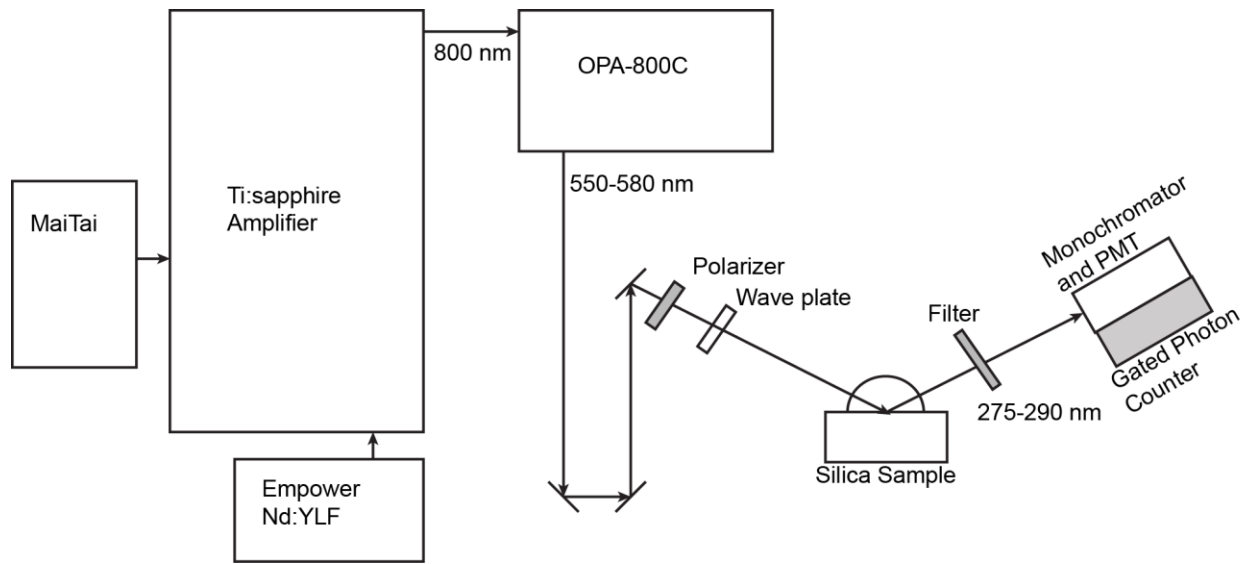


**Figure 2.1** Schematic of the SHG laser assembly. A MaiTai and Empower lasers pump a regeneratively amplified Ti:Sapphire laser system. A portion of Ti:Sapphire laser light pumps an OPA-800C which is tuned to 550-580 nm. The OPA light is focused on the silica sample and the resulting SHG light (275-290 nm) is selected, amplified and counted using a monochromator, photomultiplier tube (PMT) and gated photon counter.

## 2.2.2 Surface Preparation

A freshly cleaned fused silica hemisphere was used for all SHG experiments. The hemisphere was cleaned by sonication in: Milli-Q water (5 min), methanol (5 min), and then Milli-Q water (5 min). Next, the hemisphere surface was covered with Nochromix (Godax Laboratories, 5% w/v in  $H_2SO_4$ ) for one hour. The hemisphere was then rinsed in a copious amount of Milli-Q water, followed by sonication in: Milli-Q water (5 min X 2), in methanol (5 min), and Milli-Q water (5 min). Finally, the hemisphere was placed in a 100 °C oven for 30

minute, cooled to room temperature and plasma cleaned (PDC-32G, Harrick Plasma) in air for 2-3 min right before the experiment.

### **2.2.3 Materials**

Sodium chloride was from Sigma Aldrich ( $\geq 99.0\%$ ). Sodium hydroxide was from EMD Chemicals Inc. (97.0%) and used for all experiments with the exception of the thirty-minute wait time experiments where sodium hydroxide from Sigma Aldrich was used ( $>99.9\%$ ). Sulfuric acid and hydrochloric acid were from Caledon laboratories. All compounds were used without further purification. Ultrapure deionized water ( $18.2 \text{ M}\Omega$ ) was used immediately after deionization from a Milli-Q-Plus ultrapure water purification system (Millipore). The pH of all solutions was measured with an Orion Star A215 pH meter (Thermo Scientific) with an Ag/AgCl electrode (Orion, 9107APMD). All experiments were performed with freshly prepared solutions.

### **2.2.4 SHG Titration Experiments**

Prior to the start of each experiment, the hemisphere was first exposed to Milli-Q water until the SHG signal was optimized, at which point the solution was changed. This water pre-treatment may be important in creating the same initial surface structure, as water exposure has shown to effect the SFG spectrum at the quartz/water interface.<sup>46</sup>

For the titrations from pH 6-12, the Milli-Q water was replaced with 10 mM NaCl and the interface was equilibrated for 30 min. A NaOH solution containing 10 mM NaCl was used to adjust the pH by 0.3-0.5 pH increments until pH  $12.0 \pm 0.1$ . After the addition of each basic aliquot, the solution was mixed by repeatedly removing and dispensing the solution with a glass pipette fit with a rubber bulb. SHG was measured until the signal had leveled off (~ 5 minutes). Then ~100 s of SHG was measured, and once again the pH was determined and recorded. This

process was repeated. For the pH 7-2 titration, a 10 mM NaCl solution that had been pH adjusted to pH  $7.0 \pm 0.1$  was equilibrated with the interface after optimizing the second harmonic signal at the water/silica interface. A solution containing 10 mM NaCl in dilute HCl was used to adjust the pH 0.3-0.5 pH units until pH  $2.0 \pm 0.1$  in a similar manner described above. For experiments from pH 12 to 2, after measuring signal at the silica/water interface, the fresh Milli-Q water was replaced with a solution of pH  $12.0 \pm 0.1$  containing aqueous NaOH, which was then equilibrated for 30 min with the interface. Next a solution of 10 mM NaCl in  $\text{HCl}_{(\text{aq})}$  was added in 0.3-0.5 pH unit increments until pH  $2.0 \pm 0.1$  was reached in the same manner as above. For experiments from pH 2-12, after attaining SH signal the Milli-Q water was removed and replaced with water adjusted to pH  $2.0 \pm 0.1$  with HCl and equilibrated for 30 minutes. This was then followed by the addition of aqueous NaOH containing 10 mM NaCl in 0.3-0.5 pH unit increments up to a pH of  $12.0 \pm 0.1$ .

Regarding analysis of these titration experiments, the  $\text{pK}_a$  was determined in the same manner as was used to find the  $\text{pH}_{0.5}$  (pH where the silanols and siloxides are equal in number) value as described previously by fitting the titration curves with a sigmoid using Igor Pro.<sup>75</sup> The reported values represent the average measured  $\text{pK}_a$  from at least two titrations, whereas the error is the standard deviation of these multiple experiments. The quality of the sigmoid fit to the surface charge density versus surface pH data was excellent (the standard deviation of the  $\text{pK}_a$  fit parameter was less than  $\pm 0.1$ ) for all but the  $\text{pK}_a$ -III curves for the pH 2 to 12 and pH 12 to 2 experiments (data not shown), so we chose to report the average values and the standard deviation determined from comparing  $\text{pK}_a$  values extracted from multiple runs to emphasize the reproducibility of these experiments. Despite the poor quality of the fit yielding  $\text{pK}_a$ -III values for two of the types of experiments, we observed reasonable reproducibility of this  $\text{pK}_a$ -III value.

In contrast, the sigmoidal fits of  $E_{2\omega}$  versus solution pH yielded small standard deviations in  $pH_{0.5}$  (equivalent to  $pK_a$ ) for all of the experiments suggesting that the poorer fits yielding  $pK_a$ -III (resulting in standard deviations in the  $pK_a$  fit parameter of  $\pm 2.0$ ) stemmed primarily from the application of the Gouy-Chapman model at high pH (data not shown).

## 2.3 Results and Discussion

### 2.3.1 Theory of $\chi^{(3)}$ Technique

Second harmonic light is generated when light of frequency  $\omega$  interacts with the interface of two isotropic media, resulting in an induced polarization at the interface that oscillates at twice the incident frequency ( $P_{2\omega}$ ). This break in inversion symmetry that the interface affords is a general requirement of second-order processes within the electric dipole approximation. The square root of the intensity of the SHG response ( $I_{2\omega}$ ) is proportional to  $P_{2\omega}$  according to.<sup>26</sup>

$$\sqrt{I_{2\omega}} = E_{2\omega} \propto P_{2\omega} = \chi^{(2)} E_\omega E_\omega + \chi^{(3)} E_\omega E_\omega \int E_0 dx = \chi^{(2)} E_\omega E_\omega + \chi^{(3)} E_\omega E_\omega \Phi_0$$

**(Equation 2.1)**

In this expression,  $E_\omega$  is the incident electric field,  $E_{2\omega}$  is the electric field at  $2\omega$  generated by the oscillating polarization, and  $\chi^{(2)}$  is the second-order susceptibility, which depends on the composition of the interface. For silica, because it is a negatively charged surface above pH 2, there is also a static electric field ( $E_0$ ) that contributes to the second harmonic electric field through  $\chi^{(3)}$ , the third-order susceptibility.<sup>26</sup> Integrating the static electric field from the surface to the bulk (distance =  $z$ ) yields the interfacial potential ( $\Phi_0$ ), which depends on the surface charge density as well as the concentration and identity of ions in solution.<sup>26, 35, 75, 77</sup> In the  $\chi^{(3)}$  technique we relate changes in the SHG E-field directly to changes in  $\Phi_0$ .

### 2.3.2 Two-Step SHG Titrations Initiated at Neutral pH

As seen in our previous work, the salt identity and the concentration of the alkali chloride in the aqueous phase dramatically affected the acid-base chemistry of the planar silica/water interface.<sup>77</sup> This sensitivity led us to ask, how does the interface behave if the salt is greatly reduced? To answer this question, pH titrations were done in the presence of 10 mM Na<sup>+</sup>, which corresponds to the monovalent cation concentration at pH 12 when alkali hydroxide is used to adjust the pH. As varying the pH changed this cation concentration, we performed the experiment in three ways: first, we mapped out the acid-base chemistry of silica in two stages from pH 7 to 12 and pH 7 to 2 with a background electrolyte concentration of 10 mM NaCl. This two-step method performed on two separate samples was employed in our previous work to limit the effects of hysteresis on our measurements.<sup>75-77</sup> Next, we performed the titration from pH 12 to 2 and finally from pH 2 to 12. These three sets of experiments allowed us to determine the influence of sample history (i.e. starting pH) as well as the salt concentration on the resulting acid-base behavior.

Figure 2.2 shows the behavior of the silica/water interface in the presence of 10 mM NaCl based on the two-step method initiated at neutral pH. As the pH of the bulk solution increased, the magnitude of the normalized  $E_{2\omega}$  increased as a result of deprotonation of surface silanol sites, which resulted in a larger magnitude of  $\Phi_0$  (Figure 2.2A). Consistent with previous work from our group and others, the interface exhibited two acid-base equilibria manifested in two sigmoidal curves.<sup>26, 75, 77, 82</sup> Such bimodal behavior is indicative of two unique silanol sites on silica that have very different intrinsic acidities. However, unlike these previous experiments,

the relative cation concentration changed significantly during the titration experiments. Specifically, the  $\text{Na}^+$  concentration in the titration was effectively constant until pH 10, where it rapidly increased as the pH of the solution was increased with the addition of  $\text{NaOH}_{(\text{aq})}$  (Figure 2.2A). Thereafter, the changes in  $E_{2\omega}$  were attributed to a convolution of increased surface charge density, which should increase the magnitude of  $\Phi_0$ , and increased screening by sodium, which should decrease the magnitude of  $\Phi_0$ .

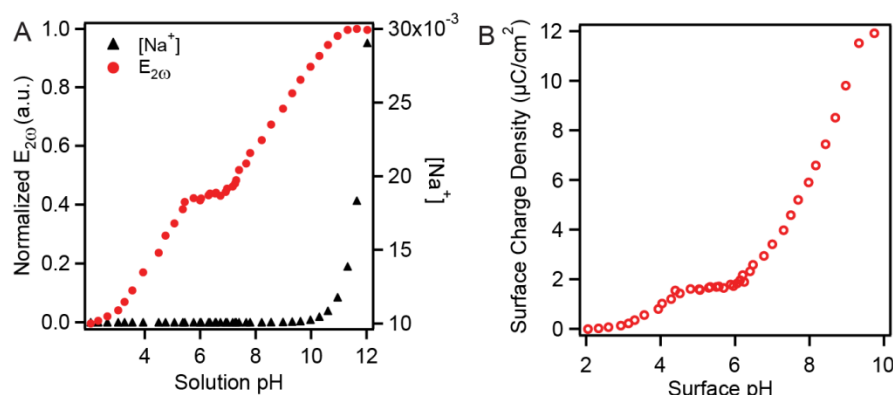


**Figure 2.2** A representative titration composed of two separate experiments: one from pH 6 to pH 12 and the other from pH 7 to pH 2 with a background electrolyte of 10 mM NaCl. A) Normalized  $E_{2\omega}$  (red circles) and concentration of  $\text{Na}^+$  (black triangles) as a function of solution pH for the silica/water interface. B) The corresponding surface charge density (open red circles) as a function of surface pH.

Assuming the interfacial potential varies linearly with  $E_{2\omega}$ , the normalized SHG E-field (depicted in Figure 2.2A) can then be used to determine the interfacial potential ( $\Phi_0$ ) at each pH utilizing a maximum  $\Phi_0$  value of -0.16 V for the silica/water interface at pH 12 based on the maximum surface charge density of silica ( $\sigma_{\max}$ ) of 14  $\mu\text{C}/\text{m}^2$ <sup>26, 91</sup> and the Equation 2.2. According to the Gouy-Chapman model, the interfacial potential is governed by the concentration of cations in a diffuse layer (starting at the d-plane or outer Helmholtz plane) that screen the negative surface sites on silica (present at the 0-plane) as described by the Grahame equation (Scheme 2.1):

$$\Phi_0 = \frac{2kT}{e} \sinh^{-1} \left( \sigma \sqrt{\frac{\pi}{2Ce kT}} \right) \quad (\text{Equation 2.2})$$

Here  $\epsilon$  is the bulk dielectric constant,  $C$  is the bulk electrolyte concentration ( $[Na^+]$ ),  $e$  is the elementary charge,  $k$  is the Boltzmann constant, and  $T$  is the temperature in Kelvin. Similarly, Equation 2.2 can be used to find the surface charge density at each pH once the interfacial potential is determined from the SHG measurements. To quantify how surface charge density changes with pH, we determined the  $-\log$  value of the acid dissociation equilibrium constant ( $pK_a$ ) that describes the relative concentrations of deprotonated siloxides and silanols as a function of surface pH:

$$pK_a = pH_{surface} - \log \frac{[SiO^-]}{[SiOH]} \quad (\text{Equation 2.3})$$

The surface pH can be determined from the bulk hydronium concentration and the interfacial potential, which accounts for enrichment of interfacial  $H_3O^+$  as a result of the presence of negative charges on silica.<sup>26</sup>

The surface charge density as a function of surface pH is shown in Figure 2.2B. The inflection point of these sigmoidal traces corresponds to the pH where half of the surface sites have been deprotonated, which is equivalent to the  $pK_a$  as shown in Equation 2.3. Thus, these  $pK_a$  values were determined to be  $3.8 \pm 0.1$  and  $8.6 \pm 0.1$  for the most acidic and least acidic silanols, respectively, from a sigmoidal fit to the titration curves. These values represent the average of at least two experiments and the error is the standard deviation. The least acidic silanol sites exhibited systematically smaller effective  $pK_a$  ( $pK_a^{eff}$ ) values with increasing NaCl concentration:  $8.6 \pm 0.1$  for 10 mM NaCl,  $7.8 \pm 0.1$  for 0.1 M, and  $7.3 \pm 0.1$  for 0.5 M NaCl.

This trend is consistent with our previous hypothesis that  $\text{Na}^+$  stabilizes the siloxide sites such that more sodium leads to a greater effective  $K_a$  and a correspondingly smaller effective  $pK_a$ .<sup>77</sup>

As mentioned before, the titration curves in Figure 2.2 were generated from two separate titration experiments that started at neutral pH and then were “stitched” together. One problem with this approach is that above pH 10 the concentration of the  $\text{Na}^+$  was changing dramatically with pH owing to the addition of NaOH (Figure 2.2A). This increase in salt concentration strongly influences the relationship between the measured interfacial potential and the corresponding surface charge density according to the Gouy-Chapman model (Equation 2.2). Additionally, hysteresis has been observed in the acid-base properties of this interface by SHG at high salt concentration<sup>82</sup> and by potentiometric titrations of silica colloids.<sup>52</sup> Hysteresis has also been seen in the water structure at the quartz/water interface by SFG<sup>46</sup> and in the electroosmotic mobility of silica capillaries,<sup>92-93</sup> which strongly suggests that the acid-base behavior should depend on the pH history of the sample. To account for the influence of the starting pH and remove the changing  $\text{Na}^+$  concentration, titration curves were started at pH 12, which had a natural background sodium concentration of 10 mM. Thereafter aqueous HCl that contained a background electrolyte of 10 mM NaCl was added to adjust the pH.

### 2.3.3 SHG Titrations from pH 12 to pH 2

In Figure 2.3, when the titration was started at pH 12, the signal decreased as the pH of the solution decreased owing to protonation of the surface siloxide sites resulting in neutral silanols ( $\text{SiO}^- \rightarrow \text{SiOH}$ ). One striking feature of this titration profile is the appearance of a third sigmoidal component. The presence of three sigmoidal curves suggests that three unique silanol sites were present when the interface was exposed to pH 12, in contrast to the two sites present

when the surface was instead exposed to neutral pH (Figure 2.3 vs Figure 2.2, respectively). The difference in the behavior of the silica/water interface when exposed to neutral pH or pH 12 water reveals that the surface structure is not at equilibrium for at least one of the samples. Both the Gouy-Chapman model and the  $pK_a$  parameter presuppose equilibrium behavior, which is clearly not the case. However, for the sake of quantifying our results we utilize these most common approaches to analyze our measurements. Moreover, if we assume that the structure of the electric double layer and the protonation state of the silanols are quickly established in their most stable configuration despite the non-equilibrium surface structure of silica, then these models are still physically meaningful. Yet we recognize the pitfalls in using thermodynamic tools to describe a metastable system and, therefore, caution against considering the  $pK_a$  values reported here as true thermodynamic quantities.

Based on the above rationale we calculate the three “ $pK_a$ ” values of the corresponding silanol groups for the pH titration initiated at pH 12, which were found to be  $3.8 \pm 0.3$ ,  $5.2 \pm 0.5$ , and  $9.6 \pm 0.6$ . The first and third  $pK_a$  values agree with the two-step method started at pH 7,<sup>75</sup> but the middle  $pK_a$  has not been observed in this type of SHG experiment on planar silica. However, we note with interest that this middle value is within error of DFT-MD calculations done by Sprik and co-workers for the planar  $\alpha$ -quartz/water interface that resulted in  $pK_a$  values of 5.6 and 8.5 for the two sites on  $\alpha$ -quartz (*vide infra*).<sup>31</sup>

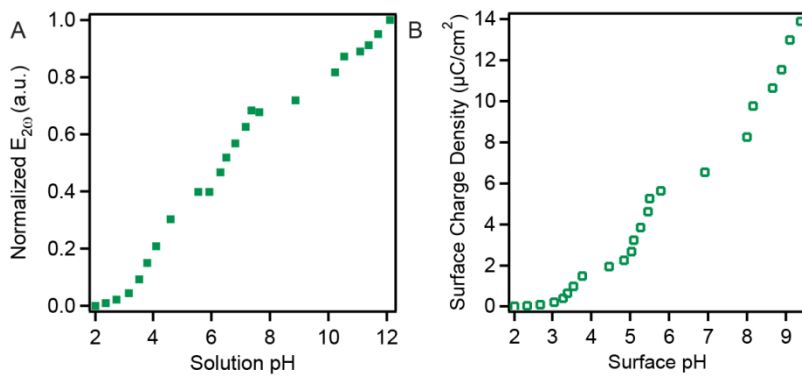


**Figure 2.3** A representative titration starting from pH 12 for the silica/water interface. A) Normalized  $E_{2\omega}$  as a function of solution pH (solid green squares). B) Surface charge density as a function of surface pH (open green squares).

The data was also analyzed using the Gouy-Chapman-Stern model which takes into account the linear drop in potential from the siloxide sites to the first layer of cations that mark the beginning of the diffuse layer (Scheme 2.1, resulting in  $|\Phi_0| > |\Phi_d|$ ).<sup>94</sup> If we assume that the  $\text{pH}_{\text{surface}}$  depends on the potential at the Stern layer ( $\Phi_d$ ) rather than at the plane of the siloxides ( $\Phi_0$ ) (Figure 2.4), then these results provide a similar picture of the acid-base chemistry of the silica interface but with somewhat different  $\text{pK}_a$  values of the surface. Although this assumption is not typically used,<sup>95</sup> the alternative results in  $\text{pH}_{\text{surface}}$  values that can differ from the bulk pH by more than 5 pH units. Thus, we chose to employ the Gouy-Chapman model, which yields more reasonable surface pH and  $\text{pK}_a$  values than that of the basic Stern model based on Figure 2.4B.

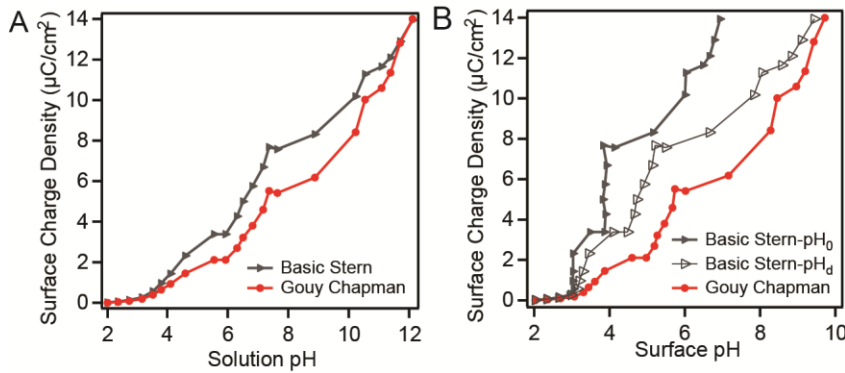


**Figure 2.4** A) Representative titrations of surface charge density calculated via the Gouy-Chapman equation (closed red circles) or the Basic Stern model (closed grey triangles) versus solution pH. B) Calculated surface charge density versus surface pH using the Basic Stern model (grey triangles) or the Gouy-Chapman model (red circles). For the Basic Stern model the surface pH was determined from the potential at the 0-plane ( $\text{pH}_0$ , closed grey triangles) and the d-plane ( $\text{pH}_d$ , open grey triangles).

We also performed another series of titrations initiated at pH 12 but unlike the experiments in Figure 2.3A where a constant  $\text{Na}^+$  concentration was kept, here the salt concentration changed throughout the experiment due to the addition of aqueous HCl without background electrolyte (Figure 2.5A). These data also clearly exhibited trimodal behavior, but these curves were not used for any of the calculations owing to the change in  $\text{Na}^+$  throughout the experiment. We also observed trimodal behavior for titrations initiated at pH 12 on samples from Almaz Optics, indicating this influence of pH history was general for fused silica as it was observed on multiple samples from multiple suppliers (Figure 2.5B).

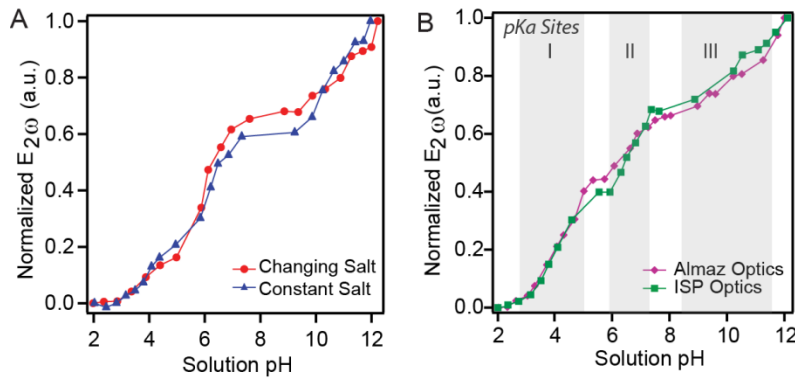


**Figure 2.5** A) Representative titrations from pH 12 to 2 with varying Na<sup>+</sup> concentration as there was no background NaCl in the aqueous HCl used to decrease the pH (red circles) with comparison of pH 12 to 2 with a constant salt concentration (blue triangles). Based on the change in volume upon decreasing the pH, the Na<sup>+</sup> concentration decreased by approximately 20%. B) Comparison between representative titrations performed on fused silica hemispheres from ISP Optics (green squares) (our standard supplier) and Almaz Optics (purple diamonds).

Finally, the duration of a pH 12 to 2 experiment was on the order of six hours including the initial 30 minute wait time at pH 12, but the time required for each data point ranged from 8-12 minutes depending on how long it took to change the pH to the desired solution value. To ensure that these time intervals captured the steady state behavior, we performed the titration experiments from pH 5.4 to pH 7 to pH 12 to pH 7 to pH 2 with 30 minute wait times rather than the ~5 minute wait times used in the above experiments (the wait time corresponded to the period after the pH was changed and before acquiring the intensity measurement for ~2 minutes). We observed little change (<5%) in the average signal with longer wait times indicating the surface reached its steady-state structure within the few minutes it took to change the pH to a stable solution value (Figure 2.6). This led us to conclude that the 5 min wait times was sufficient.

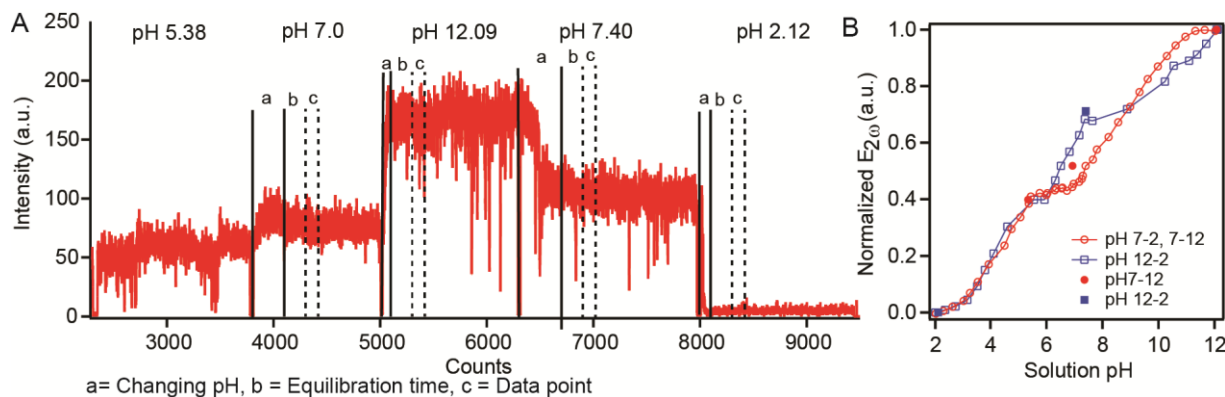


**Figure 2.6** A) Titration from pH 5.38 to pH 7.0 to 12.09, then 12.09 to 7.40 to 2.12 with 30 minute wait time at each pH point. The interval (a) between the bold lines represents where the pH was being changed and manually mixed. The interval (b) between the bold line and dotted line represents the typical wait time of 5 minutes used in all of the reported experiments, and the interval (c) between the two dashed lines is where the data would have been collected in the all reported titrations. We note that during the course of the experiment the energy/pulse dropped from 450 nJ to 330 nJ per pulse. Incidents of ~0 intensity in A correspond to where the beam was blocked and the energy of the pulse was measured. B) The data from part (A) collected with 30-minute wait times (solid symbols) is overlaid on the data from 5-minute wait times from Figure 2.3A and Figure 2.2A (open symbols). These data were power normalized and then normalized to the values at pH 2 and pH 12.

### 2.3.4 SHG Titrations from pH 2 to pH 12

In experiments initiated at the other pH extreme, pH 2, the SH E-field exhibited distinctly different behavior. Specifically, a lag in SHG response was observed from a solution pH of 2 until pH 4 was reached, whereupon  $E_{2\omega}$  increased sharply until pH 6 where it once again plateaued. From pH 8 upward the  $E_{2\omega}$  increased until the end pH was reached (pH 12, Figure 2.7A). Unlike the previous experiment initiated at pH 12, the concentration of  $\text{Na}^+$  was changing as the pH of the solution was initially increased, yet the signal change between pH 2 and 3 was negligible (Figure 2.7A). Moreover, a bimodal distribution as seen in the first two-step experiment (Figure 2.2A) was observed, rather than the trimodal behavior observed for the titration initiated at pH 12. However, unlike the two-step experiment that also exhibited two

sites, the position of the first  $pK_a$  was near  $5.2 \pm 0.5$  as compared to the much lower  $pK_a$  of  $3.8 \pm 0.1$  of the two-step experiment (Figure 2.7 vs Figure 2.2). The corresponding  $pK_a$  values for the titration initiated at pH 2 were calculated to be  $5.3 \pm 0.5$  and  $9.6 \pm 0.6$  as determined from the corresponding surface charge density vs surface pH (Figure 2.7B), which are within error of the second  $pK_a$  and third  $pK_a$  that were calculated for the titrations initiated at pH 12.

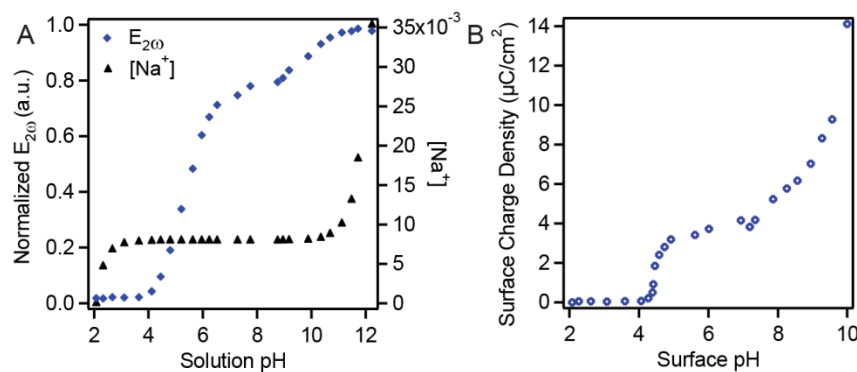


**Figure 2.7** A representative titration of the silica/water interface starting at pH 2. A) Normalized  $E_{2\omega}$  (blue diamonds) and  $Na^+$  concentration (black triangles) as a function of solution pH. B) The surface charge density as a function of surface pH (blue open diamonds).

Titration experiments with longer wait times were also performed from pH 6.4 to pH 3.7 to pH 2.1 to pH 3.7 to pH 12.0 (Figure 2.8). The average of the data after the 30 min equilibration was overlaid on top of Figure 2.2 and Figure 2.7. A close up of the pH 3.7 to pH 2.0 to pH 3.7 is shown in Figure 2.8C this showed the lack of SHG response upon increasing the pH from pH 2 to 3.75 was observable even with a 30 minute wait period.

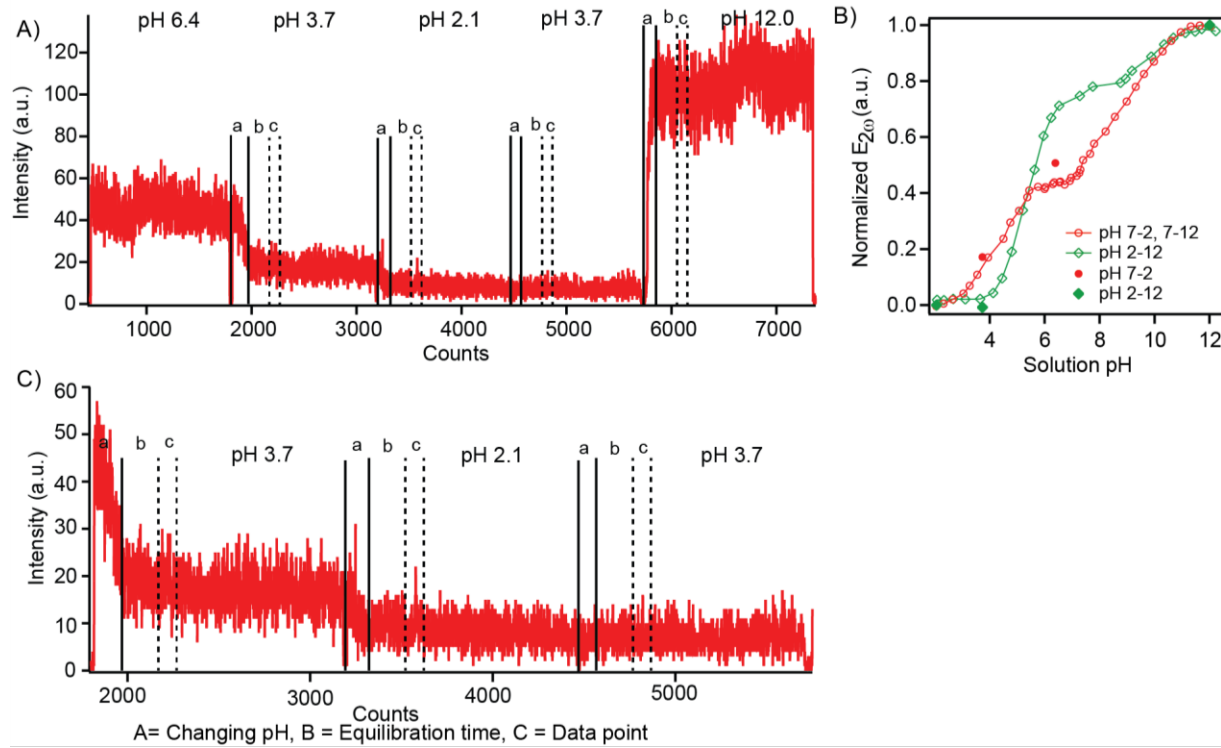


**Figure 2.8** A) Titration from pH 6.4 to pH 3.7 to 2.1, then 2.1 to 3.7 to 12.0 with 30 minute wait times at each pH point. The interval (a) between the two bold lines represents where the pH was being changed and manually mixed. The interval (b) between the bold line and dotted line represents the typical wait time of 5 min used in all of the reported experiments, and the interval (c) between the two dashed lines is where the data would have been collected in the all reported titrations. For the final pH increase to 12, the average signal increased from 101 counts per second (cps) in the (c) interval to 108 cps in the last few minutes after 30 minutes wait time. B) The average  $E_{2\omega}$  values after 30 min wait time (closed symbols, the data from part (A)) are overlaid on the data from the paper (open symbols) and show the extent of hysteresis even with longer wait times. Owing to the stability of the laser, the open-symbol data was not power normalized and just normalized to the values at pH 2 and 12. C) An expanded version of pH 3.73 to pH 2.06, then back to pH 3.73 shows the lack of the response to the change in pH. Incidents of  $\sim 0$  intensity correspond to where the beam was blocked and the energy per pulse measured.

### 2.3.5 pH History and the Origin of the Three Surface Sites

From these experiments, it is clear that hysteresis occurs in the acid-base titrations as seen in the compilation of the normalized  $E_{2\omega}$  graphs in Figure 2.9, consistent with observations at higher salt concentration.<sup>82</sup> Moreover, when we performed the same experiments with 0.1 M

NaCl background electrolyte we observed a very similar trend as observed at  $\sim$ 10 mM Na<sup>+</sup> (Figure 2.9B). These results indicated that the least acidic site with a pK<sub>a</sub> of  $\sim$  9 (pK<sub>a</sub>-III) was common to all of the interfaces regardless of their starting pH. The presence of the other acidic sites, however, depended greatly on the initial conditions. Exposure to pH 7 resulted in only one other site with a pK<sub>a</sub> of 3.8 (pK<sub>a</sub>-I) while exposure to pH 2 resulted in a second site with pK<sub>a</sub> of 5.2 (pK<sub>a</sub>-II). Yet all three sites were observed when the sample experienced an initial pH of 12. The relative distribution of the different acidic silanol sites was calculated from the surface charge density vs solution pH data (Table 2.1).

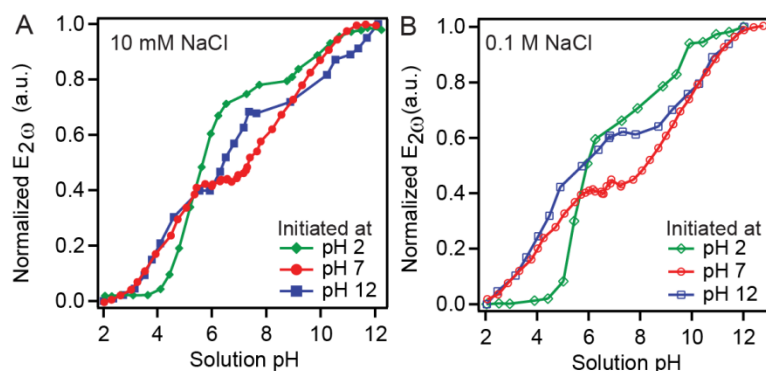


**Figure 2.9** Representative titrations of the silica/water interface with three different initial pH values: pH 2 (green diamonds),  $\sim$  pH 7 (red circle) and pH 12 (blue squares) at (A) 10 mM NaCl (closed symbols) and (B) 0.1 M NaCl (open symbols).

Before discussing the relative distribution of these sites, we note that the maximum number of silanols that *can* be deprotonated on the silica surface is much lower than the actual number of silanols present on the surface. For example, the maximum surface charge density for silica used in our calculations that was measured by Eisenthal and co-workers represents 0.87 siloxides per nm<sup>2</sup> ( $14 \mu\text{C}/\text{cm}^2$ ).<sup>11</sup> Based on a multitude of experimental data, the most accepted density value is 4-5 silanols per nm<sup>2</sup> for non-porous amorphous silica.<sup>85</sup> Therefore, the maximum surface charge density at pH 12 represents the deprotonation of only 19% of silanol

sites based on a silanol density of 4.5. The presence of a high density of silanols even at higher pH is consistent with the observations of Walker and co-workers who observed binding of substituted phenols to an equal number of silanol and siloxides sites at pH 10.5.<sup>96</sup> Moreover, other studies that observed higher surface charge densities on colloidal silica than the value utilized here still result in only a fraction of sites being deprotonated at high pH based on a silanol density of 4.5/nm<sup>2</sup>.<sup>97</sup>

Of the deprotonatable sites, we find that pH history of the sample strongly influences their identity and relative distribution. Specifically, the pK<sub>a</sub>-I silanols represented 17% of these sites while 83% were the pK<sub>a</sub>-III silanols for the two-step titrations initiated at pH 7 (Table 2.1). For the titration initiated at pH 12, the distribution was calculated as 19 ± 5% for the pK<sub>a</sub>-I silanols, 26 ± 7% for the pK<sub>a</sub>-II silanols, and 55 ± 7% for the pK<sub>a</sub>-III silanols. Lastly, the distribution of silanol sites for the titrations initiated at pH 2 was 26 ± 2% and 74 ± 2% of the pK<sub>a</sub>-II and pK<sub>a</sub>-III silanols, respectively. We were surprised to observe that the relative populations of the silanol sites corresponding to pK<sub>a</sub>-I (17 and 19%) and pK<sub>a</sub>-II (26 %) (Table 2.1) were within error for the two systems that exhibited each site. In contrast the relative population of the pK<sub>a</sub>-III silanol sites varied drastically depending on the starting pH. However, we hesitate to draw too many conclusions from the distribution percentages of each site as the changing salt concentration in two of the experiments makes analysis at high pH problematic. Specifically, for the titrations initiated at pH 2, the Gouy-Chapman model predicts that the surface charge density increased drastically as the solution was raised to the final pH of 12 (corresponding to a surface pH of 10) from pH 11.7 owing to the increase in Na<sup>+</sup>. The SH E-field, however, had leveled off, which suggests that the surface by pH 11.7 had already reached its maximum amount of deprotonated sites that it could sustain (Figure 2.9). The Gouy-

Chapman model can over predict the influence of higher salt concentrations when the surface is highly charged, which high pH affords.<sup>98</sup> Additionally, we find that the fit to  $\sigma$  vs surface pH data at high pH, required to determine pK<sub>a</sub>-III, is generally much poorer than the fit of the corresponding E<sub>2ω</sub> vs solution pH data at the same upper extreme. The difficulty in interpreting the data at high pH impacts our confidence in the highest pK<sub>a</sub> value and the relative distribution of sites, but it does not affect the overall finding of the varying number of distinct sites and their relative pK<sub>a</sub> values.

**Table 2.1** Calculated pK<sub>a</sub> Values and Site Population for Different Starting pH.

Silanol Site	Starting pH		
	pH 2	pH 6-7	pH 12
	pK <sub>a</sub> Values		
Most Acidic (pK <sub>a</sub> -I)	-	3.8 ± 0.1	3.8 ± 0.3
Mid Acidic (pK <sub>a</sub> -II)	5.3 ± 0.5	-	5.2 ± 0.5
Least Acidic (pK <sub>a</sub> -III)	9.6 ± 0.6	8.6 ± 0.1	9.6 ± 0.6
	Relative Population		
Most Acidic (pK <sub>a</sub> -I)	0	17 ± 2%	19 ± 5%
Mid Acidic (pK <sub>a</sub> -II)	26 ± 2%	0	26 ± 8%
Least Acidic (pK <sub>a</sub> -III)	74 ± 2%	83 ± 2%	55 ± 7%

Thus far the bimodal behavior of the silica/water interface has been attributed to different hydrogen bonding environments of the silanols.<sup>26, 35, 47, 49</sup> For example, the pK<sub>a</sub>-I sites have only been observed by Leung et al. in *ab initio* calculations on  $\alpha$ -quartz where the surface was first reconstructed and completely dehydroxylated before adding water to the simulation.<sup>33</sup> From the simulations, silanol sites near hydrophobic cyclic trimers exhibited low pK<sub>a</sub> values of 3.8 and 4.8.<sup>33</sup> The presence of such hydrophobic regions containing siloxane bridges is supported by SFG experiments at the silica/water vapor and silica/ethylene glycol vapor interface.<sup>55-56</sup> In another theoretical study using molecular dynamics – density functional theory, Sulpizi et al. observed two distinct pK<sub>a</sub> values of 5.6 and 8.6, close to what we observed for the pK<sub>a</sub>-II and pK<sub>a</sub>-III sites, respectively.<sup>31</sup> The silanols with a pK<sub>a</sub> of 5.6 were those that had an out-of-plane OH group donating a hydrogen bond to water. In contrast, the silanols with a pK<sub>a</sub> of 8.6 consisted of in-plane OH groups that donated a hydrogen bond to a neighboring site. Accordingly, from these studies we propose a possible origin of the three sites we observed correspond to a hydrophobic site, a site donating a hydrogen bond to water, and a site donating a hydrogen bond to a neighbor (Figure 2.10A). We attribute the variation in pK<sub>a</sub>-III values of 8.6 and 9.6 to the large uncertainty in determining the latter value.

From the hysteresis results, we observe that the hydrophobic sites with greatest acidity (pK<sub>a</sub>-I) are only present when the surface first experiences pH 7 or greater. In contrast, for samples first exposed to pH 2, the surface becomes fully hydroxylated and hydrophilic, not supporting the formation of any hydrophobic sites. Instead, the hydroxylated surface is made up of two sites, one that we propose donates hydrogen to water resulting in a pK<sub>a</sub> of 5.2, and another that donates hydrogen to a neighboring silanol resulting in a pK<sub>a</sub> of ~9. For the sample initiated at neutral pH there are two types of sites present, deprotonated hydrophobic sites with pK<sub>a</sub> of 3.8

and neighboring silanols in a hydrogen-bonded network with an average  $pK_a$  of ~9. Finally, the sample exposed to pH 12 has all three sites: those siloxides that can be protonated to form hydrogen bonds with neighboring sites, siloxides that can be protonated to form hydrogen bonds with water, and siloxides in hydrophobic regions that require low pH to protonate (Figure 2.10A). As pointed out by Leung et al. the presence of a large fraction of these hydrophobic sites is not exhibited in their simulations.<sup>33</sup> The fact that they do not form on samples exposed to pH 2 suggests that the hydrophobic sites are metastable and require specific conditions to be trapped at the interface. We also note that recent *ab initio* experiments of a fully hydroxylated amorphous silica/water interface determined that there were three different types of silanols that donate hydrogen bonds to water molecules.<sup>32</sup> These sites were: isolated silanols, geminal and vicinal disilanols (Figure 2.10B). It is possible that these three sites correspond to the three sites observed, although the authors did not determine their corresponding  $pK_a$  values from their simulations. Finally, previous observations of hysteresis in electroosmotic flow experiments have been explained by the formation of a gel layer at pH 2 that is removed at higher pH.<sup>93</sup> If the  $pK_a$ -II site is due to some gel-like morphology of silica, then our results would indicate that such a surface only forms when the surface is first exposed to one or other pH extreme, as the  $pK_a$ -II sites were not present in the sample first exposed to neutral pH.

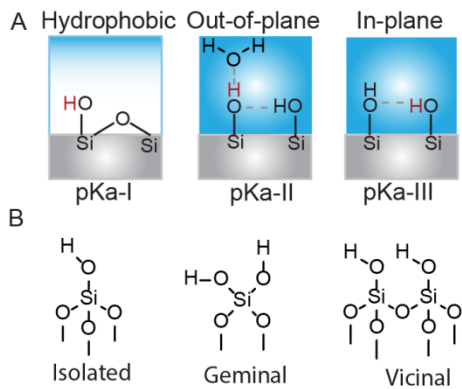


**Figure 2.10** Potential origins of the three surface sites with the three distinctive  $pK_a$  values. A) Three different hydrogen bonding environments of silanols. B) The three silanol sites that interact with water present at the amorphous silica surface according to *ab initio* calculations.<sup>27</sup>

## 2.4 Conclusions

Here we have explored how pH history plays a role in the interfacial acid-base chemistry of the silica/aqueous interface at low salt concentration using SHG. When the titrations are started at pH 7, we observe the bimodal distribution that is prevalent in the literature, with  $pK_a$  values of  $3.8 \pm 0.1$ , and  $8.6 \pm 0.1$ . However, when the titration is initiated at pH 12 we observe evidence of three sites with  $pK_a$  values of  $3.8 \pm 0.3$ ,  $5.2 \pm 0.5$ , and  $9.6 \pm 0.6$ , which has never before been seen for planar fused silica. In contrast, when the titration began at pH 2 we observed a lag in the pH response of the signal until a solution pH of 5, which resulted in two  $pK_a$  values of  $5.3 \pm 0.5$  and  $9.6 \pm 0.6$ . From recent computational investigations at the silica/water interface, we propose that three distinct hydrogen-bonding environments give rise to these  $pK_a$  values. This work indicates that the pH history of the sample influences not only the surface charge density, but the type of surface sites present at the interface, which has implications in accurate modeling of environmental systems. However, whether this hysteresis persists for days is not clear based on this work and must be the subject of future inquiry. Hysteresis in the measurements shows that the value depends on the initial conditions, yet equilibrium constants, like the acid dissociation constant, only depend on the equilibrium

concentrations not prior conditions. As such, the presence of hysteresis calls into question the validity of utilizing acid dissociation constants and equilibrium electric double layer models such as Gouy-Chapman that are routinely used to understand the silica/water interface. The development of new electric double layer models that can incorporate non-equilibrium behavior is needed to more accurately quantify the behavior of this widely used material; the generation of such models, however, lies outside the scope of this thesis.

## **CHAPTER 3**

**Using SFG to Study the Effects of Ion Concentration and pH History at the  
Silica/Water Interface**

### 3.1 Introduction

Among the techniques that can be used to study interfaces, optical techniques are often utilized because they are generally fast, are nondestructive, and can access buried interfaces. Of these optical techniques, sum frequency generation (SFG) is often utilized because of its ability to distinguish between molecules at the surface and the molecules in the bulk.<sup>1, 9-10</sup> In particular, the organization water molecules at mineral interfaces like silica are of great interest because of the ubiquitous nature of this interface. The arrangement of water molecules at an interface will depend on the chemical nature of the interface, the charge of the interface, the hydrophobicity/hydrophilicity of the interface, and the composition of the aqueous phase in the interfacial region. Depending on the location of the interface in the environment, the silica surface can experience a variety of conditions. For example, in fresh water systems, the interface will typically experience lower concentration of ions (millimolar range). Moreover, the divalent ions,  $\text{Ca}^{2+}$  and  $\text{Mg}^{2+}$  tend to be double the concentration of the monovalent ions  $\text{Na}^+$ ,  $\text{K}^+$ , etc. in the fresh water systems.<sup>99</sup> In contrast, if the surface is located in seawater the main ionic components tend to be  $\text{Na}^+$  and  $\text{Cl}^-$  at roughly 0.7 M.<sup>99</sup> The pH in these systems also tends to vary greatly. Around the world lakes can be basic, neutral, or acidic depending on the environmental causes or through anthropogenic causes. The ocean, which has a pH of 8.1,<sup>100</sup> has areas with hydrothermal vents that can also vary widely in pH (2-3 and 9-11).<sup>101</sup>

At the majority of pH's in the environment, silica is negatively charged.<sup>23</sup> The negative charge of the silica can align the dipole moments of water molecules. In 1992, Eisenthal and coworkers theorized that the increase in the SHG signal upon deprotonation of the surface silanols was a result of the increased alignment of water molecules at the interface.<sup>26</sup> SFG in the presence of no salt showed the expected result where SFG signal intensity increased with

increasing pH.<sup>36</sup> However, Eisenthal's original SHG work in 1992 was done in the presence of 0.5 M NaCl. Subsequent SFG studies tend to focus on the effect changing the ionic strength,<sup>47</sup><sup>50, 53-54</sup> or on the difference of ion polarizability<sup>40, 53, 79, 81</sup> as opposed to changes in pH and surface charge.<sup>49</sup> The one study that has looked at surface charge with higher ionic strength NaCl (0.1 M) reported all data with respect to the SFG intensity of water at the same pH. This makes it very hard to discriminate differences in the SFG spectra at high concentrations of NaCl because the addition of salt to the water dramatically decreases the SFG intensity due to the screening of the negative charges by the ions.

In addition, high concentrations of monovalent ions have been shown to affect the silica surfaces. Reversal of the double layer charge has been observed for the monovalent ion Li<sup>+</sup>, Na<sup>+</sup>, K<sup>+</sup>, and Cs<sup>+</sup> in zeta potential measurements.<sup>71, 102</sup> As the concentration of these ions increased, the pH where the charge reversal occurred increased from pH 2, which is typically recorded as the point of zero charge of silica,<sup>84</sup> to closer to pH 4-5 at the higher concentration of ions (up to 0.4 M ions).<sup>71, 102</sup> In addition, overcharging of the double layer was theorized as the reason behind why atomic force microscopy (AFM) measurements between two silica surfaces start repulsive and then turn attractive as the concentration of ions increases. In particular, at pH 5.5 NaCl caused attraction between the two surfaces between 100 and 200 mM, whereas KCl and CsCl cause attraction between the two surfaces at lower ion concentrations.<sup>70</sup> However, not all AFM measurements displayed the charge reversal behavior in the presence of the monovalent ions. Yet in comparing all AFM studies on this aqueous interface, one important observation was studies that reported attractive behavior had samples characterized by relatively lower surface charge densities compared to the samples in studies that did not report charge reversal behavior. This could be attributed to the multitude of silica colloids that were utilized in all the

different experiments. Thus the high concentration of ions that were present in Eisenthal's original work could have an impact on the resulting structure of the electric double layer. As SFG is sensitive to water molecules in different hydrogen bonding environments it is well suited to probe the electrical double layer more directly than SHG.

## 3.2 Experimental

### 3.2.1 Laser Assembly

For the SFG setup, 2/3 of the 800 nm from a regeneratively amplified Spitfire Assembly (Spectra Physics) light is used to pump a TOPAS-C and nDFG laser system (Light Conversion Ltd) to produce tunable IR light. The Tunable IR light is sent through a tunable half wave plate (ALPHALAS GMBH) and polarizer (Thor Labs) to select *p*-polarized light. The IR light is focused on a custom built sample cell that holds a 1 inch diameter IR grade fused silica hemisphere (ISP Optics and Almaz Optics) at an angle of 66°. In addition, a portion of the 800 nm light from the Spitfire is broadened in time from fs to ps via an air spaced etalon (Fabray-Perot) and focused through a polarizer (Thor Labs) and half wave plate to select the desired polarization of light. The 800 nm visible light is aligned spatially and temporally with the IR laser light at the silica/water interface. At the interface light that is the sum of the visible and IR laser light is collimated and directed through a bandpass filter that filters out the 800 nm laser light (Chroma HQ 617/70 M). The SFG light is then focused onto a (Acton SP-2556 Imaging Spectrograph, grating: 1200 G/mm with 500-nm blaze wavelength) connected to a thermoelectrically cooled, back-illuminated, charge coupled device camera (Acton PIXIS 100B CCD digital camera system, 1340 x 100 pixels, 20 mm x 20 mm pixel size, Princeton Instruments). For these experiments SFG was performed with *ssp* polarized light (*s*-polarized SFG, *s*-polarized visible and *p*-polarized IR, respectively).

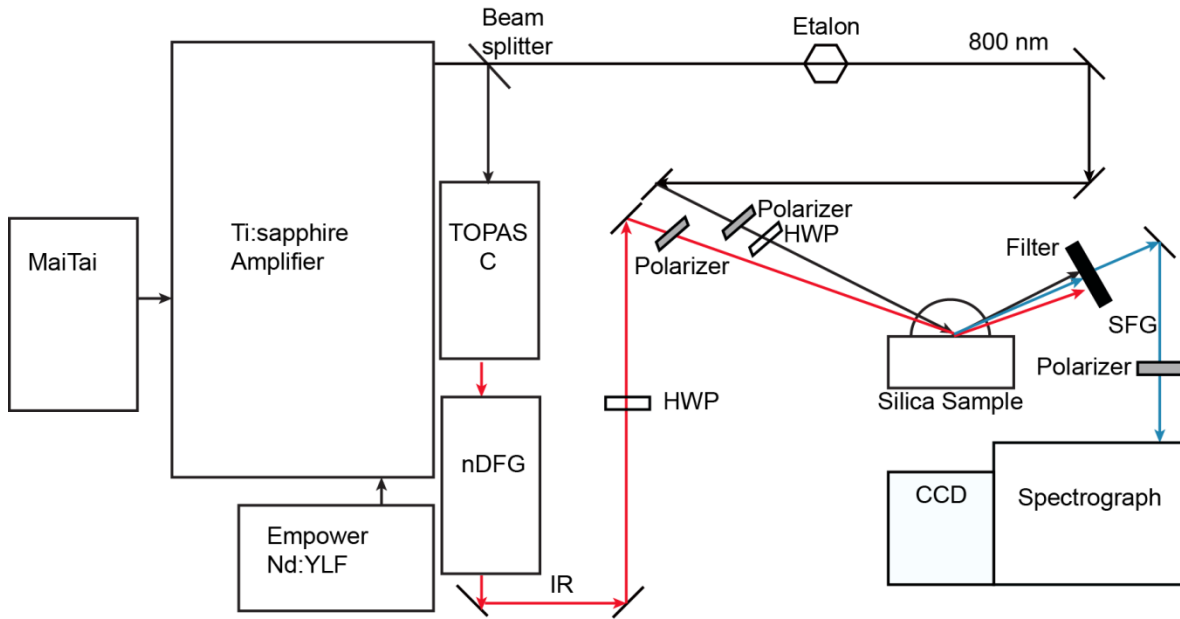


**Figure 3.1** Depiction of SFG laser assembly. IR light from the TOPAS-C and nDFG is focused on to the silica/water interface. Visible light at 800 nm is broadened in time and is overlapped with the IR light spatially and temporally at the interface. The sum of the light (Visible + IR) is filtered and collected on the spectrograph and CCD camera. HWP = half wave plate.

### 3.2.2 Surface Preparation

A 1 inch diameter IR grade hemisphere was sonicated in Milli-Q water for 5 min and rinsed with Milli-Q water. The hemisphere was then sonicated in methanol and rinsed with Milli-Q water. The hemisphere was then sonicated in Milli-Q water and rinsed with Milli-Q water. The hemisphere was then placed in a glass beaker with piranha solution (3:1 ratio of concentrated  $\text{H}_2\text{SO}_4$ :30 % hydrogen peroxide) for 1 h. The hemisphere was then rinsed copiously with Milli-Q water (at least 1 L of water) and sonicated in Milli-Q for 5 min and rinsed with Milli-Q. After this 1 L rinse, the hemisphere was sonicated in Milli-Q for 5 min and rinsed with Milli-Q 3 more times. The sample was then placed in a 100 °C oven for 30 min. Once the hemisphere was cooled to room temperature, it was plasma cleaned (Harrick plasma cleaner) in air for 2 min.

### **3.2.3 Materials**

Sodium chloride with a purity of greater than 99% was from Sigma Aldrich. Sodium hydroxide with purity >99.99% was from Sigma Aldrich. Concentrated hydrochloric acid and sulfuric acid was from Caledon laboratories. All compounds were used without further purification. Ultra-pure deionized water (Milli-Q water) was used immediately after purification from a MilliQ-Plus ultrapure water purification system (Millipore). The pH of all solutions was measured with an Orion 2–Star Benchtop pH meter (Thermo Scientific) with a Ag/AgCl pH electrode. All experiments were performed with freshly prepared solutions.

### **3.2.4 SFG Experiments**

A gold-coated IR grade fused silica hemisphere was mounted to the sample cell. IR and visible light were spatially and temporally aligned at the interface. To fully cover the OH vibrational stretching region 5-6 broadband IR pulses were used. At this point a polystyrene calibration film was placed in the IR beam path and a spectra was collected in the CH stretching region. The polystyrene was used to calculate the offset of the spectrograph from the expected value. The gold coated silica hemisphere was then replaced with a freshly cleaned fused silica hemisphere and exposed to water. The hemisphere was adjusted on the sample cell so that the resulting SFG was aligned through the center on the alignment disk. The alignment disk was removed from the SFG line, and the water spectrum was collected at the same 5-6 IR pulses. The water was then replaced with the salt solution and was equilibrated for 30 min. The pH was adjusted using the NaOH or HCl that was dissolved in the salt solution. The samples were equilibrated for 5 min after the pH change; then the 5-6 IR pulses were collected. The data was analyzed by taking the sum of the water spectra divided by the sum of the gold spectra.<sup>103</sup>

### 3.3 Results and Discussion

#### 3.3.1 Background Theory on SFG

Within the electric dipole approximation, SFG is only generated in non-centrosymmetric media or at an interface. When visible laser light ( $E_{Vis}$ ) and IR laser light ( $E_{IR}$ ) are spatially and temporally aligned at the interface they induce a polarization that oscillates at the sum of the two laser lights ( $P_{Sum}$ ). This oscillating polarization generates an electric field that also oscillates at the sum of the two incident frequencies ( $E_{Sum} = E_{Vis} + E_{IR}$ ). The intensity of the SFG signal ( $I_{SFG}$ ) is given in the below equation.

$$I_{SFG} \propto |E_{Sum}|^2 = |\chi^{(2)} E_{Vis} E_{IR}|^2 \quad (\text{Equation 3.1})$$

where the second-order susceptibility ( $\chi^{(2)}$ ) is specific for the interface. Because the IR light that is used is in resonance with the O-H vibrational mode, any molecules that contain this vibrational mode can be excited. In the case of the silica/water interface, only water molecules that have a net alignment, *i.e.*, are non-centrosymmetric, will be observed by SFG. A change in the intensity of  $I_{SFG}$  stems from a change in the  $\chi^{(2)}$  term.

$$\chi^{(2)} = \sum N_{H_2O} \langle \beta_{H_2O} \rangle \quad (\text{Equation 3.2})$$

where  $N_{H_2O}$  is the number density of water molecules,  $\beta_{H_2O}^{(2)}$  represents the second-order molecular hyperpolarizability of water and the brackets  $\langle \rangle$  represent the orientationally averaged value. Because silica is negatively charged, the static electric field that is set up by the negative siloxides contributes to the  $I_{SFG}$  through a third-order susceptibility ( $\chi^{(3)}$ ). Integrating the static electric field from the surface to the bulk yields the interfacial potential ( $\Phi$ ).

$$|E_{Sum}|^2 = |\chi^{(2)} E_{Vis} E_{IR} + \chi^{(3)} E_{Vis} E_{IR} \Phi|^2 \quad (\text{Equation 3.3})$$

The contribution of  $\chi^{(3)}\Phi$  can be written as:

$$\chi^{(3)}\Phi = N_{H_2O} \left( \frac{\mu_{H_2O}\Phi}{ck_B T} \beta_{H_2O} \right) + N_{H_2O} \gamma_{H_2O} \Phi \quad (\text{Equation 3.4})$$

This equation shows that the water molecules dipole moment ( $\mu_{H_2O}$ ) that are aligned due to the interfacial potential in the presence of thermal energy  $k_B T$ , where  $c$  is a constant, as well as the contributions of the third-order molecular hyperpolarizability ( $\gamma_{H_2O}$ ).

### 3.3.2 Effect of 0.5 M and 0.1 M NaCl

In Eisenthal and coworkers original 1992 paper, it was theorized that the increase of the SHG signal intensity was a result of an increase in the number of water molecule that are aligned at the surface. If this is true, then at 0.5 M NaCl, the same overall trend should be observed for the SFG spectra. Based on this hypothesis, if a two-step titration is performed the SFG signal intensity should decrease from pH 7 to pH 2 and the signal should increase from pH 6 to 12. In Figure 3.2 when the two-step titration was performed the *ssp* polarized SFG intensity in the presence of 0.5 M NaCl deviated significantly from the hypothesis. In the presence of 0.5 M NaCl the SFG signal intensity increases from pH 6 to 2 (Figure 3.2A). When the titration was performed from 6 to 12 the SFG intensity initially decreases until pH 7-8, then the SFG intensity increases from pH 9-12 (Figure 3.2B). In contrast, when the same two step titration was performed in the presence of 0.1 M NaCl from pH 7 to 5 there is a slight decrease in the intensity of the SFG, while from 4 to 2 the SFG signal increases (Figure 3.2C). If the titration is performed from pH 6 to 12 the SFG signal intensity only increases (Figure 3.2D). Because this data was so strikingly different than what was expected, it was externally verified by Dr. Dennis Hore and Tasha Jarisz from the University of Victoria to ensure the data was reproducible on

other laser systems and other silica samples. They found that the same general trends were observed for 0.1 and 0.5 M NaCl at the silica/water interface.

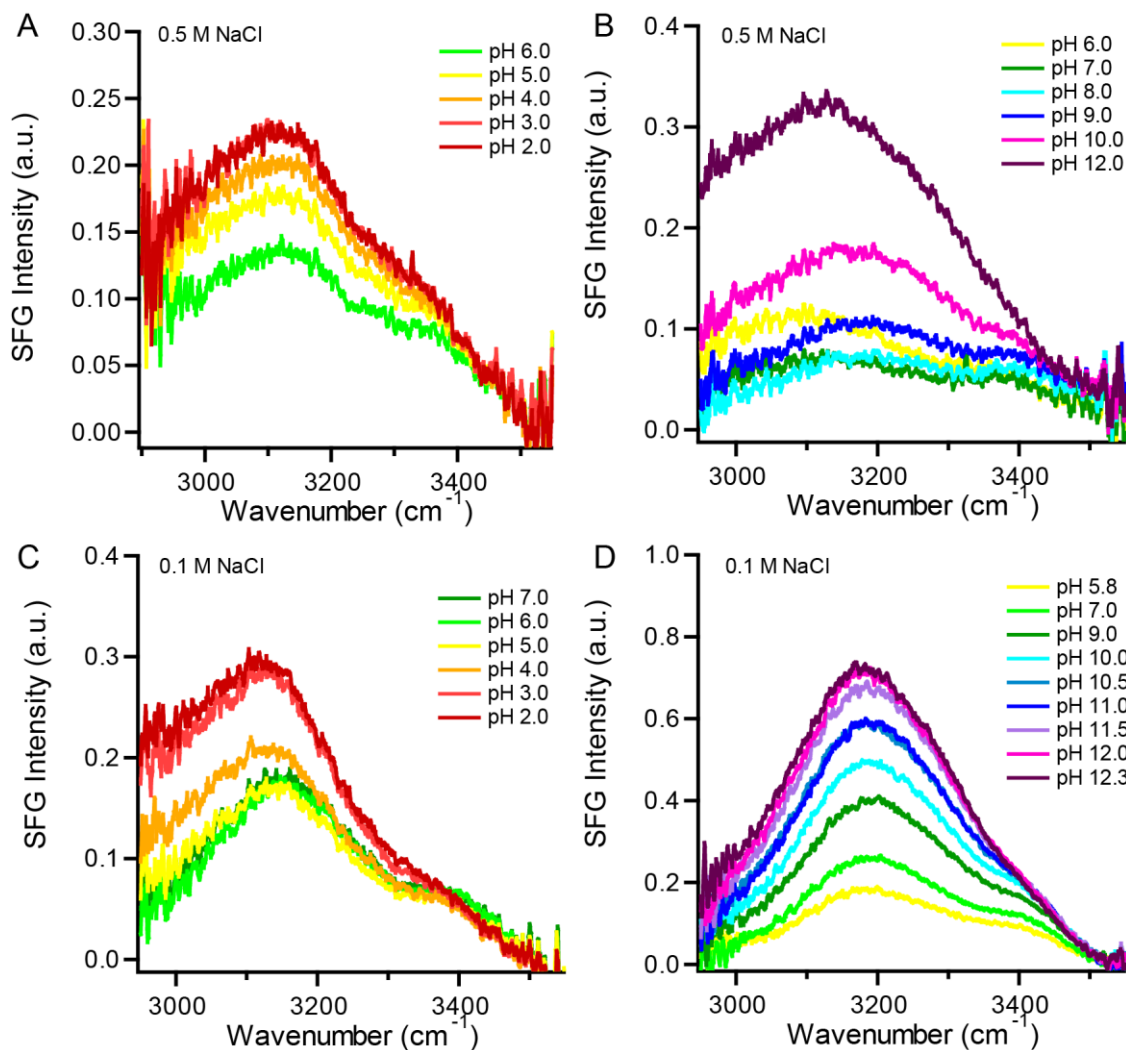


**Figure 3.2** Representative titrations of *ssp* polarized SFG of: A) 0.5 M NaCl pH 6.0 to 2.0; B) 0.5 M NaCl pH 6.0 to 12.0; C) 0.1 M NaCl pH 7.0 to 2.0; and D) 0.1 M NaCl pH 5.8 to 12.0.

To compare the experiments at different salt concentrations, the integrated area of each spectrum was calculated between 2950 to 3500  $\text{cm}^{-1}$ . In Figure 3.3 the data from the integrated area clearly shows a minimum as a function of pH for each salt concentration. For 0.5 M NaCl the minimum in the SFG intensity is between pH 7 and 8, while the minimum in SFG of 0.1 M NaCl is between pH 5 and 6.

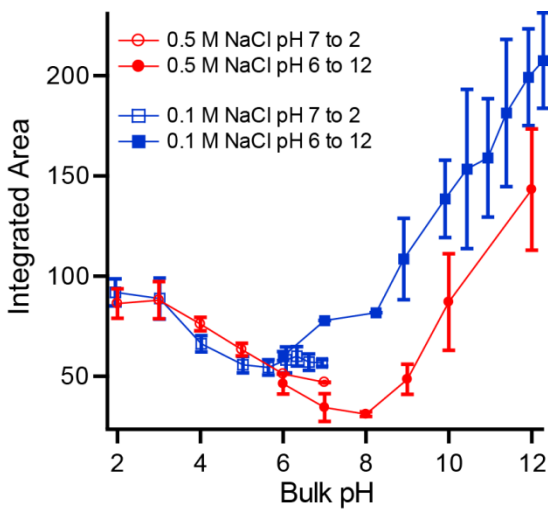


**Figure 3.3** Integrated area of 0.5 M NaCl (red) and 0.1 M NaCl (blue) representative titrations between 2950-3500  $\text{cm}^{-1}$ .

The original hypothesis that the increased signal intensity in the 0.5 M SHG is due to the increased alignment of water molecules does not match the *ssp* polarized SFG spectra. Interestingly, this non-monotonic trend has been previously reported in the literature; the SFG spectrum at pH 1.5 was observed to have a higher intensity than the SFG spectrum at pH 3.8 when salt was present.<sup>35, 40</sup> The previous studies attributed the effect to the hydrogen bonding between the oxygen of the water with the hydrogen of surface silanol moieties.<sup>35, 40</sup> The minimum in the integrated area as a function of pH in the *ssp* polarized SFG resembles the SFG behavior of interfaces where the pH is varied through the point of zero charge (PZC).<sup>37-39, 41</sup> The PZC is the pH that corresponds with a surface that has no electrical charge density.<sup>84</sup> Interfaces like  $\text{Al}_2\text{O}_3$ ,<sup>37, 104</sup>  $\text{TiO}_2$ ,<sup>39, 41, 105</sup> and  $\text{CaF}_2$ <sup>41</sup> have a PZC at much higher pH compared to silica, which is thought to have a PZC around pH 2-3.<sup>23, 84</sup> The minimum observed in the SFG intensity as the pH is varied suggests that the surface is undergoing charge reversal, where the water is experiencing a positively charged interface at pH below the minimum in the SFG titration. However, it is unlikely that the PZC of silica would change to pH 5 or pH 8 where we observe the minima for silica interfaces with 0.1 M and 0.5 M NaCl, respectively. Instead it is

possible that there is overcharging in the double layer next to the interface. Overcharging would result in the water molecules in the diffuse part of the electric double layer sensing a positive charge from an excess of ions in the Stern layer even though the surface charge remains negative. In zeta potential experiments at the concentrations that were studied (0.1 – 0.5 M) there was a change of sign in the electrokinetic potential on silica colloids in the presence of monovalent ions.<sup>71, 102</sup> As the concentration increased, the point where the electrokinetic potential changed sign shifted to a higher pH.<sup>71</sup> The authors attributed this shift in the isoelectric point to the ions adsorbing to the surface at concentrations that are higher than needed to neutralize the surface charge.<sup>71</sup> There have also been studies on SFG that show charge reversal. In one example positively charged CaF<sub>2</sub> was able to be overcharged with sodium dodecyl sulfate (SDS) surfactant. The SFG signal intensity was lowest where the surface was thought to be neutralized by higher concentrations of the SDS. Upon increasing the concentration of SDS even further an aggregate at the CaF<sub>2</sub> surface, where the hydrophobic tails of the SDS were in the interior of the aggregate, whereas the negatively charged head groups faced outward towards the surface or the bulk water. As the aggregate formed, the authors observed more SFG in the water region, which they attributed to the negative charge on the head groups of the SDS molecule aligning water molecules.<sup>106</sup> In our case, as the concentration of the solution was increased, the pH where the minimum in the SFG was observed shifted to a higher pH value. This shift indicates that as more ions are present in the solution, the more effective the screening of the negative surface charge.

The charge reversal behavior is depicted in Figure 3.4. At higher pH where more surface sites are deprotonated, the ions are not able to fully screen the negative surface charge (Figure 3.4A). In this case the water molecules in the diffuse layer as well as those next to the surface

would have their hydrogens orientated toward the surface. In the case where the surface has less of a negative surface charge (Figure 3.4B), the ions fully screen and overcharge the interface. At this point the water molecules in the diffuse layer would experience an effectively positive charge and orient with the hydrogens pointing away from the surface.

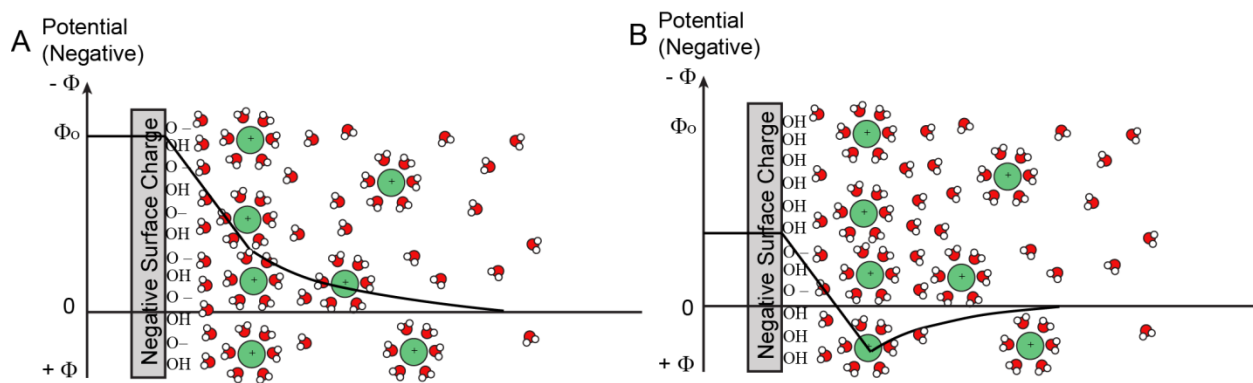


**Figure 3.4** Schematic of A) a more negatively charged surface that behaves as a negative surface B) a less negatively charged surface that is overcharged due to the ions at the interface and behaves as a positive surface.

Another possible interpretation of the changes in the SFG signal is that the  $\text{Na}^+$  ion dehydrates at the interface and becomes specifically adsorbed at the surface. In this case, if part of the hydration layer still surrounds the  $\text{Na}^+$  ions, they could contribute to the  $\chi^{(2)}$  signal, but would be orientated with the hydrogens pointed out towards the bulk (as if the surface were positive). The dehydration of  $\text{NaCl}$  at a charged interface has been investigated in molecular dynamics – density function theory simulations by Dewan *et al.*<sup>78</sup> They found that at 0.35 M concentration,  $\text{Na}^+$  was dehydrated at the interface, and most hydrogens of the water molecules in the electric double layer pointed away from the surface. This was in contrast to  $\text{CsCl}$ , which was hydrated at the silica/water interface and had hydrogens pointed towards the silica surface throughout the electrical double layer.

Experimental support for our hypothesis that the waters associated with the low wavenumber modes are flipping as the pH is increases is found in recent phase-sensitive measurements by Tahara,<sup>14</sup> Shen,<sup>13</sup> and coworkers. Specifically, phase-sensitive measurements can determine the absolute net orientation of the molecules at the interface. In the case of water, a positive  $\text{Im}[\chi^{(2)}]$  corresponds with water molecules that have their hydrogens pointed toward the surface. In contrast, a negative  $\text{Im}[\chi^{(2)}]$  value corresponds with water molecules that have their hydrogens pointed away from the surface.<sup>13-15</sup> Shen and coworkers found that the  $3200 \text{ cm}^{-1}$  region could be decomposed into two different peaks: one at  $3200 \text{ cm}^{-1}$  whose  $\text{Im}[\chi^{(2)}]$  flipped from negative to positive upon increasing the pH. This change in sign suggested these water molecules flipped orientation at around pH 4.5. The other peak had a center frequency around  $3000 \text{ cm}^{-1}$ , and had a negative  $\text{Im}[\chi^{(2)}]$  that remained negative even as the pH was varied. In contrast, the  $3400 \text{ cm}^{-1}$  peak only had a positive  $\text{Im}[\chi^{(2)}]$  value over the studied pH range. More recently, Tahara and coworkers had a very similar finding with the HOD/silica interface.<sup>14</sup> They observed that the HOD/silica water interface had one major peak in the intensity spectrum (the “regular” not phase-sensitive SFG) centered around  $3400 \text{ cm}^{-1}$  with a broad shoulder towards the lower wavenumber range ( $3000\text{-}3200 \text{ cm}^{-1}$ ). Using phase-sensitive measurements they found the  $\text{Im}[\chi^{(2)}]$  corresponding with the peak at  $3000 \text{ cm}^{-1}$  rather than that at  $3200 \text{ cm}^{-1}$  flipped its sign, becoming positive somewhere between pH 7 and 12. (In Tahara and coworkers’ study only three pH values were studied (2.1, 7.2, 12.1) so the actual transition pH was missed.) However, the fact remains, that both the silica/ $\text{H}_2\text{O}$  and silica/HOD show the presence of the  $3000 \text{ cm}^{-1}$  peak with a negative  $\text{Im}[\chi^{(2)}]$  even at fairly high pH values (at least pH 7). This similarity suggests that there is an OH oscillating mode that is orientated such that its hydrogen is pointed away from the surface for both  $\text{H}_2\text{O}$  and HOD. Similar to Shen and coworkers’ findings, the  $3400 \text{ cm}^{-1}$

<sup>1</sup> peak only had a positive  $\text{Im}[\chi^{(2)}]$ , which grew in intensity from pH 2 to 7, but did not grow between pH 7 and 12. In contrast the  $3200 \text{ cm}^{-1}$  peak had little to no contribution at the acidic pH, and appeared at pH 7 and increased in magnitude at pH 12.

The water molecules at  $3400 \text{ cm}^{-1}$  that do not flip orientation in the phase-sensitive SFG could be the water molecules that are closest to the surface and experience the 0-plane potential, which is negative above pH 2. Further support for this hypothesis comes from experimental X-ray photoelectron spectroscopy data that shows the thickness of the stern layer, which includes water, hydrated ions, and dehydrated ions, closely follows the changes in the amplitude of the  $3400 \text{ cm}^{-1}$  peak in SFG very well.<sup>107</sup> Moreover, if a layer of water exists between the 0-plane and the layer of cations, as some electrical double layer models have hypothesized,<sup>27</sup> then these waters would be orientated with the hydrogens pointed toward the silica surface at all pH. In addition, both reports of phase sensitive measurements show that low wavenumber peak changes sign corresponding with a flip in the orientation of the waters. This low wave number mode has been attributed to water further from the surface,<sup>47</sup> which would be consistent with these waters primarily residing in the diffuse layer and experiencing a change in sign of the zeta potential from pH 2 -12.<sup>13-14</sup> However, both these studies (references 13 and 14) were performed with no background electrolyte except what was needed to change the pH of the bulk solution. Thus the phase sensitive measurements of the silica/water interface in the presence of high concentration salts would be interesting to explore.

### 3.3.3 pH History of 0.1 M NaCl

Within the natural environment, pH can vary drastically. The previous thesis chapter showed that the pH history (*i.e.*, starting pH of the experiment) had a significant impact on the

shape of the SHG signal intensity.<sup>108</sup> We wanted to see if there were observable changes in the SFG intensities when the starting pH was different.

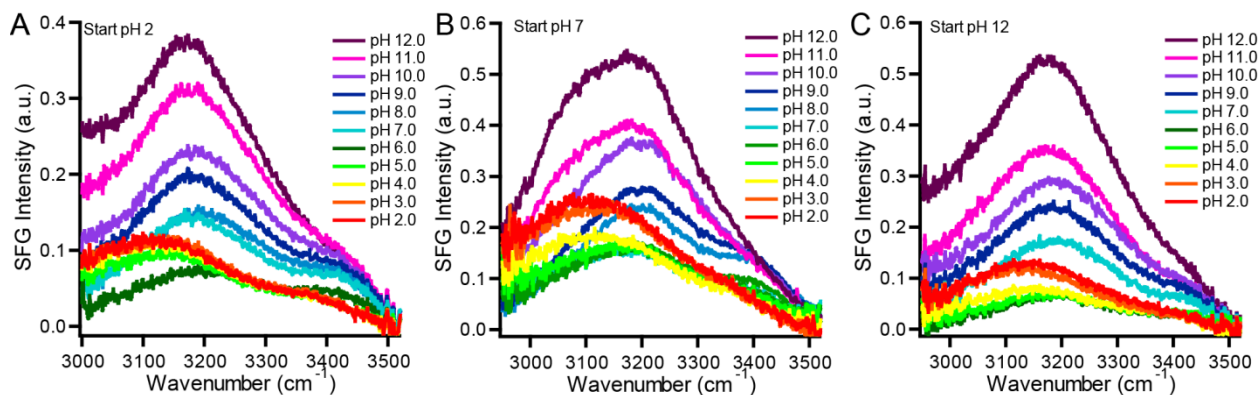


**Figure 3.5** Representative titrations of *ssp* polarized SFG spectra of the silica/NaCl (0.1 M) interface A) from pH 2.0 to 12.0; B) from pH 6.0 to 12.0 and pH 7.0 to 2.0; and C) from pH 12.0 to 2.0.

In all cases when the titrations were initiated from different pH values in the presence of 0.1 M NaCl, the SFG signal intensity decreased from pH 2.0 to pH 5.0-6.0, then increased in intensity from pH 6.0 to 12.0 (Figure 3.5). The integrated area was determined for all of the above spectra and their replicates. Overall, the shape of the data appears very similar when the experiments are initiated at different pH values. There are some slight differences in the spectra between the two step initiated data and those that were initiated at the pH extremes (pH 2 or 12). For example, the integrated area data of the titration initiated at pH 7 is not as low as the data initiated at pH 12 or 2. The *ssp* polarized SFG initiated at different pH values shows very little differences in the SFG spectra. This is in contrast to the SHG, which showed major hysteresis based on the initial starting pH.

In addition, one very interesting feature of the above SFG graphs (Figure 3.5) is that there appears to be a contribution from a mode around  $3050\text{ cm}^{-1}$  that is very apparent at the lower pH values (Figure 3.5). Literature has suggested that this mode is a result of the hydronium ion at

low pH,<sup>109-111</sup> and the hydroxide ion at high pH.<sup>112</sup> Through this work, we have clearly shown that SFG and SHG in the presence of high salt, do not measure the same thing.

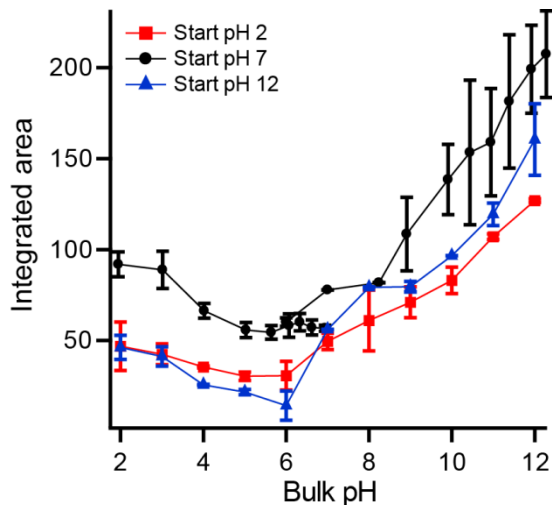


**Figure 3.6** Average integrated area of the SFG titrations from: pH 2.0 to 12.0 (red squares), pH 6.0 to 12.0 or pH 7.0 to 2.0 (black circles), and pH 12.0 to 2.0 (blue triangles).

### 3.4 Conclusions

Using SFG, we have shown that the water molecules that are probed by *ssp* polarized SFG do not show the same behavior as the interfacial species that are probed in SHG. In the presence of 0.5 M NaCl, the SFG intensity had a minimum around pH 7-8. This was in contrast to 0.1 M NaCl which showed a minimum in the SFG intensity between pH 5-6. We theorized that the SFG intensity behavior that was observed in the presence of 0.1 M and 0.5M NaCl could be due to overcharging of the electrical double layer or to dehydration of the Na<sup>+</sup> ions at the silica surface suggesting that the *ssp* polarization combination was most sensitive to water molecules in the diffuse part of the electric double layer. In addition, the experimental starting pH has no effect on the shape of the *ssp* polarized SFG as a function of pH, which is also very different from our SHG studies. The next chapter will discuss the possible origin of the difference in the SHG and *ssp*-SFG results by exploring other polarization combinations. Finally, one striking feature that was observed in all *ssp*-SFG titrations was the prominent

appearance of the  $3000\text{ cm}^{-1}$  peak when the pH was varied, particularly at the pH extremes. We attribute this peak to the OH vibrational mode of  $\text{H}_3\text{O}^+$  at low pH and  $\text{OH}^-$  at high pH.

## **CHAPTER 4**

### **Reinterpreting the Origin of the SHG Intensity by Comparing Nonlinear Optical Methods**

## 4.1 Introduction

The silica/water interface has been the subject of enormous amounts of mystery, speculation and debate as it is one of the most relevant interfaces to human civilization owing to its prevalence in nature and the ubiquity of glass and silica substrates in materials applications.<sup>1, 10, 113</sup> One challenge in aligning the conflicting views of the behavior of the silica/water interface is the vast difference in silica samples that have been utilized in investigations of its interfacial behavior. From gels,<sup>93</sup> to colloids,<sup>58, 84</sup> to macroscopic slabs of crystalline<sup>35-36, 46</sup> and amorphous silica,<sup>73, 75, 77, 82, 108, 114</sup> all have been explored with a battery of techniques, as well as a wide variety of pre-treatments that can influence the resulting measurement like prior exposure to different pH or aqueous compositions.<sup>52, 92-93, 108</sup> Among these controversies one of the strangest contrasts in the literature has been the distinctly bimodal behavior observed in non-resonant second harmonic generation (SHG) pH titration experiments on macroscopic fused silica/water aqueous salt samples,<sup>26, 75-77, 108</sup> which was observed but less pronounced in an electrokinetic experiment on silica colloids.<sup>115</sup> Otherwise such behavior has not been reported despite the decades of research on silica. The origin of this bimodal titration was attributed to two different types of silanol sites that had markedly different acidities due to the local hydrogen-bonding environment.<sup>26, 35-36</sup> The reason this bimodal behavior was not as obvious for other experiments was attributed in part to the higher salt concentrations and different pre-treatments made possible by the SHG experiments, that limit electrokinetic or potentiometric measurements owing to the instability of colloidal silica to high salt concentrations. Planar silica samples are often utilized to combat these problems, and are compatible for use in nonlinear optical methods like SHG and SFG. Sum frequency generation (SFG) is often used in conjunction with SHG to obtain a clearer picture of the molecular interactions at the interface.<sup>1, 7, 116</sup>

In many instances SHG and SFG measurements on mineral oxide/water interfaces have been completed by different groups. For systems like the TiO<sub>2</sub>/water interface, the data are fairly consistent. For example, Eisenthal and coworkers measured the TiO<sub>2</sub> (110)/water interface to have a point of zero charge (PZC), or the pH where the surface has no net charge of 4.8.<sup>105</sup> In the case of the SHG, the PZC is typically calculated based on the cross over point of SHG titrations completed at multiple salt concentrations. As the SHG electric field depends only on the concentration of the electrolyte through the screening of surface charges, SHG will be independent of the salt concentration at the pH where the surface has no net charge. Additionally, consistent with the PZC identified by these salt variation experiments, *ssp* polarized SFG experiments of TiO<sub>2</sub> thin films showed the lowest SFG intensities between pH 4 and 6.<sup>39</sup> Both the SHG and SFG results are consistent with the PZC calculated on TiO<sub>2</sub> particles from zeta potential measurements.<sup>84, 117-118</sup> However, investigations of the Al<sub>2</sub>O<sub>3</sub>/water interface have had variable results. For example, Eisenthal and coworkers measured the  $\alpha$ Al<sub>2</sub>O<sub>3</sub> (0001) and  $\alpha$ Al<sub>2</sub>O<sub>3</sub>(1̄102) to have PZC's of 4.1 and 5.2 respectively.<sup>119</sup> In addition, SHG and AFM studies by Eggleston and coworkers showed Al<sub>2</sub>O<sub>3</sub> to have a PZC between pH 5-6. This contrasted highly with colloidal measurements of Al<sub>2</sub>O<sub>3</sub> which were typically between pH 8-10.<sup>84</sup> One possible explanation for this observed deviation is that the Al<sub>2</sub>O<sub>3</sub> particles contain more defect sites than the single crystal faces which contribute more to the surface charging behavior. Between SFG measurements there was variability as well. Sung et al. used conventional and phase sensitive SFG to probe where the minimum in the SFG intensity was in the water stretching region, and monitored the net orientation of the water molecules.<sup>37</sup> The authors found that the hydrogens of the water molecules flipped from having the hydrogens pointed towards the bulk to the hydrogens pointed towards the surface at a pH of 6.7 for

$\alpha\text{Al}_2\text{O}_3(1\bar{1}02)$ .<sup>37</sup> However, this value differed from the results of Pink and coworkers who found  $\alpha\text{Al}_2\text{O}_3$  to have a PZC around pH 8.<sup>38</sup> In this case no crystalline surface was specified, which may impact the results.<sup>38</sup>

Many of these interfaces will have different behavior in the presence of ions. Silica for example has a reported PZC around pH 2-3,<sup>23, 84</sup> yet silica behaves very differently in the presence of ions. One example is where monovalent ions cause overcharging in the double layer at the surface of silica. In zeta potential measurements, as the salt concentration increases, the pH where the zeta potential turns from negative to positive increases from about pH 2 to pH 4-5 depending on the monovalent ion.<sup>71, 102</sup> In addition, AFM measurements have observed the repulsion between two silica surfaces changes to an attractive force at higher concentrations of the monovalent ions.<sup>70</sup> There have been multiple AFM experiments that have both observed and not observed the repulsion between two silica plates becoming attractive in the presence of the monovalent electrolytes.<sup>70</sup> One common feature in the AFM studies that observed the repulsion changing to attraction was that the corresponding surfaces had lower surface potentials compared to the surfaces measured in AFM studies that showed just repulsion in the presence of the monovalent electrolytes.<sup>70</sup> These differences could be due to different types of silica utilized in the studies. Sodium, in particular, behaves in a distinct manner separate from the other monovalent alkali ions.<sup>75, 77-78</sup> For example, when the bimodal SHG acid-base titrations were explored with multiple concentrations (0.1 M and 0.5 M) of the alkali chlorides, the higher pK<sub>a</sub> value was sensitive to both the cation identity and concentration. In the presence of sodium, when the concentration was lowered, the higher pK<sub>a</sub> in the bimodal titration curve shifted to a higher pH value. The opposite happened when the concentration was lowered in the presence of lithium, potassium or cesium, which caused the higher pK<sub>a</sub> to shift to a lower pH value.<sup>75, 77</sup>

These unusual results were attributed to a combination of interactions between the surface sites, the water and the electrolytes.<sup>77</sup> In addition molecular dynamics simulations of the silica/water interface at high salt concentrations have shown that Na<sup>+</sup> orients the water molecules with the hydrogens pointed towards the bulk, which is opposite to how cesium orients the water molecules at the negatively charged silica/water interface.<sup>78</sup>

To determine if the interpretation of the bimodal behavior was consistent with complementary techniques sensitive to different interfacial parameters, we decided to compare the non-resonant SHG experiments with resonantly enhanced SFG of interfacial water in the presence of 0.1 M NaCl.

## 4.2 Experimental

### 4.2.1 Laser Assembly

A thorough description of both the SHG and SFG laser assemblies can be found in Section 2.2.1 and Section 3.2.1, respectively. Briefly for SHG, *p*- or *s*-polarized 580 nm (from OPA) or 800 nm (from Spitfire) light was focused towards the silica/water interface at an angle of 62° from the surface normal. SHG was generated at 290 or 400 nm, respectively, and was collimated and refocused through the appropriate colored glass filter (dependent on the wavelength of light). The SHG light was selected via a monochromator and was subsequently amplified and counted using a gated photon counter and PMT system. The only difference between the SHG assembly in Section 2.2.1 and the one used in these experiments is that a polarizer was placed on the SHG output line between the glass filter and the monochromator for the *pss* experiments with the polarizer selecting *p*-SHG.

For SFG, a portion of 800 nm light from the Spitfire was broadened in time from fs to ps via an air-spaced etalon. The ps pulse was passed through a polarizer and half wave plate to select the desired polarization and focused onto a cleaned silica hemisphere (IR grade, Almaz Optics). To generate the tunable IR laser light, 2/3 of the Spitfire output was directed into a TOPAS-C and nDFG assembly. The IR light from the nDFG was directed through a half wave plate, polarizer, and focusing lens and aligned spatially and temporally with the visible laser light (800nm). The SFG beam was collimated, and passed through a bandpass filter to remove the 800 nm visible. The SFG was then sent through a polarizer and was focused on a spectrograph and CCD camera.

#### **4.2.2 Materials**

Sodium chloride (> 99% purity) and sodium hydroxide (>99.99% purity) was from Sigma Aldrich. Hydrochloric acid and sulfuric acid were from Caledon laboratories. 30 % Hydrogen peroxide was from Sigma Aldrich. All chemicals were used as received. Freshly purified water (18 MΩ) from a Millipore system was used. For SFG an Orion 2–Star Benchtop pH meter (Thermo scientific) was used and for SHG an Orion Star A215 pH meter was used.

#### **4.2.3 Surface Preparation**

A 1-inch fused silica hemisphere (IR-grade) that is transparent in the IR region was first sonicated in Milli-Q water and rinsed multiple times with Milli-Q water. The hemisphere was then sonicated in methanol and then rinses with Milli-Q water. This was followed by sonication and rinsed with Milli-Q water. The hemisphere was then immersed in piranha solution (3:1 mixture of concentrated sulfuric acid: 30% hydrogen peroxide). The hemisphere was then rinsed with copious amounts of Milli-Q water. The hemisphere was then sonicated and rinsed 4 more times with Milli-Q water. The hemisphere was then placed in an oven at 100°C to dry for 30

min. The hemisphere was allowed to cool to room temperature, and was plasma cleaned in air for 2 min. the sample was then immediately placed on the sample cell.

#### **4.2.4 SHG Experiments**

The freshly cleaned hemisphere was mounted in the sample cell and exposed to pure Milli-Q water. SHG signal was optimized and verified on water. The water was then replaced with the 0.1 M NaCl solution at pH 5.6 for the increasing pH titrations or pH 7.0 for the decreasing pH titrations and equilibrated with the interface for 30 min. The pH was then adjusted either with HCl or NaOH solution that was made up in 0.1 M NaCl to limit the change in the ionic strength of the solution. The NaCl/HCl or NaCl/NaOH was used to adjust the pH by 0.3-0.4 pH units and was equilibrated with the surface for 5 min. After equilibration, 1.5 min of data was taken and the pH of the solution recorded. This step was repeated until either pH 12.7 or pH 2 was reached. The average of the SHG signal was obtained and was divided by the average water SHG signal at the same incident laser power.

#### **4.2.5 SFG Experiments**

Firstly, a gold coated, IR grade hemisphere was mounted on the sample cell. SFG was optimized for the polarization setting to be used. 6 IR pulses were used, spaced  $100\text{ cm}^{-1}$  apart from each other to cover the OH stretching region. The SFG was collected at the 6 identified wavelengths as a reference. A polystyrene calibration film was placed in the IR beam path and the offset of the detector determined. The gold coated silica hemisphere was then replaced with a freshly cleaned IR grade silica hemisphere. The sample cell was filled with pure Milli-Q water and was adjusted so that the SFG was aligned through the center of an alignment disk, in the same alignment as the SFG from the gold-coated silica hemisphere. The spectrum was collected at the same 6 IR wavelengths that were collected for the gold coated silica. Next, the water was

replaced with the salt solution and equilibrated for 30 min. The spectrum was collected at the same 6 IR wavelengths that were collected for the gold coated silica for all subsequent pH values. The pH of the solution was adjusted to the desired value using HCl or NaOH that was dissolved in 0.1M NaCl and was equilibrated with the surface. The spectra were taken and the pH was measured. After each pH adjustment the sample was equilibrated for 5 min and then the spectra were taken.

### 4.3 Results and Discussion

#### 4.3.1 Theory of SHG and SFG

Before comparing the two spectroscopies, we begin by briefly outlining the theory behind the sensitivity of SHG (and SFG) to the interfacial potential set-up by deprotonated sites at the silica/water interface. Both techniques are second-order nonlinear optical spectroscopies that depend primarily on the second-order susceptibility  $\chi^{(2)}$ , which depends on the extent of ordering and the molecular identity of the species that make up the interface.

$$P^{(2)} = \chi^{(2)} E_{(\omega_1)} E_{(\omega_2)} = \sum_i N_i \langle \beta_i \rangle \quad (\text{Equation 4.1})$$

where  $P^{(2)}$  is the second-order induced polarization oscillating at the sum of  $\omega_1$  and  $\omega_2$ ,  $E(\omega_1)$  and  $E(\omega_2)$  are the electric fields from the incident light source,  $N$  is an interfacial species and its corresponding molecular hyper polarizability ( $\beta$ ), which are summed over all interfacial species. The  $\langle \rangle$  brackets represent an orientational average of  $\beta_i$ . Within the electric dipole approximation,  $\langle \beta_i \rangle$  is zero for molecular ordering that is isotropic within length scales on the order of the wavelength of light. Consequently, the second-order response requires a break in inversion symmetry to garner a non-zero  $\langle \beta_i \rangle$  and thus  $\chi^{(2)}$ . For SHG both frequencies are the same ( $\omega_1 = \omega_2$ ) and are in the visible for our experiments, whereas  $\omega_1$  is in the visible and  $\omega_2$  is in

the infrared for our SFG experiments. However, in the presence of a static field  $E_0$  that is set-up by charged surface sites like siloxides another term must be considered.

$$\sqrt{I_{\omega_1+\omega_2}} = E_{\omega_1+\omega_2} \propto P^{(2)} = \chi^{(2)}E\omega_1E\omega_2 + \chi^{(3)}E\omega_1E\omega_2E_0 \quad (\text{Equation 4.2})$$

Here  $\chi^{(3)}$  is the third-order susceptibility, which contains both contributions from the molecular hyper polarizability ( $\beta$ ) as well as the third-order hyper polarizability ( $\gamma$ ) of interfacial molecules. To clarify the meaning behind  $\chi^{(3)}$  of water, it is helpful to write the product of and  $\chi^{(3)}$  and  $E_0$ :

$$\chi_{H_2O}^{(3)}E_0 = \frac{\mu_{H_2O}E_0}{ck_B T} \beta_{H_2O} + \gamma_{H_2O}E_0 \quad (\text{Equation 4.3})$$

where  $\mu_{H_2O}$  is the permanent dipole moment of water,  $c$  is a constant,  $k_B$  is Boltzmann's constant and  $T$  is temperature.<sup>26</sup> The first term was determined considering a Boltzmann distribution of water that is aligned within the presence of the static field  $E_0$  under conditions where the electrostatic aligning energy ( $\mu_{H_2O}E_0$ ) is much less than the thermal energy ( $k_B T$ ).<sup>26, 120</sup> More succinctly, the first term describes the amount of water ordered by the field and as such it depends on the hyper polarizability  $\beta$ , identical to the  $\beta$  in the expression for  $\chi^{(2)}$ , multiplied by the orientation distribution  $\mu_{H_2O}E_0/ck_B T$ . The second term describes the direct coupling of the static field  $E_0$  with the two incident oscillating fields through a third-order process. Thus,  $\gamma$  is utilized which is analogous to the third-order hyper polarizability that determines third harmonic generation upon coupling three incident light fields. Using non-resonant values from Kusalik and co-workers for  $\beta$  and  $\gamma$  of water<sup>121</sup> and the dipole moment at 300 K,<sup>122</sup> we calculated the values of each term neglecting the constant  $c$ . With these values the  $\gamma$  term is only 10% of the  $\beta$  term (that of aligned water) in  $\chi^{(3)}$ . However, using the values of  $\beta$  and  $\gamma$  of water determined experimentally from SHG by Bethea and Levine,<sup>120</sup> we found that the  $\gamma$  term was 50% of the  $\beta$

term. The resonant values of  $\beta$  and  $\gamma$  are not known for the water OH stretching region, but we assume they differ from one another similarly to the off-resonant values. Consequently, we interpret the data in terms of aligned water as that is the biggest contributor based on our calculations, but we recognize that the contribution of the  $\gamma$  term may be important, particularly as the calculated values of  $\beta$  and  $\gamma$  have significant variability and may not be accurate.

$$E_{\omega_1+\omega_2} \propto (N_{Silica}\langle\beta_{Silica}\rangle + N_{H_2O}\langle\beta_{H_2O}\rangle + N_{ions}\langle\beta_{ions}\rangle)E_{\omega_1}E_{\omega_2} \\ + (N_{H_2O}\frac{\mu_{H_2O}\Phi_0}{ckT}\beta_{H_2O} + N_{H_2O}\gamma_{H_2O}\Phi_0)E_{\omega_1}E_{\omega_2} \quad (\text{Equation 4.4})$$

In addition, Equation 4.4 assumes that the alignment of water is due only to changes in the interfacial potential and that this alignment varies linearly with the interfacial potential. However this assumption ignores the contribution of hydrogen bonding and how this bonding changes as the water molecules orientation changes as they are aligned.

#### 4.3.2 Typical Polarizations for SHG and SFG of the Silica/Water Interface

To probe the silica/water interface, SHG typically uses either “*p*-in/all out” or “*s*-in/all out” polarization, while SFG typically utilizes *ssp* polarization (*s*-polarized SFG, *s*-polarized visible and *p*-polarized IR) for the OH vibrational stretches of interfacial water molecules. Figure 4.1A illustrates the typical SHG pH titration observed for the silica/aqueous interface with 0.1 M. Two sigmoidal regions were observed, one below and the other above neutral pH. According to Equation 4.4, the minimum in SHG should be observed at pH 2 because this would correspond to the smallest magnitude of  $\Phi_0$ . This was consistent with the point-of-zero charge of silica being between pH 2 and 3.<sup>84</sup> In contrast, Figure 4.1B illustrates the polarization-resolved SFG spectra in the O-H stretching region (*s*-polarized SFG, *s*-polarized visible light, *p*-polarized

IR) from Section 3.3.2. As is clear, unlike SHG the signal intensity increased upon decreasing the pH from pH 7 to pH 2.

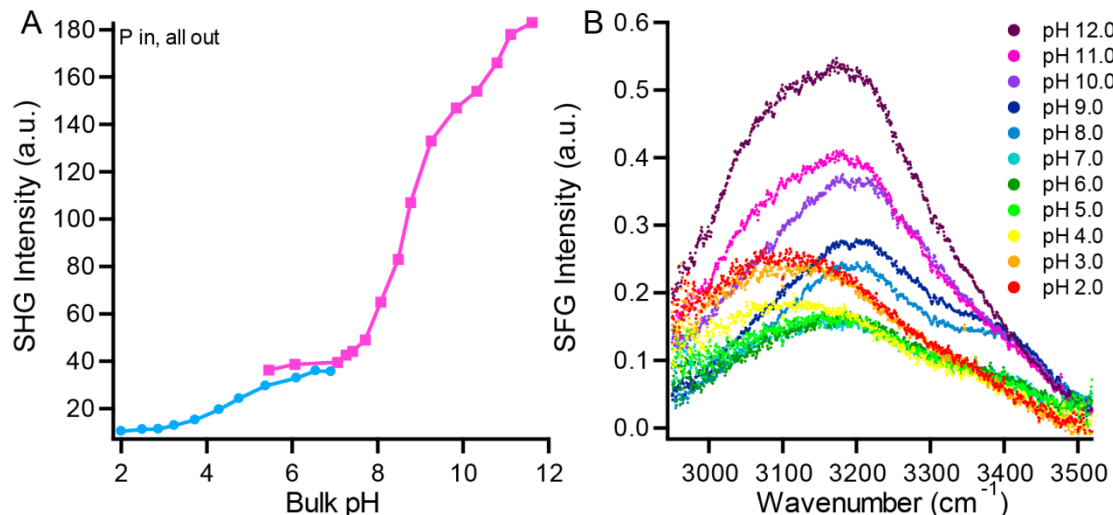


**Figure 4.1** A) SHG intensity (determined from previously published SH electric field vs pH data in supporting information of reference 107) vs pH from the silica/aqueous interface with 0.1 M NaCl SHG using *p*-in/all out polarization. The SHG plot is composed to two titrations, from pH 6 to 12 and from pH 7 to 2. B) Representative *ssp* polarized SFG from the silica/aqueous interface with 0.1 M NaCl, also composed of two titrations from pH 6 to 12 and from pH 7 to 2.

One problem with the current set up for probing the silica/water interface is that the chosen polarization combinations probe different  $\chi^{(2)}$  tensor elements (Table 4.1), which could lead to the observed differences. To ensure that the same  $\chi^{(2)}$  tensor element was probed, a polarization combination that could be performed on both the SHG and SFG laser lines was utilized. With many experimental SHG setups, including ours, the two incident photons need to have the same polarization. This effectively eliminates the use of *sps* and *ssp* polarizations for a direct comparison between SHG and SFG. This leaves *pss* and *ppp* polarizations for experiments that can be used for a direct comparison of SHG and SFG. From Table 4.1, *ppp* polarization probes multiple tensor elements.<sup>9, 12</sup> Therefore, if this polarization is used for a comparison, it will be difficult to determine which tensor element is contributing to the signal as the

experimental geometry influences the relative weighting of each element's contribution.<sup>9, 12</sup>

Therefore *pss* polarization was chosen because it only probes the tensor element  $\chi_{zyy}^{(2)}$  and can also be utilized in SHG measurements.

**Table 4.1** All unique, non-zero polarizations and the elements of  $\chi_{ijk}^{(2)}$  that contribute to the spectrum for a C<sub>∞</sub> interface

Polarization combinations	Elements of $\chi_{ijk}^{(2)}$
<i>pss</i>	$\chi_{zyy}^{(2)}$
<i>sps</i>	$\chi_{yzy}^{(2)}$
<i>ssp</i>	$\chi_{yyz}^{(2)}$
<i>ppp</i>	$\chi_{zzz}^{(2)}, \chi_{zxx}^{(2)}, \chi_{xzx}^{(2)}, \chi_{xxz}^{(2)}$

#### 4.3.3 *pss* Polarized SHG and SFG

The *pss* polarized SHG, which probes  $\chi_{zyy}^{(2)}$ , (Figure 4.2) appears similar in shape to that of bimodal SHG collected in *p*-in/all out polarization in the presence of 0.1 M NaCl (Figure 4.1). As our previous experimental set-up, the polarization combination *p*-in/all out, probes all tensor elements, we conclude that the  $\chi_{zyy}^{(2)}$  tensor is most important given the similarities between the *pss* and *p*-in/all out data, which could be in part due to our experimental geometry. However, unlike SHG the shape profile of the SFG collected in *pss* polarization in the presence of 0.1 M NaCl (Figure 4.2) is vividly different than the *ssp* polarized SFG of 0.1 M NaCl (Figure 4.1). In the *pss*-polarized SFG of 0.1 M NaCl, the 3400 cm<sup>-1</sup> peak is much more prominent than the 3200 cm<sup>-1</sup> peak, unlike *ssp*-SFG where the 3200 cm<sup>-1</sup> peak dominates the spectrum. Thus the biggest difference in the *pss* polarized SFG spectra is that the signal decreased with decreasing pH from pH 7 to 2 compared to the *ssp* polarized SFG of 0.1 M NaCl where the SFG signal increased

from about pH 5 to 2. As such the *pss* SFG trend more closely follows the trend observed in the SHG.

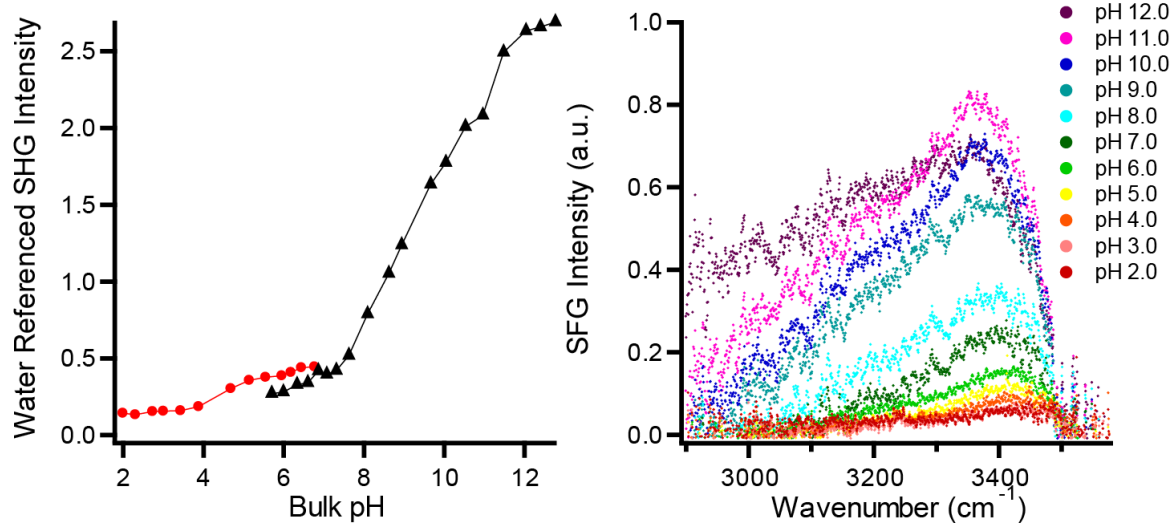


**Figure 4.2** A) Representative titrations of *pss* polarized SHG from the silica/aqueous interface with 0.1 M NaCl that is referenced to the SHG of pure water/silica (all SHG values were divided by the value of the SHG of water). Here two separate titrations were completed, pH 6.0 to 12.0, and pH 7.0 to 2.0. B) Representative titrations of *pss* polarized SFG of silica/aqueous interface with 0.1 M NaCl also collected via two separate titrations pH 6.0 to 12.0 and pH 7.0 to 2.0.

From the SFG spectra, the  $\chi^{(2)}$  can be approximated as the sum of oscillators with Lorentzian line shapes.

$$\chi_R^{(2)} = \sum_n \frac{A_n}{(\omega_{IR} - \omega_n + i\Gamma_n)} \quad (\text{Equation 4.5})$$

In the equation,  $\omega_{IR}$  is the frequency of the IR laser beam,  $A_n$ ,  $\omega_n$  and  $\Gamma_n$  are the amplitude, frequency and width of the  $n^{\text{th}}$  vibrational mode respectively. As the SFG intensity depends on the absolute square of  $\chi^{(2)}$ , each of the SFG intensity spectra (*pss* and *ssp*) can be fit to the absolute square of the sum of two Lorentzian peaks (equation 4.5), one centered around 3200  $\text{cm}^{-1}$  and another peak centered 3400  $\text{cm}^{-1}$ . The summed total of the  $A/\Gamma$  determined from the fits is given for both *pss* (Figure 4.3A) and *ssp* (Figure 4.3C) show the marked differences between

the two data sets. When the separate contributions are plotted for both the *pss* (Figure 4.3B) and for *ssp* (Figure 4.3D) it is clear that the  $3200\text{ cm}^{-1}$  peak dominates the *ssp* spectra, but has very little contribution to the intensity of the *pss* spectra.

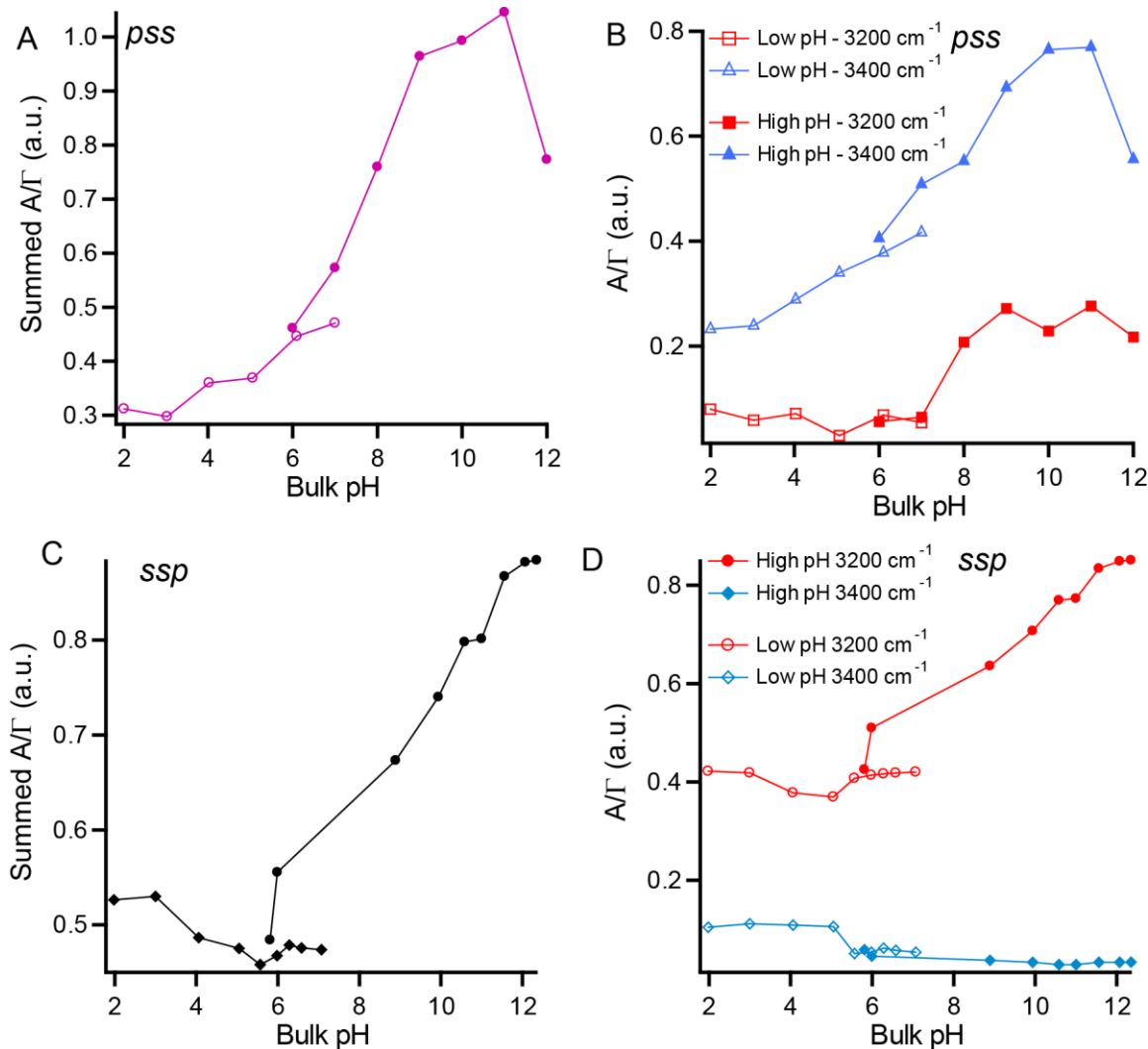


**Figure 4.3** Representative 0.1 M NaCl titrations that have been fit using two Lorentzian peaks. A) Summed  $A/\Gamma$  values of the *pss* SFG high pH and low pH titrations. B) The separate  $A/\Gamma$  contributions of the  $3200\text{ cm}^{-1}$  (red) and  $3400\text{ cm}^{-1}$  (blue) centered modes from the *pss* polarization combination. C) The summed  $A/\Gamma$  values of the *ssp* SFG high pH and low pH titrations. D) The separate  $A/\Gamma$  contributions of the  $3200\text{ cm}^{-1}$  (red) and  $3400\text{ cm}^{-1}$  (blue) centered modes in *ssp* polarization combination.

Based on symmetry rules, *pss* and *sps* polarization should be equivalent in their SFG response. The prominence of the  $3400\text{ cm}^{-1}$  peak compared to the  $3200\text{ cm}^{-1}$  peak has been

previously observed for both *pss* and *sps* spectra of the silica/water interface.<sup>43, 45, 47</sup> The trends observed in both the *ssp* and *pss/sps* were confirmed by Dr. Dennis Hore and Tasha Jarisz as collaborators on this project from the University of Victoria. Interestingly, the cross polarized Raman of bulk water also shows the 3400 cm<sup>-1</sup> more prominently than the 3200 cm<sup>-1</sup> peak, whereas the parallel polarized Raman is dominated by the 3200 cm<sup>-1</sup> when waters interact with other molecules.<sup>123</sup>

One general school of thought is that the two peaks at 3200 cm<sup>-1</sup> and 3400 cm<sup>-1</sup> represent two different populations of orientated water molecules. In the *pss* polarized SFG spectra, there is very little contribution from the 3200 cm<sup>-1</sup> peak compared to the large contribution of the 3200 cm<sup>-1</sup> peak in the *ssp*-polarized spectra. One possible explanation for this result is that the water molecules in resonance with 3200 cm<sup>-1</sup> that are probed in *ssp* are oriented in a way that they are not probed by the *pss* polarization combination. To determine if indeed the *pss* polarization is sensitive to the orientation of the water molecules while *ssp* polarization is not, we used a nonlinear optical prediction program (NLOPredict) developed by Dr. Garth Simpson to determine the magnitude of  $\chi^{(2)}$  as a function of tilt angle (angle between the surface normal and the principle axis of the molecule), which assumes a delta function distribution.<sup>124</sup> One difficulty in utilizing NLOPredict is finding suitable values for the hyperpolarizability tensor elements of water. Given the complexity of the hydrogen bonding between water molecules, hyperpolarizabilities calculated from gas phase measurements often do not match experimental data.<sup>47, 125</sup> The hydrogen bonding between water molecules is known to red shift the experimental spectra by as much as several hundred cm<sup>-1</sup> from the expected values.<sup>125-126</sup> Morita and Hynes have had some success of simulating the SFG of a water spectrum.<sup>125</sup> Utilizing the  $\alpha$  and  $\mu$  values from Morita and Hynes's calculations<sup>125</sup> we were able to calculate the  $\beta$  values for

water and use them in NLOPredict<sup>124</sup> to determine the  $\chi^{(2)}$  response of the water molecules for the different polarizations combinations as a function of water tilt angle (Figure 4.4). From our calculations there are clearly some angles of  $\theta$  where you have a large magnitude of  $\chi^{(2)}$  in the *ssp* polarization spectrum and a small magnitude of  $\chi^{(2)}$  in the *pss* polarization spectrum. As the *pss* polarization is much more sensitive to the orientation of water molecules compared to the *ssp* polarization, the very little contribution from the  $3200\text{ cm}^{-1}$  peak indicates it is oriented sub-optimally to generate *pss*-SFG, while a large contribution from the  $3400\text{ cm}^{-1}$  peak indicates these waters are oriented such that they are very *pss*-SFG active. In contrast, both the  $3200\text{ cm}^{-1}$  and  $3400\text{ cm}^{-1}$  peaks are present in the *ssp*-SFG as this polarization combination probes most water orientations.

Jena and Hore varied the concentration of NaCl in two different polarization (*ssp* and *sps*) and found that the  $3200\text{ cm}^{-1}$  peak was more sensitive to the increasing NaCl compared to the  $3400\text{ cm}^{-1}$  peak.<sup>47</sup> As the concentration of the NaCl was increased, it screens more of the surface charge and therefore the water molecules further from the surface no longer feel the potential. Thus, Jena and Hore proposed that the lower coordinated water molecules, *i.e.*, the water molecules that contribute to the  $3400\text{ cm}^{-1}$  peak, corresponded to water molecules that were closer to the silica surface.<sup>47</sup> Brown and coworkers established that the amplitude of the  $3400\text{ cm}^{-1}$  peak provided quantitative agreement to their X-ray photoelectron spectroscopy measurements of the thickness of the Stern layer, which supported the Hore group's argument.<sup>28</sup>

<sup>47</sup> Specifically, Brown and coworkers found that as the NaCl concentration increased the thickness of the Stern layer decreased, which correlated with the amplitude of the  $3400\text{ cm}^{-1}$ .<sup>107</sup> Thus they found that for silica colloids, concentrations of 0.1 M NaCl consistent with less than one monolayer of water molecules within the Stern layer between the surface sites and the

cations of the electric double layer, 0.05 M consistent with about one monolayer of water, and 0.01 M NaCl consistent with more than one monolayer of water.<sup>28</sup> This evidence leads us to assign the 3400 cm<sup>-1</sup> peak to water molecules closest to the surface sandwiched between the surface and the sodium ions. Consequently the 3200 cm<sup>-1</sup> peak would then be water molecules that were further from the silica surface, in the diffuse portion of the electric double layer. In the diffuse part of the double layer the water molecules could be affected more by the identity of the ions and their relative hydration as well as the zeta potential which is approximately equal to the potential at the outer Helmholtz plane where the cations lie.<sup>28</sup>

In Chapter 3, we hypothesized that the *ssp*-polarized SFG could be due to overcharging of the double layer. This would mean that the 3200 cm<sup>-1</sup> peak is sensitive to the potential at the outer Helmholtz plane, while the 3400 cm<sup>-1</sup> peak is sensitive to the 0-plane. If this is true, then in equations the  $E_0$  should be substituted with  $\zeta$  instead of  $\Phi_0$  when looking at when the integral is performed. One way to test if this hypothesis is correct, would be to run streaming potential measurements for our samples, which would allow the zeta potential to be calculated, and see if the data follows the trends in the *ssp* polarized SFG.

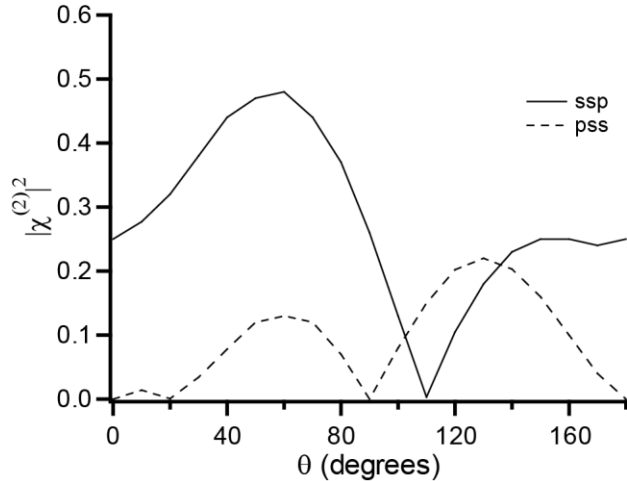


**Figure 4.4** Nonlinear optical predict of the magnitude of the  $\chi^{(2)}$  for resonant water molecules as a function of the tilt angle  $\theta$  between the surface normal and the principle axis. The solid line is the *ssp* polarization and the dashed line is *pss* polarization.

If the alignment of the  $3400\text{ cm}^{-1}$  water is the only cause of the SHG signal, the changes in the magnitude of the intensity spectra should be the same based on the linear relationship of water molecules oriented by the static electric field to the second-order susceptibility ( $\chi^{(2)}$ ). Yet, when the magnitude of both SHG and SFG are referenced to pure water, a common data point in all the data sets, we see that the magnitude in the signal change is drastically different. Figure 4.5 shows the water referenced SHG intensity is enhanced compared to the water referenced SFG intensity. This difference suggests the alignment of the  $3400\text{ cm}^{-1}$  water molecules by the interfacial potential contributes to the overall SHG signal, but it does not explain all of the SHG intensity.

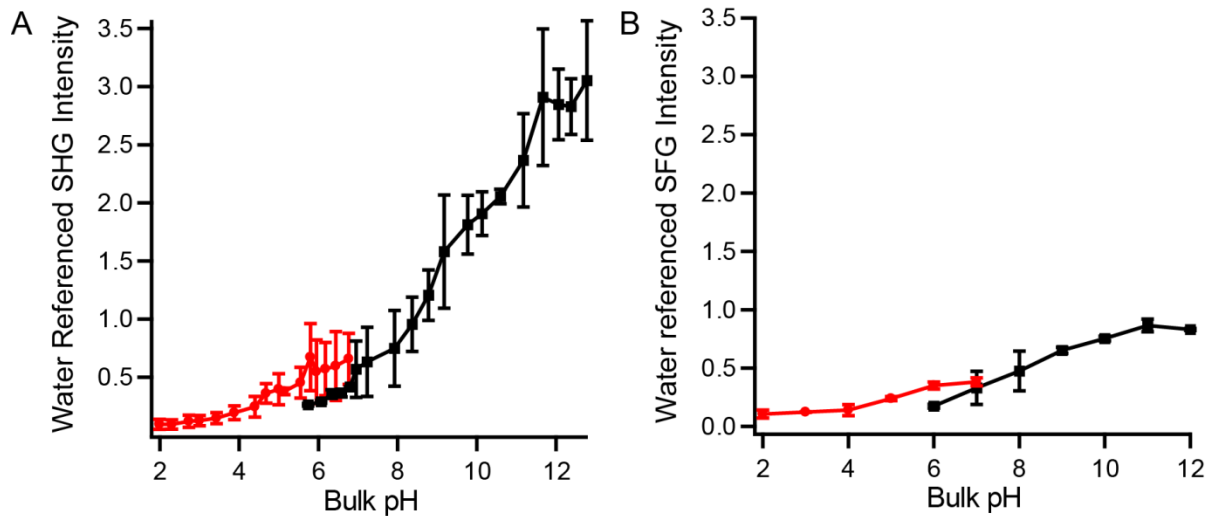


**Figure 4.5** Averaged titrations that have been referenced to the intensity of the water for each experiment. A) Average *pss* polarized SHG intensity and B) Average *pss* polarized SFG intensity.

Equation 4.4 shows that SHG takes into account the contributions from all interfacial species, which are: the water molecules experiencing the electric field, the silica (silanols and siloxides), and ions at the interface. Based on the intensities of the SHG and SFG not matching when referenced to pure water, we have ruled out that only the water molecules contributes to the SHG signal intensity. Thus, one of the other interfacial species must also contribute to the SHG signal intensity. As the surface is deprotonated, the silanols lose a hydrogen and become a negatively charged siloxide group. This increase in the electron density at the silica surface could cause the siloxides to have a larger  $\beta$  value, and consequently contribute more to the  $\chi^{(2)}$  of silica. If this is true, the  $\chi^{(2)}$  of silica would contribute significantly to the magnitude of the SHG intensity, particularly in the high pH regime. Moreover, as the alignment of these surface waters and the formation of siloxides are strongly correlated, it is possible that the SHG, which probes both, would exhibit very similar trends with SFG that only probes the former. This correlation should be particularly strong at high salt concentrations where the surface charge density varies linearly with the interfacial potential (where the constant capacitance model is most valid).

#### 4.4 Conclusions

We have demonstrated that the same polarization combinations must be used to directly compare SHG and SFG. The  $3400\text{ cm}^{-1}$  peak is most prominent in the *pss* polarized SFG and is thought to be due to water molecules closest to the surface. In contrast, the  $3200\text{ cm}^{-1}$  peak is significantly weaker in the *pss* polarization and is thought to be due to the water molecules further from the surface. Using *pss* polarized SFG and studying the OH vibrational region, we found that the magnitude of the intensity of the  $3400\text{ cm}^{-1}$  waters experiencing the static electric field at the surface cannot account for the entire SHG intensity observed. Instead there has to be a contribution from another element. We propose that the enhancement in the SHG signal intensity is due to the increased electron density upon deprotonation of the silanol to the siloxide. The increased electron density at the silica surface could increase the  $\chi^{(2)}$  of silica, making it a significant contributor to the resultant SHG intensity.

## **CHAPTER 5**

### **Effect of Calcium on the Silica/Water Interface**

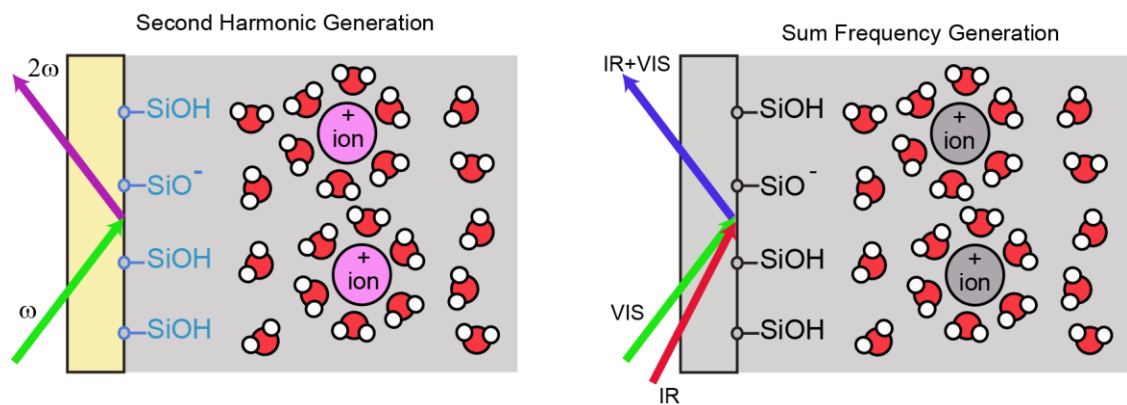
## 5.1 Introduction

Second harmonic generation (SHG) and sum frequency generation (SFG) have contributed immensely to the understanding of the orientation and distribution of water, ions and other species at environmentally relevant interfaces like the air/water and mineral oxide/water interface. For example, vibrational sum frequency generation (SFG) is commonly employed to monitor the amount of ordered water at these interfaces as a function of aqueous composition.<sup>4, 7, 10, 35-36, 43, 48-49, 116</sup> More recently, the *absolute* orientation of water at these interfaces has been the focus of research using new methods of vibrational SFG.<sup>13, 15, 17, 42, 44, 127-129</sup> For second harmonic generation (SHG), resonance enhanced experiments have been conducted using the intrinsic electronic signatures of ions such as chromate<sup>73-74</sup> and iodide<sup>130</sup> to monitor their surface activity. Another approach for probing electrostatic interactions at interfaces is to utilize non-resonant second harmonic generation.<sup>26, 105, 119</sup> As discussed in previous chapters, the method known as the  $\chi^{(3)}$  technique, proposed that SHG depended on the interfacial potential of the interface, and thus could be used to observe ion screening and binding events as such processes modulate the interfacial potential.<sup>26</sup>

The origin of the interfacial dependence of the non-resonant SHG signal was described by Eisenthal and co-workers in their seminal work, which demonstrated that SHG was very sensitive to the pH at the silica/water interface.<sup>26</sup> The resulting pH variation experiments appeared very much like typical sigmoidal acid-base titrations of surface sites. As a result of the sigmoidal behavior in the SHG intensity versus pH curves, in addition to other supporting observations, the authors attributed the signal changes to changes in the interfacial potential that arose from deprotonation of silanol sites as the pH was increased.<sup>26</sup> According to their model, two different factors contributed to the  $\chi^{(3)}$  term which contained the interfacial potential: the first

involved the presence of the static electric field arising from deprotonated siloxide sites orienting the water dipoles, while the second involved the interaction of the two incident fields and this static field through the third-order polarizability of water.<sup>26</sup>

Similar to the case of SHG, this interfacial potential dependence has also been proposed to play a significant role in the signal intensities of the vibrational SFG of water based on similar observations of the pH sensitivity of the intensity spectra.<sup>7, 35-36</sup> The main difference in these two nonlinear optical experiments, however, is that vibrational SFG is in resonance with water stretching modes, while the SHG experiments depend on the non-resonant response of all of the ordered species present at the interface as seen in Scheme 5.1. However, the theory of the interfacial dependence of non-resonant SHG, sometimes referred to as the  $\chi^{(3)}$  technique, attributes most of the signal to the water present at the interface.<sup>26</sup> As such, it should be possible to compare the resonantly enhanced SFG with the off resonant SHG owing to their proposed similar origins.



**Scheme 5.1** Cartoon depiction of the contributions of different  $\chi^{(2)}$  elements in second harmonic generation and sum frequency generation. SHG depends on the non-resonant response of all species at the interface;  $\text{SiOH}$ ,  $\text{SiO}^-$ , bulk water, aligned water, and ions. SFG depends on the resonant response of aligned water.

Although  $\chi^{(3)}$  models of both SFG and SHG are common in the literature, very few do comparisons of the two experiments. Here we reveal that the behavior of SFG and SHG can vary starkly for systems with interesting charging behavior. Alkaline earth ions like calcium, which are divalent, are known to behave very differently compared to monovalent ions.<sup>52, 65, 69, 131-132</sup> One of these differences is the propensity to cause charge reversal in streaming potential measurements, where the electrokinetic charge on silica in the presence of calcium appears to change sign at a particular pH or calcium concentration.<sup>65, 133</sup> A change in sign of the zeta potential has also been observed for colloidal silica in the presence of higher concentrations of calcium chloride.<sup>69</sup> Anecdotally, the tendency of silica particles to aggregate at high pH in the presence of calcium, which causes low extraction efficiency in Athabasca oil sands processing of crude oil, has been attributed to charge reversal in the electric double layer.<sup>2, 132</sup> Because of its unique features, divalent calcium represents an interesting system for exploration by these complementary techniques. Moreover, observed differences in SHG and SFG provide insight into the origin of the signal in these experiments.

## 5.2 Experimental

### 5.2.1 Laser Assembly

The laser system consists of a regeneratively amplified Ti:Sapphire laser assembly (Spitfire Pro 3.3W , Spectra Physics,) which produce 800 nm pulses (<100 fs, full width half max (FWHM) ~12 nm, 1 kHz repetition rate). For the SHG experiments a portion of light from the Spitfire (30%) was used to pump an optical parametric amplifier (Spectra Physics OPA-800CF) to generate laser light tunable in the visible region. In the SHG experiments, the wavelength of the incident light was tuned to either  $550 \pm 2$  nm or  $580 \pm 2$  nm. The light from the OPA was attenuated by a dual wheel neutral-density filter (New Focus, cat. # 5215) to 300 –

500 nJ per pulse. A  $\lambda/2$  wave plate and Glan-Thompson polarizer (B. Halle, UV-grade Calcite) were used to generate *p*-polarized light which was focused through a silica hemisphere at an angle of 62° from the surface normal, mounted on a custom-built Teflon cell such that the interface was perpendicular to the laser table. The cell provided access to the aqueous phase from the top so that the pH could be easily changed. The reflected light was collimated and focused through a bandpass colored glass filter (Thorlabs, UG5), which was used to filter out the reflected fundamental, onto a monochromator (Optometrics Corp., Mini-Chrom MC1-02) coupled to a photomultiplier tube (PMT) (Hamamatsu Photonics). The electrical response of the PMT was amplified and counted with a gated photon counter (Stanford Research Systems).

For the SFG experiments, a portion of light from the Spitfire (70%) was used to pump a TOPAS-C/NDFG (Light Conversion) to generate broadband infrared (IR) light. The resulting IR was tuned in the 3000 – 3600  $\text{cm}^{-1}$  range for probing the resonant O-H stretch of water. The IR light was passed through a polarizer (LPMIR050 Thor Labs) and  $\frac{1}{2}$  wave plate (Alphalas GMBH) to control the incident polarization. Spitfire visible light (~800 nm, 100 fs) was broadened to a pico second (ps) pulse using a Fabry-Perot etalon and passed through a polarizer (LPVI5050 Thor Labs) and  $\frac{1}{2}$  wave plate to control the incident polarization. The IR and visible beam were focused through a fused silica hemisphere (ISP Optics, 1 inch diameter, IR-grade  $\text{SiO}_2$ ), assembled in a custom made Teflon cell assembly described previously, such that the beam were temporally and spatially overlapped at the interface.<sup>75-76</sup> The incident angles of the IR and visible beam onto the silica/water interface were kept at roughly 66° and 64°, respectively, from the surface normal. The resulting SFG emitted from the interface was collimated and filtered with a bandpass filter (Chroma, HQ 617/70 M) to remove residual 800-nm incident light. This light was passed through a polarizer to select the *s*- or *p*-polarized SFG, and focused onto a

spectrograph (Acton SP-2556 Imaging Spectrograph, grating: 1200 G/mm with 500-nm blaze wavelength) connected to a thermoelectrically cooled, back-illuminated, charge coupled device camera (Acton PIXIS 100B CCD digital camera system, 1340 x 100 pixels, 20 mm x 20 mm pixel size, Princeton Instruments).

### **5.2.2 Materials**

Calcium chloride hexahydrate (Sigma Aldrich, >99%), magnesium chloride hexahydrate (Caledon Laboratory, >99%), sodium chloride (Sigma Aldrich, ≥99%), sodium hydroxide (Sigma-Aldrich, ≥99.99%) hydrochloric acid (Caledon Laboratory) and sulfuric acid (Caledon Laboratory) were used in the SHG and SFG experiments. Freshly purified ultrapure deionized water (18.2 MΩ·cm water from a Milli-Q-Plus ultrapure water purification system (Millipore Corporation) was used in all experiments. The pH of all the solutions was measured using an Orion 2–Star Benchtop pH meter (Thermo Scientific) with a double-junction Ag/AgCl (Orion, 9107APMD).

### **5.2.3 Second Harmonic Generation (SHG)**

#### ***5.2.3.1 Sample Cleaning***

For SHG which utilized a UV-grade silica sample (1-inch diameter, ISP Optics), the hemisphere cleaning process comprised of sonication and rinsing in fresh ultrapure Milli-Q water, then sonication and rinsing in methanol, followed by sonication and rinsing in Milli-Q water. The flat surface of the hemisphere was then treated with Nochromix solution (Godax Laboratories, 5% w/v solution in H<sub>2</sub>SO<sub>4</sub>) for 1 h. This was followed by extensive rinsing and sonication in Milli-Q water. The hemisphere was finally sonicated in Milli-Q water and dried in

an oven at 100 °C for 30 min. The hemisphere was then cooled to room temperature and plasma cleaning was performed using a plasma cleaner (Harrick Plasma PDC-32G) in air for 3 min.

#### **5.2.3.2 SHG Titration Experiments**

Prior to performing all pH-titration and salt titration experiments, we examined the power dependence and wavelength dependence for confirmation of SHG. The SHG signal optimization was always performed with Milli-Q water. The cell was then rinsed with the experimental solution (aqueous 0.1 M CaCl<sub>2</sub> and 10 mM NaCl solution), and then the cell was filled with experimental solution and the sample was equilibrated for 30 min. The high pH experiments were started at unaltered pH of electrolyte solution (pH ~5.8) followed by addition of NaOH in 0.3-0.5 pH unit increments. The volume of each addition was monitored to ensure that the total volume changed by less than 5% during the course of the experiment. Since NaOH provides Na<sup>+</sup> ions in the aqueous medium, a question was raised if such a small amount of Na<sup>+</sup> ions could influence the experimental results. To resolve this issue, we have used 10 mM concentration of NaCl in the background for all solutions of 100 mM CaCl<sub>2</sub>.

#### **5.2.4 Sum Frequency Generation (SFG)**

##### **5.2.4.1 Sample Cleaning**

For SFG IR-Grade silica samples were used (1-inch diameter, ISP Optics). This hemisphere was sonicated in Milli-Q water for 5 min, methanol for 5 min, and in Milli-Q water for 5 min. The hemisphere was dried in an oven at 100 °C for 30 min. The hemisphere was then covered in a piranha solution (3:1 concentrated H<sub>2</sub>SO<sub>4</sub>:30% H<sub>2</sub>O<sub>2</sub>) for 1 h. The hemisphere was then copiously rinsed with Milli-Q water. This was followed by another sonication in Milli-Q water for 5 min, methanol for 5 min, and in Milli-Q water for 5 min. The hemisphere was dried

in an oven at 100 °C for 30 min. The hemisphere was then cooled to room temperature and plasma cleaned in air for 3 min.

#### **5.2.4.2 SFG Experiments**

At the start of each SFG experiment, 5-6 reference spectra covering 2850-3650 cm<sup>-1</sup> of the IR range were collected from a gold coated IR-grade silica hemisphere. The experiments were done in *ssp* polarization (*s*-SFG, *s*-visible and *p*-IR). The gold coated hemisphere was replaced with a freshly cleaned IR grade fused silica hemisphere (Almaz Optics, 1 inch diameter) and exposed to water. Five spectra, with the same center frequencies as above, were measured for the water spectrum. The final spectrum of the silica/water interface was obtained by adding the recorded spectra at the above mentioned wavelengths and dividing them by the summed gold-coated reference spectra.<sup>103</sup> Prior to this normalization, the background was subtracted from the individual gold spectra by measuring the background spectrum with the visible beam blocked.

### **5.3 Results and Discussion**

#### **5.3.1 Background SHG and SFG**

SHG results when light of frequency  $\omega$  interacts with an interface. Specifically, under the right symmetry conditions the incident electric field induces a polarization that oscillates at twice the frequency of  $\omega$  ( $P_{2\omega}$ ), thereby generating an electric field that oscillates at the same frequency ( $E_{2\omega}$ ). For an uncharged interface, this second harmonic electric field is dependent on the second order susceptibility ( $\chi^{(2)}$ ) and the incident electric field ( $E_\omega$ ) according to:

$$\sqrt{I_{2\omega}} = E_{2\omega} \propto P_{2\omega} = \chi^{(2)} E_\omega E_\omega \quad (\text{Equation 5.1})$$

However, because silica is negatively charged above pH 2,<sup>23</sup> according to the  $\chi^{(3)}$  model the  $E_{2\omega}$  signal is enhanced by the static electric field set up by negatively charged surface sites, which can be described by the product of the third-order susceptibility ( $\chi^{(3)}$ ) and the interfacial potential ( $\Phi_0$ ).<sup>26</sup> Thus,  $E_{2\omega}$  can be expressed as:

$$E_{2\omega} \propto \chi^{(2)} E_\omega E_\omega + \chi^{(3)} E_\omega E_\omega \Phi_0 \quad (\text{Equation 5.2})$$

For the  $\chi^{(3)}$  technique of SHG, which is off resonance, the second-order susceptibility  $\chi^{(2)}$  encompasses contributions from all interfacial species, namely silica ( $\chi_{Silica}^{(2)}$ ), the surface water ( $\chi_{H_2O_{surface}}^{(2)}$ ), and ions at the interface ( $\chi_{ions}^{(2)}$ )

$$\chi^{(2)} = \chi_{Silica}^{(2)} + \chi_{H_2O_{surface}}^{(2)} + \chi_{ions}^{(2)} \quad (\text{Equation 5.3})$$

These can be related to their respective molecular hyperpolarizabilities ( $\beta$ ) and the number of interfacial species ( $N$ ) as shown by:

$$\chi^{(2)} = N_{Silica} \langle \beta_{Silica} \rangle + N_{H_2O} \langle \beta_{H_2O} \rangle + N_{ions} \langle \beta_{ions} \rangle \quad (\text{Equation 5.4})$$

According to the theory by Eisenthal and coworkers,<sup>26</sup> the third order susceptibility ( $\chi^{(3)}$ ) also originates from the second-order molecular hyperpolarizability of water as well as its third-order molecular hyper polarizability:

$$\chi^{(3)} \Phi_0 = N_{H_2O} \frac{\mu_{H_2O} \Phi_0}{c k_B T} \beta_{H_2O} + N_{H_2O} \gamma_{H_2O} \Phi_0 \quad (\text{Equation 5.5})$$

where  $\mu_{H_2O}$  is the dipole moment of  $k_B$  is the Boltzmann constant,  $T$  is the temperature,  $\gamma_{H_2O}$  is the third-order hyperpolarizability. When these terms are substituted in Equation 5.2, it yields:

$$E_{2\omega} \propto (N_{Silica}\langle\beta_{Silica}\rangle + N_{H_2O}\langle\beta_{H_2O}\rangle + N_{ions}\langle\beta_{ions}\rangle)E_\omega E_\omega + (N_{H_2O} \frac{\mu_{H_2O}\Phi_0}{ckT} \beta_{H_2O} + N_{H_2O}\gamma_{H_2O}\Phi_0)E_\omega E_\omega \quad (\text{Equation 5.6})$$

For vibrational SFG the underlying theory is similar to SHG except that it is generated when infrared light ( $E_{IR}$ ) and visible light ( $E_{VIS}$ ) interact with the interface, generating an electric field that oscillates at the sum frequency of the two incident beams ( $E_{SFG}$ ). For charged interfaces like silica, the SFG response also depends on the contributions from the static electric field which also contributes to  $\chi^{(3)}$  through the interfacial potential ( $\Phi_0$ ):

$$E_{SFG} \propto P_{SFG} = \chi^{(2)}E_{VIS}E_{IR} + \chi^{(3)}E_{VIS}E_{IR}\Phi_0 \quad (\text{Equation 5.7})$$

The  $\chi^{(2)}$  and  $\chi^{(3)}$  term can also be similarly broken down into the interfacial components, however because we are employing a technique that is in resonance with the OH vibrational modes, the contributions of the  $\chi^{(2)}$  and  $\chi^{(3)}$  that correspond to water molecules will dominate the resulting spectra. Thus the equation simplifies to:

$$E_{SFG} \propto (N_{H_2O}\langle\beta_{H_2O}^{(2)}\rangle)E_{VIS}E_{IR} + (N_{H_2O} \frac{\mu_{H_2O}\Phi_0}{ckT} \beta_{H_2O} + N_{H_2O}\gamma_{H_2O}\Phi_0)E_{VIS}E_{IR} \quad (\text{Equation 5.8})$$

One major conclusion from Eisenthal and coworkers' original work was that the major source of the SHG off resonance signal is the interfacial water as opposed to other interfacial species like silanol and siloxide sites owing to the low signal intensity near the point-of-zero charge (pH 2).<sup>26, 84</sup> In Section 4.3.3 the SHG and SFG monitored in the *pss*-polarization combination behave in similar ways at high pH, where increased intensity upon an increase in pH is observed. Consequently, we hypothesized that the pH-dependent SHG should match the vibrational pss SFG spectrum of water in the presence of  $\text{CaCl}_2$ .

### 5.3.2 Effect of CaCl<sub>2</sub> on SHG

There have been very few SHG studies done on the effects of Ca<sup>2+</sup> at the silica/water interface. Those SHG studies have focused on the adsorption behavior of the divalent metals (Ca<sup>2+</sup>, Mg<sup>2+</sup>, Sr<sup>2+</sup>, and Ba<sup>2+</sup>) onto the silica/water interface at pH 7.<sup>114, 134</sup> They showed that the binding constants of the alkaline earth cations generally increased with increasing ion polarizability.<sup>114, 134</sup> Thus there is a need to study the role that pH plays in the behavior of more concentrated Ca<sup>2+</sup> ions. This will hopefully lead to a better understanding of the unusual phenomena that is observed in the presence of higher concentrations of calcium.

The effects of 0.1 M CaCl<sub>2</sub> with a background electrolyte of 0.01 M NaCl on the SHG electric field as the pH of the bulk solution is varied is shown in Figure 5.1. The 0.01 M NaCl was added to the sample solution to keep the Na<sup>+</sup> or Cl<sup>-</sup> concentration fairly constant due to the addition of NaOH. The addition of these solutions changed the volume of the sample solution less than 5% and was considered to be negligible. These 0.1 M CaCl<sub>2</sub> titrations done at high pH (pH 6-12) were dramatically different from the reference 0.1 M NaCl titration over a similar pH range. In the high pH titrations with CaCl<sub>2</sub>, the SHG intensity increased with increasing pH until a maximum SHG signal was reached. This was then followed by a decrease in the SHG signal intensity with a further increase in bulk solution pH (Figure 5.1). Although we performed the SHG measurements until pH 12, we observed that at this pH the sample solution precipitated Ca(OH)<sub>2</sub>. Based on the K<sub>sp</sub> of Ca(OH)<sub>2</sub> the sample solution should not precipitate until about 11.7.<sup>135</sup> The absorbance of the calcium solutions at the different pH values was measured by UV-Vis absorbance spectroscopy to ensure no scattering was observed, which would signify precipitation of the solution (data not shown).

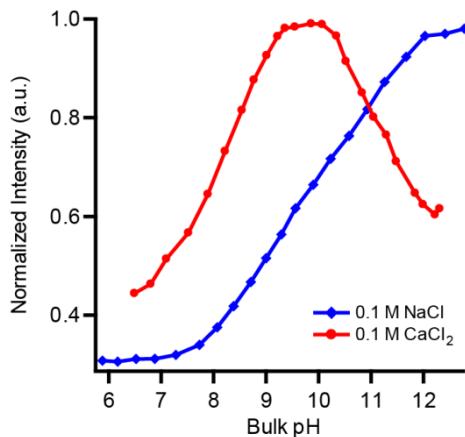


**Figure 5.1** Representative SHG titrations (*p*-in/all out polarization) on fused silica in the presence of 0.1 M NaCl and 0.1 M CaCl<sub>2</sub> with 10 mM NaCl. The spectra were divided by the highest intensity signal to normalize the spectra to 1.0.

Decreasing the concentration of the calcium in the bulk solution to 0.01 M caused the pH where maximum SHG was observed to shift to higher pH (Figure 5.2). The net decrease in SHG upon further increasing the pH after the maximum was reached was also less pronounced at lower concentration. One possible explanation for the concentration dependence is that as the surface is deprotonated, the negative surface (*i.e.*, the siloxides) attract more Ca<sup>2+</sup> ions to the interface until it is neutralized. If a greater amount of ions are present in the bulk solution, then the surface does not need to be as negatively charged to attract the same amount of ions to the surface. Consequently at higher concentration, the decrease in SHG happens at a lower pH value. To verify whether the SHG and our proposed mechanism of calcium binding could be further explained by the direct measurement of water at this interface, we performed the complementary SFG experiments.

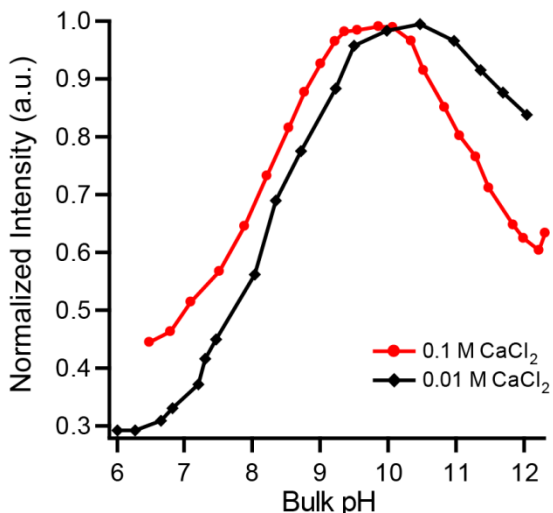


**Figure 5.2** Representative SHG titrations (*p*-in/all out polarization) of the silica interface in the presence of 0.1 M  $\text{CaCl}_2$  (red circles) and 0.01 M  $\text{CaCl}_2$  (black diamonds). The intensity at each pH point was divided by the maximum intensity in the titration. All titrations had a background electrolyte of 0.01 M NaCl to account for changes in sodium concentration with the addition of sodium hydroxide.

### 5.3.3 Effect of $\text{CaCl}_2$ on SFG

With regard to the SFG studies, one study on silica conducted at pH 10 found that  $\text{Mg}^{2+}$  attenuated the water signal more than  $\text{Ca}^{2+}$  at low concentrations of the electrolytes (0.033 mM).<sup>79</sup> However it is typically the higher concentrations of the divalent ions that cause the unusual behavior of the silica.<sup>2, 65, 69, 131-132</sup> Indeed, while we were working on this study Chou, Bertram and co-workers found that the water structure decreased substantially upon adding high concentrations (4 M) of calcium or magnesium chloride.<sup>136</sup> To understand the interplay between pH and high concentrations of calcium chloride as well as the unusual pH dependence of the SHG signal we performed similar experiments as those above but monitored the water structure at the interface by SFG. In the *ssp* SFG spectra, we observed two peaks, one at  $\sim 3200 \text{ cm}^{-1}$  and another one at  $\sim 3400 \text{ cm}^{-1}$ , which is typical of the SFG spectrum observed for the planar silica/water interface.<sup>35</sup> The surface was first exposed to pure water and then the solution was replaced with the salt solution at pH 5.5-5.8. When the 0.1 M calcium was added, the intensity of

the *ssp* SFG water spectra decreased dramatically, which is consistent with the ions screening the charge of the interface leading to less aligned water, particularly in the diffuse layer which we associate with the mode at  $3200\text{ cm}^{-1}$  (Section 4.3.3).<sup>49</sup> However, as the pH of the solution was increased in the presence of  $\text{CaCl}_2$  the SFG intensity decreased and reached a minimum in the SFG signal around pH 10.0-10.5 (Figure 5.3A). As the pH of the bulk solution was increased further, the SFG signal began to increase. Moreover, as the signal increased with increasing pH (pH 10 and higher) a peak at lower wavenumber around  $3000\text{ cm}^{-1}$  became prominent in the SFG spectra.

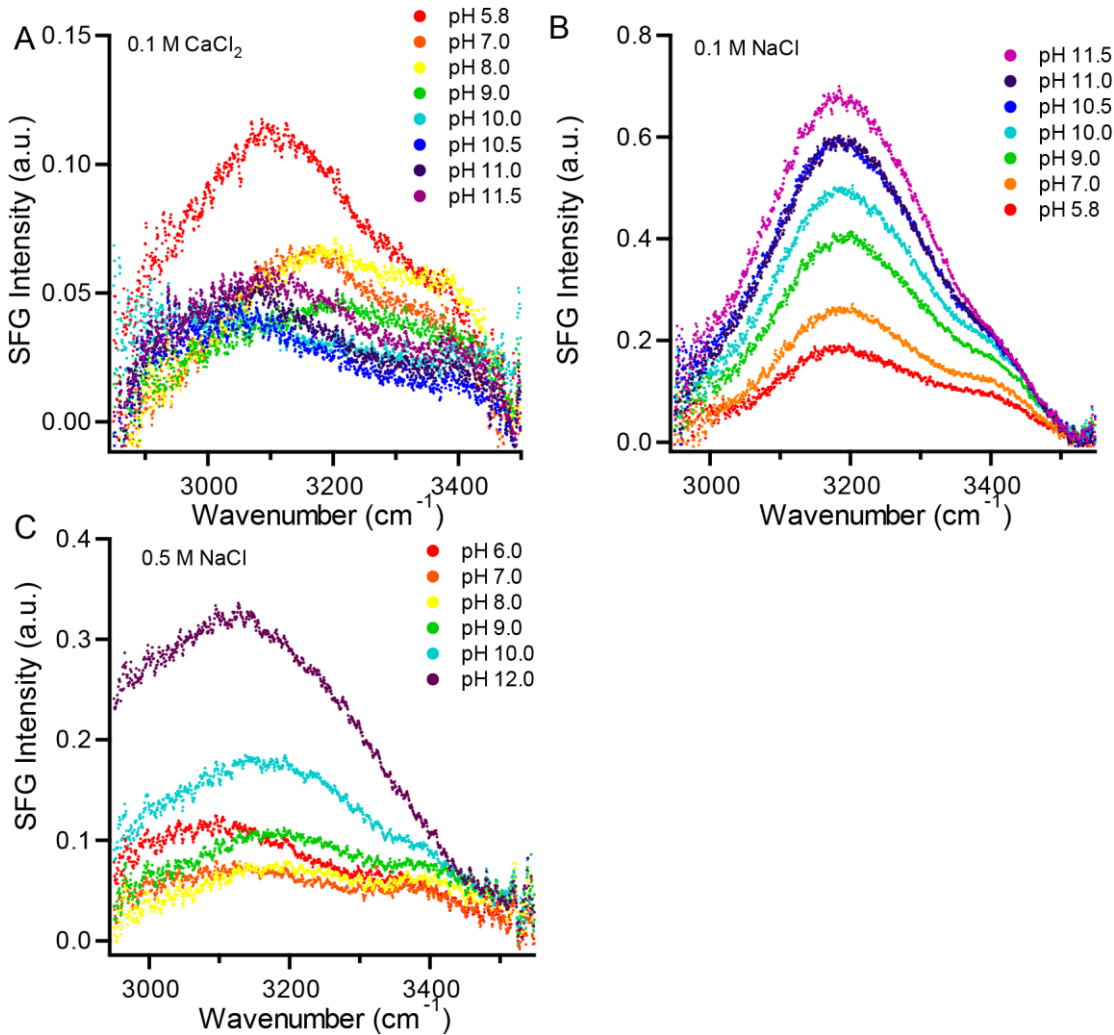


**Figure 5.3** *ssp* polarized SFG of: A) Silica/CaCl<sub>2</sub> aqueous interface (0.1 M + 0.01 M NaCl) from pH 6.0 to pH 11.5. B) Silica/0.1 M NaCl interface from pH 6.0 to pH 12.0 C) Silica/0.5 M NaCl interface from pH 6.0 to 12.0.

The trend that is observed in SFG signal in the presence of calcium (Figure 5.3A) is not what is typically observed when the pH is increased on a silica surface in the presence of 0.1 M monovalent ions like Na<sup>+</sup>, where the SFG signal generally increases as the silica surface is deprotonated from pH 6 to 11.5 (Figure 5.3B).<sup>35-36, 49</sup> When we compare 0.5 M NaCl, the SFG intensity decreases from pH 6 to 7, then increases from pH 8-12. In Section 3.3.2 we showed that the minimum of the SFG for 0.1 M was around pH 5-6 and the minimum was between pH 7-8 for 0.5 M NaCl. If CaCl<sub>2</sub> behaved similar to monovalent NaCl, we would expect the minimum

of the SFG in the presence of 0.1 M CaCl<sub>2</sub> (ionic strength of 0.3 M) to be between pH 5-8. Instead, CaCl<sub>2</sub> causes the minimum in the SFG to occur between pH 10.0 - 10.5. In addition, the minimum intensity observed is much lower in the presence of 0.1 M CaCl<sub>2</sub> compared to 0.5 M NaCl. The effect of CaCl<sub>2</sub> decreasing the overall SFG intensity more than NaCl has been previously observed at both low<sup>79</sup> and high concentrations.<sup>136</sup>

### 5.3.4 *pss* Polarized SFG

In the previous Section 4.3.3, the *pss* polarized SFG has similar trends to *pss* polarized SHG. Furthermore, the *pss* polarized SHG data resembled both the *p*-in/all out polarizations and *s*-in/all out polarizations in SHG experiments indicating that the common  $\chi^{(2)}$  element for all of these polarization combinations,  $\chi_{zii}^{(2)}$  (where ii = xx or yy), is the dominant contributor. In this case for the silica water interface in the presence of NaCl (0.1 or 0.5 M), the water mode at 3400 cm<sup>-1</sup> which is most sensitively probed by *pss* did follow the trend observed in the SHG. In Section 4.3.3 it was concluded that the *pss* SFG polarization combination probes the behavior of the water molecules that are closest to the surface as there is little no contribution in the spectra from the mode at 3200 cm<sup>-1</sup>. Therefore, determining how the surface waters are behaving could provide insight on the mechanism of interaction of calcium with the surface as well as the origin of the unusual SHG behavior.

In the *pss* polarization combination, the SFG behaves in a unique manner compared with what was observed for the silica interface in the presence of 0.1 or 0.5 M NaCl (Section 4.3.3). The SFG signal of the 3400 cm<sup>-1</sup> peak increased from pH 5.3 to pH 8, then decreased from pH 9 to 11, and then increased slightly from pH 11.0 to pH 11.5. In contrast, there appears to be a peak growing in at 3000 cm<sup>-1</sup> at the higher pH values (Figure 5.4).

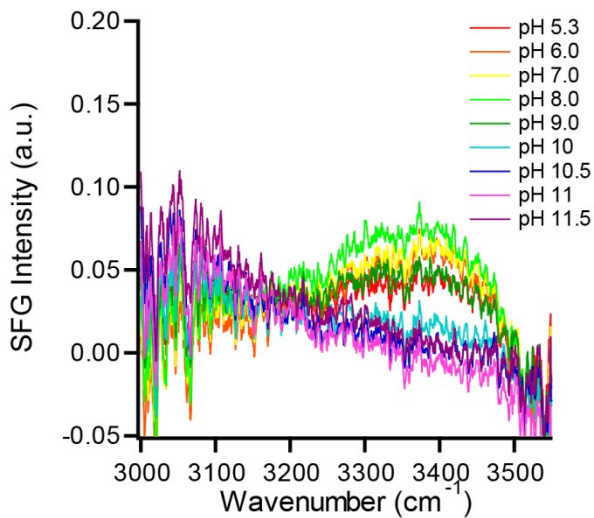


**Figure 5.4** Representative SFG titration of the silica interface with the *pss* polarization combination in the presence of 0.1 M  $\text{CaCl}_2$  and 0.01 M  $\text{NaCl}$ .

When the integrated area is calculated for the above graph and its three replicates, two trends emerge. The peak between  $3000\text{-}3200\text{ cm}^{-1}$  increases with pH, while the peak between  $3200\text{-}3400\text{ cm}^{-1}$  generally decreases with pH. The average of the integrated area was plotted for each peak range  $3000\text{-}3200\text{ cm}^{-1}$  (Figure 5.5A) and  $3200\text{-}3400\text{ cm}^{-1}$  (Figure 5.5B). It is noted the integrated area region  $3000\text{-}3200\text{ cm}^{-1}$  has significant noise and therefore may not be reliable. The high noise in this region is caused by low IR power, and thus would need to be repeated with either longer acquisition times or more IR power.

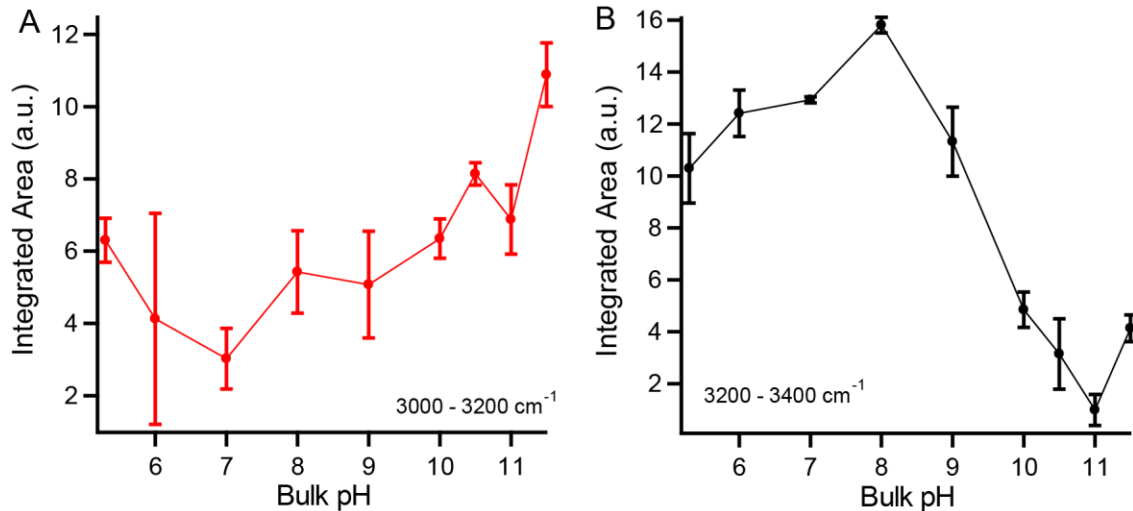


**Figure 5.5** Average integrated area of *pss* polarized SFG of the silica/0.1 M CaCl<sub>2</sub> with 0.01 M NaCl background electrolyte. A) Integrated from 3000 – 3200 cm<sup>-1</sup> B) Integrated from 3200 – 3400 cm<sup>-1</sup>. The error bars represent the standard deviation of the three replicates of the titrations on cleaned silica samples.

From the *pss* polarized SFG, it is clear that as one population of water decreases (~3400 cm<sup>-1</sup>) another population grows in (~3000 cm<sup>-1</sup>). Consequently the alignment of water cannot be the only reason for the shape of the SHG (*p*-in/all out polarization combination, Figure 5.1). From pH 8-11 the amount of water appears to be decreasing for the 3400 peak and level for the 3000 cm<sup>-1</sup> peak yet the SHG is increasing at the same pH region. In our assessment of the possible contributions to the second-order susceptibility ( $\chi^{(2)}$ ) we assumed that there was very little contribution from  $\chi_{ions}^{(2)}$ . At low pH, Ca<sup>2+</sup>, Cl<sup>-</sup>, and Na<sup>+</sup> will be the dominant species in the bulk solution; however at higher pH's Ca<sup>2+</sup> can complex with OH<sup>-</sup>. If the CaOH<sup>+</sup> species has a net orientation at the interface, then the SFG in the OH region would also contain the contribution of the CaOH vibrational mode, albeit at higher wavenumber than the water molecules.

### 5.3.5 Probing the CaOH Vibrational Mode

To verify if CaOH was present at the interface, SFG was performed at higher wavenumber. The Ca-OH vibrational mode has been previously observed around 3630-3650  $\text{cm}^{-1}$  at the  $\text{CaF}_2$ /water interface.<sup>41, 137</sup> Therefore by expanding the OH range that is probed, we can monitor if a CaOH vibrational mode appears at the silica/ $\text{Ca}^{2+}$  interface at high pH.

In Figure 5.6 the range over which the SFG of the silica/aqueous calcium spectra was measured was expanded to include the CaOH vibrational region. As our experimental laser set up was not able to reach these high IR wavenumber, I visited the lab of Prof. Eric Tyrode at KTH Institute of Technology in Stockholm who had developed a set-up that was optimized for the high IR wavenumber range. In collaboration with his student, Adrian Sthoer, we performed the same *ssp* SFG experiments (and the *ppp* polarization combination) using their silica samples and cleaning procedures, which differed slightly from our procedure but also involved a strong acid wash step. For the pure water spectrum at the silica interface, in addition to the 3200 and 3400  $\text{cm}^{-1}$  peaks that are typically detected, a prominent peak at 3600  $\text{cm}^{-1}$  was observed (Figure 5.6). This 3600  $\text{cm}^{-1}$  peak has been reported in only a small fraction of the silica/water literature, likely because most experimental set-ups are not optimized for the high wavenumber region.<sup>43, 46-49</sup> Although the origin of this 3600  $\text{cm}^{-1}$  peak in the absence of calcium is not fully understood, the corresponding oscillator is solvent exposed because  $\text{D}_2\text{O}$  is able to exchange this OH to an OD based on the appearance of the OD vibrational mode at the corresponding high wavenumber (Figure 5.6).<sup>43</sup>

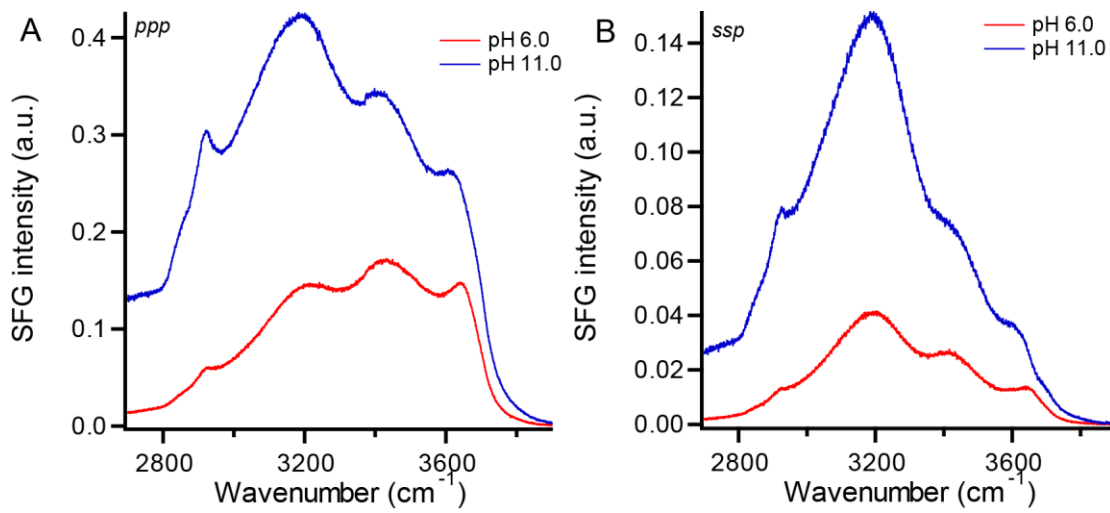


**Figure 5.6** Representative SFG spectra of the OH vibrational region of the silica/ 0.01 M NaCl interface at A) *ppp* polarization and B) *ssp* polarization on Dr. Tyrode's laser assembly.

Upon introducing calcium chloride at 0.1 M with 0.01 M NaCl also present, similar trends were observed at the silica/Ca<sup>2+</sup> interface for these two different SFG platforms in the 3000-3500 cm<sup>-1</sup> range. In general in both laboratories we observed the least amount of SFG signal around pH 10-10.5 with an increase in the SFG signal at pH 11.5. There was a slight difference at pH 8 in the data between the two labs. However the overall trend of the SFG spectra were the same. Most excitingly, at pH 10.5 we observed the presence of an interfering spectral peak in the SFG that caused a dip in the spectra around 3610 cm<sup>-1</sup> and increased in intensity as the pH of the bulk solution was increased to 11.5.

Due to the coherent nature of the SFG process, the OH stretching modes of both the H<sub>2</sub>O and the CaOH will either add constructively or destructively. If the OH modes of the H<sub>2</sub>O and the CaOH add destructively, meaning they are orientated in opposite directions, a dip will appear in the resulting SFG spectra.<sup>106</sup> To ensure that the interfering mode is a result of the presence of calcium at high pH, SFG in the presence of 0.01 M NaCl at pH 6 and pH 11 was collected

(Figure 5.6). When only NaCl was present, there was no interfering peak seen in the SFG spectrum at high pH. This confirms that the interfering mode can be attributed to the presence of calcium in the system.

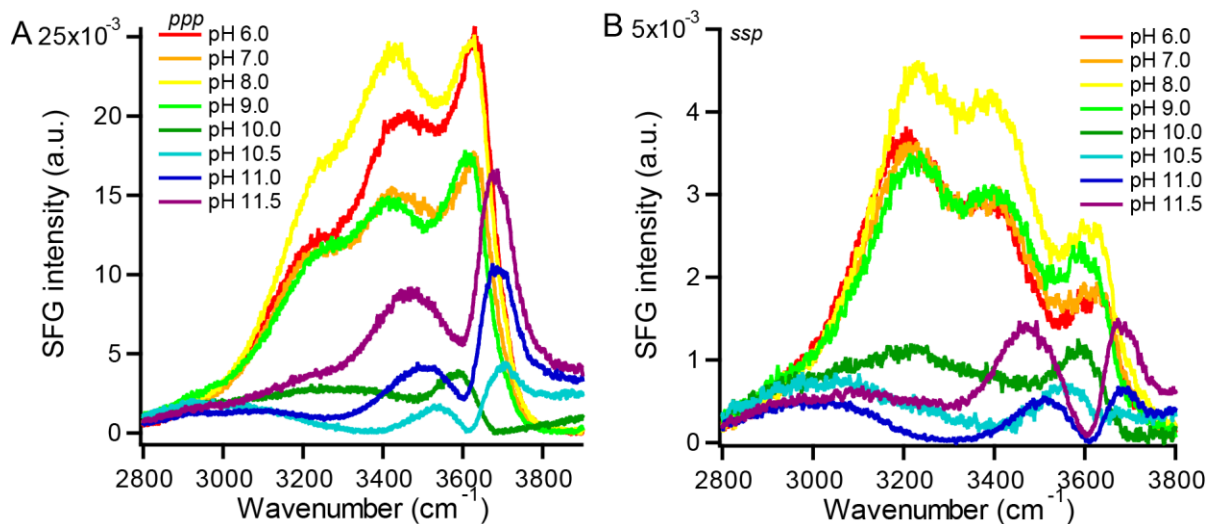
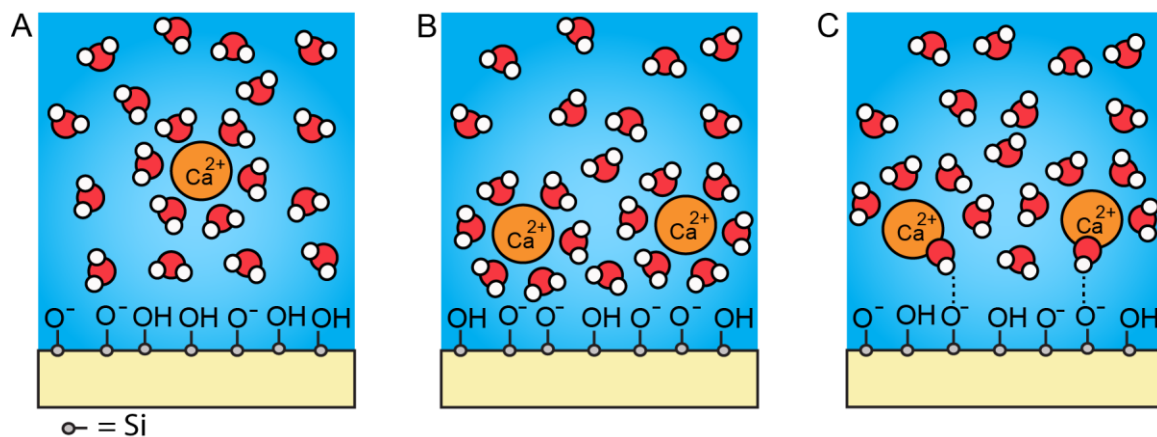


**Figure 5.7** Representative SFG of the silica/0.1 M  $\text{CaCl}_2$  interface at A) *ppp* polarized SFG; and B) *ssp* polarized SFG collected on Dr. Tyrode's laser assembly.

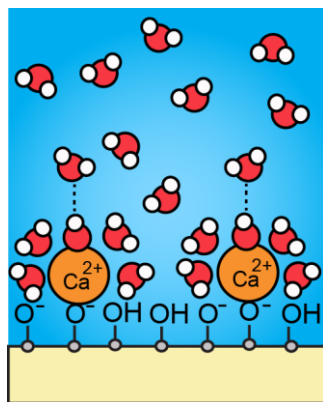
The only other interface that has been reported to have a CaOH mode present in the SFG spectrum is the  $\text{CaF}_2$ /water interface. At the  $\text{CaF}_2$ /water interface, the CaOH mode was observed as a narrow peak with a center wavenumber of  $3657\text{ cm}^{-1}$ , which only appeared at high pH values (above pH 9.3).<sup>41</sup> The position and width of the peak at the  $\text{CaF}_2$ /water interface indicated that it was a weakly hydrogen-bonded OH oscillator with a long vibrational lifetime. Further studies on the  $\text{CaF}_2$ /water interface with phase-sensitive SFG observed the CaOH mode did not significantly hydrogen bond with water molecules.<sup>137</sup> The experiments and supporting molecular dynamics simulations also found that the CaOH mode had a negative  $\text{Im}(\chi^{(2)})$ , indicating that the hydrogen of the OH was directed away from the surface out into the bulk.<sup>137</sup> The direction of the OH can be rationalized as ion exchange at high pH between the fluoride and the hydroxide ions at the interface. At the silica interface, however, the calcium ions are free in solution and not in a

crystalline form. The CaOH in our system, therefore, can have more possible orientations than the CaOH group at the  $\text{CaF}_2$ /water interface. In our experiments at the silica interface, the interference in the spectra is likely caused by the CaOH and the weakly hydrogen bonded  $\text{H}_2\text{O}$  at  $3600 \text{ cm}^{-1}$  having opposite orientations.<sup>106</sup> Studies have shown that zeta potentials in the presence of higher concentrations calcium ( $0.01 \text{ M } \text{Ca}^{2+}$ ) reverse from a negative to positive potential at around pH 10.<sup>69</sup> If we assume that the electrical double layer is overcharged above pH 10 in the presence of  $0.1 \text{ M } \text{CaCl}_2$ , then water molecules might have their hydrogens pointed away from the surface. In addition, the surface waters corresponding to the  $3400 \text{ cm}^{-1}$  peak, were disrupted by the high concentration of the calcium ions at the interface (Scheme 5.2B). For interference of the OH vibrational mode to occur, the hydrogen in the CaOH mode has to be pointed towards the surface. The CaOH could then hydrogen bond with the surface siloxides (Scheme 5.2C). Interaction of the CaOH bond with the surface would be help to dissipate the energy of the OH excited vibrational state and broaden the CaOH vibrational mode in the resulting SFG spectra.



**Scheme 5.2** Depiction of the silica/calcium interface as pH is increased. A) The pH where surface waters are being aligned by the surface siloxides. B) The pH where calcium disrupts the surface waters. C) The pH when a CaOH species forms and hydrogen bonds with the surface siloxides.

To review, the *pss* polarized SFG of the  $3400\text{ cm}^{-1}$  peak shows the surface waters to be orientated below pH 10 (Scheme 5.2A). Around pH 10, however, the surface waters are completely disrupted by the high concentration of the calcium ions at the interface (Scheme 5.2B). If this calcium were hydrated as expected, it could still result in no water signal owing to the centrosymmetry of the hexahydrate calcium ion. This explains the disappearance of the water signal for all but the weakly hydrogen bonded water mode at  $3600\text{ cm}^{-1}$  which is not associated with pH sensitive sites. As the pH of the bulk solution was further increased, the new mode at  $3610\text{ cm}^{-1}$  suggests that  $\text{CaOH}^+$  species are formed at the interface. These species can hydrogen bond with the surface siloxides or silanol groups with the hydrogen of the hydroxide pointed down (Scheme 5.2C). Another scenario is if the  $\text{CaOH}^+$  species electrostatically interacts with the interface where the  $\text{CaOH}$  would point up towards the bulk (Scheme 5.3). In this scenario, as the water signal still remains absent at  $3200$  and  $3400\text{ cm}^{-1}$  wavenumber, we propose that the surface siloxide displaces one of the water ligands around  $\text{Ca}(\text{H}_2\text{O})_5(\text{OH})^+$  resulting in an centrosymmetric structure and no SFG signal from the coordinated waters. As the absolute phase of the  $\text{CaOH}^+$  mode is unknown at the silica/water interface, either scenario is possible. It is noted that in Scheme 5.2 the water are drawn with six coordinated water molecules, which results in an octahedral structure. This depiction of the hydrated calcium ion is only one of the many forms the water molecules can coordinate to the calcium ion. Higher coordination of water molecules to the calcium ion has been predicted, although the structure of the hydrated calcium ion still appears to possess a centrosymmetric structure.



**Scheme 5.3** Alternative CaOH formation at high pH values where the OH vibrational mode is pointed with hydrogen towards the bulk.

One advantage of the latter proposed mechanism is that it explains why the water signal at 3200 and 3400 cm<sup>-1</sup> remains very small as the CaOH mode grows in. Indeed, one of the problems with the recent report by Chou, Bertram and co-workers is that they rationalize the disappearance of water signal by the formation of a partially hydrolyzed water on hexahydrate calcium.<sup>136</sup> As this structure is not centrosymmetric just as the calcium hydroxide pentahydrate is not centrosymmetric, one would expect it to contribute to the water signal. As we can separately monitor the formation of the CaOH species, we are able to show in Figure 5.7 that the water signal first disappears followed by the formation of CaOH. Therefore, it seems more reasonable that hydrated calcium ion directly dehydrates the surface. At higher pH, new species form including calcium hydroxide, which may be proceeded by the partially hydrolyzed calcium hydrate species. Consequently, our work disagrees with the overarching conclusion of the work of Chou, Bertram and coworkers that the absence of water signal necessitates the formation of a partially hydrolyzed species.<sup>136</sup>

It is interesting to compare the results of SHG of the silica/aqueous calcium interface to our SFG data of the OH vibrational stretch region. Figure 5.8 shows the water referenced signal intensities for SHG (Figure 5.8A), and for the water referenced integrated areas of the *ssp*

polarized SFG from the Gibbs-Davis laser assembly (Figure 5.8B), *ssp* polarized SFG from the Tyrode laser assembly which includes the modes at  $3600\text{ cm}^{-1}$  (Figure 5.8C), and the *pss* polarized SFG from the Gibbs-Davis laser assembly (Figure 5.8D).

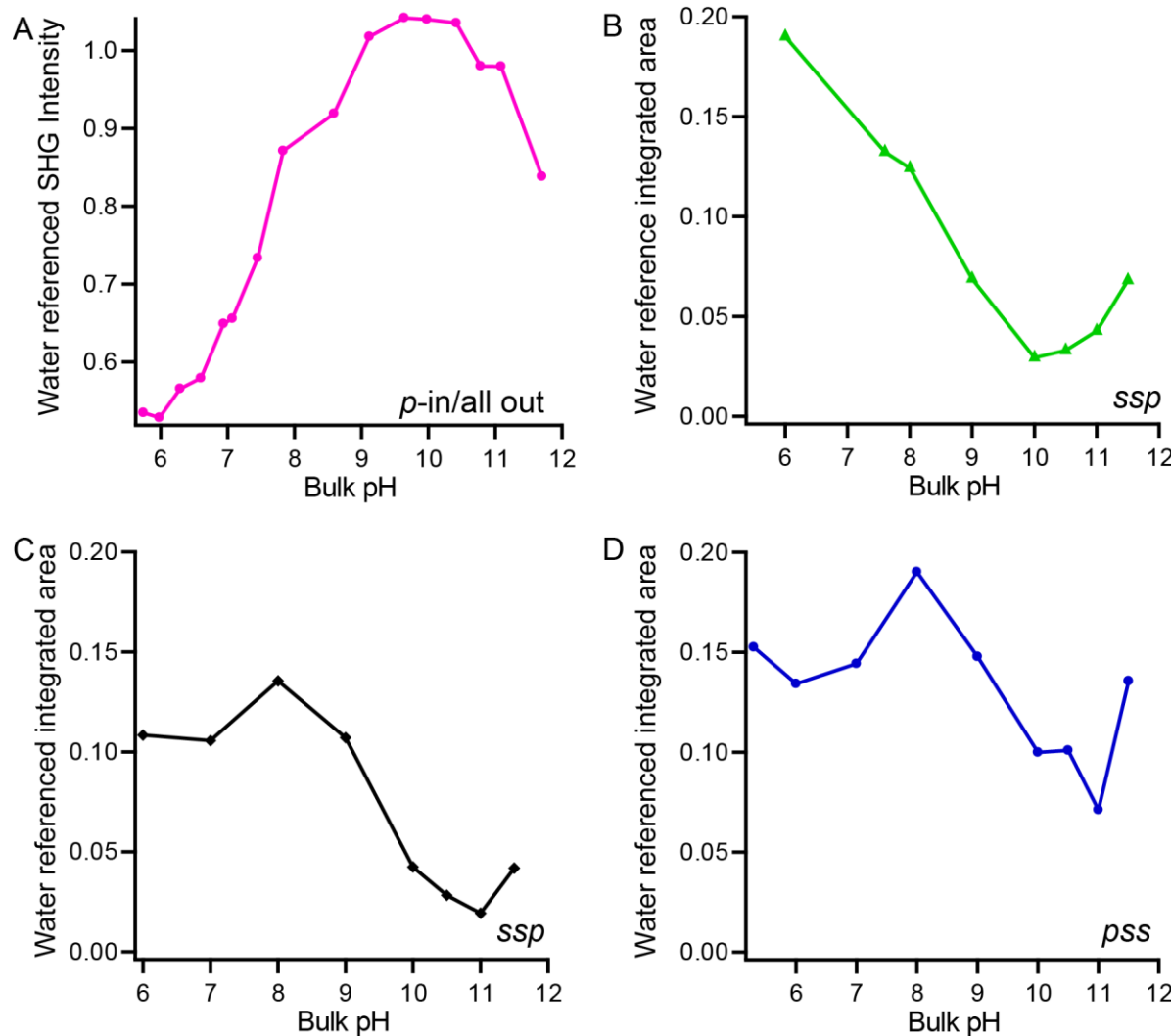


**Figure 5.8** Representative titrations of water referenced data for the silica/CaCl<sub>2</sub> (0.1 M + 0.01 M NaCl) interface A) *p-in/all out* SHG intensity. Representative titrations SFG of the OH vibrational region for the silica/CaCl<sub>2</sub> (0.1 M+ 0.01 M NaCl) interface: B) Integrated area (3000-3450  $\text{cm}^{-1}$ ) of the *ssp* polarized SFG spectra measured on the Gibbs-Davis laser assembly; C) Integrated area (2800-3800  $\text{cm}^{-1}$ ) of the *ssp* polarized SFG on the Tyrode laser assembly; and D) Integrated area (3000-3450  $\text{cm}^{-1}$ ) of the *pss* polarized SFG on the Gibbs-Davis laser assembly.

The SFG data (Figure 5.8B and Figure 5.8D) does not explain the trend observed in the SHG (Figure 5.8A). For example, with the CaOH peak (around  $3600\text{-}3650\text{ cm}^{-1}$ ) increasing in intensity at high pH (greater than pH 10), this would mean an increase in the magnitude of the SHG at high pH, which is not what we observed. In addition, when all of the data is referenced to water, the SHG signal is significantly larger compared to any of the SFG data sets. In the previous Section 4.3.3 we theorized that the enhancement in SHG signal could be a result of a larger  $\beta$  of the deprotonated siloxide owing to the increased electron density. The interaction of the CaOH mode with the siloxide site either through hydrogen bonding or electrostatic interactions could decrease the electron density around the surface silanols. This could account for the decrease at high pH observed in the SHG at the silica/water interface in the presence of calcium.

## 5.4 Conclusions

We have conducted one of the first studies on the effects of calcium at the silica/water interface as a function of pH. Molecular level pictures of the pH-dependent behavior at the silica/water interface in the presence of calcium is key for understanding mineral processing from calcium rich soils. The effect of calcium on the silica/water interface is more complex than originally thought. Closer to neutral pH values, the surface water is orientated by the static electric field set up by the negative charge on the silica. As the pH of the bulk solution increases calcium disrupts the interfacial water to a degree where there is very little aligned water. At high pH values a CaOH vibrational mode becomes prominent in the SFG spectra and is observed as an interfering peak at about  $3600\text{ cm}^{-1}$ . This CaOH vibrational mode increases in intensity as the bulk pH is further increased. In addition, the SHG (*p*-in/all out) does not match the SFG water

spectra in either *ssp* or *pss* polarization. The data suggest that the SHG signal has contributions from the water molecules, the CaOH mode, and the siloxides at the surface.

## **CHAPTER 6**

General Conclusions

## 6.1 General Conclusions

The nonlinear optical techniques second harmonic generation (SHG) and sum frequency generation (SFG) are well suited to study how interfacial molecules behave. These nonlinear optical techniques provide many advantages such as being able to distinguish molecules that are aligned at the surface versus those in the bulk solution at buried interfaces of insulators like silica. The goal of this thesis was to gain insights into how the silica/water interface is perturbed by ion identity, concentration and pH using both non-resonant SHG and SFG. The silica/water interface is ubiquitous in nature and in industry, and thus studying how the silica/water interface responds to perturbations allows for a better molecular understanding of the interface. The results of this thesis allowed us to further our understanding of the underlying equations in SHG and SFG and what contributes to the signal intensity.

Specifically I have explored how the effects of experimental starting pH change the interfacial acid-base chemistry of the silica/water interface in the presence of 10 mM NaCl using SHG.<sup>108</sup> When the titrations are initiated at pH 7, we observe the bimodal distribution that is prevalent in the literature for acid-base titrations of the silica/water interface.<sup>26, 75-77</sup>. The pK<sub>a</sub> values were calculated to be 3.8 for the most acidic silanol group and 8.6 for the least acidic silanol group. When the titration was initiated at pH 12, the silica/water interface exhibited trimodal behavior, which has never been observed for a planar silica surface before. The pK<sub>a</sub> values of the three sites were 3.8, 5.2 and 9.6 for pK<sub>a</sub>-I, pK<sub>a</sub>-II, and pK<sub>a</sub>-III. In contrast when the titration was initiated at the other pH extreme, pH 2, we observed a lag in the response of the SHG till pH 4, which resulted in two pK<sub>a</sub> values of 5.3 and 9.6. Based on recent computational studies of the silica/water interface,<sup>31-33</sup> we proposed that the three distinct pK<sub>a</sub> values were due to three distinct hydrogen bonding environments. This work indicated that the pH history that the

sample experienced influenced both the surface charge density and the type of surface sites present at the silica water interface. In addition, the presence of hysteresis questions our use. Equilibrium constants, like the acid dissociation constant, are calculated based on the equilibrium concentration of the products and reactants. If changing the starting pH of the experiment causes metastable states to form at the interface that are not at thermodynamic equilibrium then the use of acid dissociation constants and equilibrium double layer models like the Gouy-Chapman model to quantify the behavior of the silica/water interface could be problematic.

In Eisenthal and coworkers original SHG study of silica, they theorized that the changes observed in the SHG intensity upon deprotonation of the interface was due to the increase in water molecules that were orientated due to the increase of the static electric field. Vibrational SFG can be utilized to study the alignment of water directly at the silica surface. Therefore, in Chapter 3, we focused on high concentration ions for our SFG to emulate the conditions used in Eisenthal and coworkers seminal work from 1992.<sup>26</sup> Specifically, we focused on the effects of ion concentration and experimental starting pH on the alignment of water molecules at the silica/water interface in the presence of NaCl. If the observed changes in SHG intensity upon variation of the solution pH are due only to the alignment of water molecules, then SHG and SFG should have the same pH-dependent behavior. Using *ssp* polarized SFG, the most common SFG polarization to probe interfacial water; we found that the integrated intensities of the *ssp*-SFG spectra as a function of pH did not match the intensity of the SHG in Eisenthal and coworkers original paper. Because the collected data challenges the models governing SHG at the silica/water interface, the results of our SFG experiments were externally verified by Dr. Dennis Hore and Tasha Jarissz. Based on the changes in intensity as a function of pH, we believe that *ssp* polarization mainly probes water molecules that are further from the surface. Moreover,

in the case of high salt concentrations, sodium can either overcharge the silica surface at low pH, or it could become partially dehydrated at the interface, breaking the symmetry of the hydrated cation. Both of these scenarios could cause the water molecules to flip their net orientation. Water molecules that change their orientation upon changes in pH have been previously suggested in the literature from phase-sensitive SFG measurements at the low salt silica/aqueous interface.<sup>13-14</sup> Finally, the effect of the experimental starting pH had little effect on the *ssp* polarized SFG, unlike SHG where the experimental starting pH had significant impact on the shape of the SHG intensity. These results further confirm that *p*-in/all out SHG (*i.e.*, *spp* + *ppp* SHG) and *ssp* polarized SFG are probing different aspects of the silica/water interface.

In the SHG and SFG literature, it is sometimes difficult to compare results because different polarization combinations, samples, cleaning procedures, and laser setups are used. Consequently, to be able to make a direct comparison between SHG and SFG, the *pss* polarization combination was utilized because only one tensor element is probed and it is easily set up on both SHG and SFG. When *pss* polarization was utilized, both SHG and SFG exhibited similar trends in the changes in signal intensity to pH. In *pss* polarized SFG, the 3400 cm<sup>-1</sup> peak was most prominent and was thought to be due to water molecules that were closest to the silica surface. However, we found that the magnitude of the intensity of these aligned waters cannot account for the entire SHG intensity change that is observed. Therefore there must be a contribution from another of the interfacial species contributing to the magnitude of the SHG signal. We proposed that the enhancement in the SHG signal intensity was due to the increased electron density at the silica surface upon deprotonation of the silanol to siloxides. The increased electron density would increase the contribution of  $\chi_{Silica}^{(2)}$ , which resulted in a larger contribution to the resultant SHG signal intensity. These results show that the original theory

about the changes in SHG intensity as a response to pH changes is not due entirely to the alignment of water molecules, but is also a result of the changing  $\chi_{Silica}^{(2)}$  upon deprotonation of the interface. This is a significant discovery for the nonlinear optics community as it may change interpretations of previous data where the SHG signal intensity changed as a response to changes in pH.

Chapter 5 of the thesis focused on the effects of divalent calcium on both SHG and SFG. Calcium is an interesting system to study because calcium is known to cause low extraction efficiencies of bitumen crude oil from silica sands in the Athabasca Oil Sands processing at high concentrations.<sup>2, 132</sup> In the presence of CaCl<sub>2</sub>, both the pH-dependent SHG and SFG did not behave like SHG and SFG observed in the presence of monovalent NaCl. In SHG the signal intensity increased as the pH was increased to pH 10.0-10.5. The SHG signal intensity then decreased from pH 10.5 -12.0. This is in contrast to the behavior of the SFG of the OH vibrational stretch region in the presence of calcium, where the SFG intensity decreased until pH 10.0-10.5. The SFG signal intensity then increased upon further increasing the pH. In addition, when the range of SFG was expanded to higher wavenumber, a mode at 3610 cm<sup>-1</sup> caused interference in the water spectra, which was assigned to a CaOH vibration. As in the case of the SHG in the presence of NaCl, the SHG intensity in the presence of CaCl<sub>2</sub> also cannot be explained by changes in the alignment of waters due to the static electric field. Instead, we believe that the SHG signal increased from pH 6.0-10.5 because of the increase in the  $\chi_{Silica}^{(2)}$  upon deprotonating the surface. At pH 10.5 the formation of a CaOH<sup>+</sup> species and its direct complexation with surface siloxide sites caused a decrease in the  $\chi_{Silica}^{(2)}$ , which consequently decreased the SHG signal intensity. Overall the data presented in this thesis challenges the

models that govern the understanding of the causes of the SHG intensity, which is one of the greatest accomplishments of this work.

Another major accomplishment of this thesis is the work on the effects of NaCl on interfacial water structure. We have definitively shown that at high concentrations, NaCl considerably changes the behavior of water molecules and that the different layers of water molecules can be separately probed with different polarization combinations of light. In addition the work performed on the silica/water interface could be used to help understand the effects of these salts at other silicate mineral/water interfaces. However there is still much research that needs to be explored. For example, this thesis focused on the use of conventional SFG to monitor the behavior of water molecules at the silica/water interface. In conventional SFG the absolute square of the  $\chi^{(2)}$  is measured, which causes information of the phase of  $\chi^{(2)}$  to be lost. Phase sensitive SFG allows for the retention of this phase information. Applying phase sensitive SFG measurements to the studies performed in this thesis would either support or challenge our hypotheses about the effect of both NaCl and CaCl<sub>2</sub> on the silica/water interface. In addition, measurements of the zeta potentials in the presence of both NaCl and CaCl<sub>2</sub> would be helpful in confirming our hypotheses.

Studying different interfaces like, Al<sub>2</sub>O<sub>3</sub>, TiO<sub>2</sub>, and CaF<sub>2</sub> in the presence of high concentrations of salts like NaCl would also be interesting. These interfaces have points of zero charges at higher pH compared to silica, which has a point of zero charge around pH 2-3. Determining how the water molecules in the diffuse layer are behaving (3200 cm<sup>-1</sup> peak) and the water molecules close to the surface is important for understanding and modelling environmental systems. These interfaces will have different surface properties that will affect how the water

molecules can bind with the surface. Their different charging behavior, will also affect the alignment of the water molecules at the surface.

Another interesting feature that can be explored is the presence of CO<sub>2</sub> in the water and how the presence or absence of CO<sub>2</sub> affects the SHG and SFG. In our system, the CO<sub>2</sub> can diffuse freely into the system. In other systems, such as flow cells or air free systems, CO<sub>2</sub> cannot diffuse freely into the system. When CO<sub>2</sub> contacts water, a weak acid is formed. The presence of this acid could change the structure of the interface, and could also change how the water molecules respond to changes in pH. In order to study this, we will compare our normal SFG and SHG experiments (the ones described in this thesis) to experiments that are constantly bubbled with nitrogen or argon to remove the CO<sub>2</sub> from the sample solutions. This will allow us to study the effect of CO<sub>2</sub> at the silica/water interface.

## References

1. Geiger, F. M., Second Harmonic Generation, Sum Frequency Generation, and X(3): Dissecting Environmental Interfaces with a Nonlinear Optical Swiss Army Knife. *Annu. Rev. Phys. Chem.* **2009**, *60*, 61-83.
2. Masliyah, J.; Zhou, Z. J.; Xu, Z.; Czarnecki, J.; Hamza, H., Understanding Water-Based Bitumen Extraction from Athabasca Oil Sands. *Can. J. Chem. Eng.* **2004**, *82*, 628-654.
3. Schrödle, S.; Richmond, G. L., In Situ Non-Linear Spectroscopic Approaches to Understanding Adsorption at Mineral–Water Interfaces. *J. Phys. D: Appl. Phys.* **2008**, *41*, 033001.
4. Jubb, A. M.; Hua, W.; Allen, H. C., Organization of Water and Atmospherically Relevant Ions and Solutes: Vibrational Sum Frequency Spectroscopy at the Vapor/Liquid and Liquid/Solid Interfaces. *Acc. Chem. Res.* **2012**, *45*, 110-119.
5. Ball, P., Water - an Enduring Mystery. *Nature* **2008**, *452*, 291-292.
6. Richmond, G. L., Molecular Bonding and Interactions at Aqueous Surfaces as Probed by Vibrational Sum Frequency Spectroscopy. *Chem. Rev.* **2002**, *102*, 2693-2724.
7. Shen, Y. R., Surface Properties Probed by Second-Harmonic and Sum-Frequency Generation. *Nature* **1989**, *337*, 519-525.
8. Shen, Y. R., Optical Second Harmonic Generation at Interfaces. *Annu. Rev. Phys. Chem.* **1989**, *40*, 327-350.

9. Lambert, A. G.; Davies, P. B.; Neivandt, D. J., Implementing the Theory of Sum Frequency Generation Vibrational Spectroscopy: A Tutorial Review. *Appl. Spectrosc. Rev.* **2005**, *40*, 103-145.
10. Covert, P. A.; Hore, D. K., Geochemical Insight from Nonlinear Optical Studies of Mineral–Water Interfaces. *Annu. Rev. Phys. Chem.* **2016**, *67*, 233-257.
11. Boyd, R. W., *Nonlinear Optics*; Academic Press: San Diego, California, 1992.
12. Wang, H.-F.; Velarde, L.; Gan, W.; Fu, L., Quantitative Sum-Frequency Generation Vibrational Spectroscopy of Molecular Surfaces and Interfaces: Lineshape, Polarization, and Orientation. *Annu. Rev. Phys. Chem.* **2015**, *66*, 189-216.
13. Ostroverkhov, V.; Waychunas, G. A.; Shen, Y. R., New Information on Water Interfacial Structure Revealed by Phase-Sensitive Surface Spectroscopy. *Phys. Rev. Lett.* **2005**, *94*, 046102.
14. Myalitsin, A.; Urashima, S.-h.; Nihonyanagi, S.; Yamaguchi, S.; Tahara, T., Water Structure at the Buried Silica/Aqueous Interface Studied by Heterodyne-Detected Vibrational Sum-Frequency Generation. *J. Phys. Chem. C* **2016**, *120*, 9357-9363.
15. Shen, Y. R., Phase-Sensitive Sum-Frequency Spectroscopy. *Annu. Rev. Phys. Chem.* **2013**, *64*, 129-150.
16. Sovago, M.; Vartiainen, E.; Bonn, M., Determining Absolute Molecular Orientation at Interfaces: A Phase Retrieval Approach for Sum Frequency Generation Spectroscopy. *J. Phys. Chem. C* **2009**, *113*, 6100-6106.

17. de Beer, A. G. F.; Samson, J.-S.; Hua, W.; Huang, Z.; Chen, X.; Allen, H. C.; Roke, S., Direct Comparison of Phase-Sensitive Vibrational Sum Frequency Generation with Maximum Entropy Method: Case Study of Water. *J. Chem. Phys.* **2011**, *135*, 224701.
18. Velarde, L.; Zhang, X.-Y.; Lu, Z.; Joly, A. G.; Wang, Z.; Wang, H.-F., Spectroscopic Phase and Lineshapes in High-Resolution Broadband Sum Frequency Vibrational Spectroscopy: Resolving Interfacial Inhomogeneities of “Identical” Molecular Groups. *J. Chem. Phys.* **2011**, *135*, 241102.
19. Velarde, L.; Wang, H.-F., Unified Treatment and Measurement of the Spectral Resolution and Temporal Effects in Frequency-Resolved Sum-Frequency Generation Vibrational Spectroscopy (Sfg-Vs). *Phys. Chem. Chem. Phys.* **2013**, *15*, 19970-19984.
20. Grahame, D. C., The Electrical Double Layer and the Theory of Electrocapillarity. *Chem. Rev.* **1947**, *41*, 441-501.
21. Stojek, Z., The Electrical Double Layer and Its Structure. In *Electroanalytical Methods: Guide to Experiments and Applications*, Scholz, F.; Bond, A. M.; Compton, R. G.; Fiedler, D. A.; Inzelt, G.; Kahlert, H.; Komorsky-Lovrić, Š.; Lohse, H.; Lovrić, M.; Marken, F.; Neudeck, A.; Retter, U.; Scholz, F.; Stojek, Z., Eds. Springer Berlin Heidelberg: Berlin, Heidelberg, 2010; pp 3-9.
22. Lyklema, J., *Fundamentals of Interface and Colloid Science Volume II: Solid-Liquid Interfaces*; Academic Press, 1995.
23. Iler, R. K., *The Chemistry of Silica*; John Wiley & Sons, Inc.: United States of America, 1979.

24. Srinivasan, S., *Fuel Cells from Fundamentals to Applications*; Springer: New York, 2006.
25. Chapman, D. L., A Contribution to the Theory of Electrocapillarity. *Philos. Mag. Series 6* **1913**, *25*, 475-481.
26. Ong, S.; Zhao, X.; Eisenthal, K. B., Polarization of Water Molecules at a Charged Interface: Second Harmonic Studies of the Silica/Water Interface. *Chem. Phys. Lett.* **1992**, *191*, 327-335.
27. Bockris, J. O. M.; Devanathan, M. A. V.; Muller, K., On the Structure of Charged Interfaces. *P. Roy. Soc. A - Math. Phy.* **1963**, *274*, 55-79.
28. Brown, M. A.; Goel, A.; Abbas, Z., Effect of Electrolyte Concentration on the Stern Layer Thickness at a Charged Interface. *Angew. Chem. Int. Ed.* **2016**, *55*, 3790-3794.
29. Zhao, X.; Ong, S.; Wang, H.; Eisenthal, K. B., New Method for Determination of Surface Pka Using Second Harmonic Generation. *Chem. Phys. Lett.* **1993**, *214*, 203-207.
30. Wang, H.; Zhao, X.; Eisenthal, K. B., Effects of Monolayer Density and Bulk Ionic Strength on Acid–Base Equilibria at the Air/Water Interface. *J. Phys. Chem. B* **2000**, *104*, 8855-8861.
31. Sulpizi, M.; Gaigeot, M.-P.; Sprik, M., The Silica–Water Interface: How the Silanols Determine the Surface Acidity and Modulate the Water Properties. *J. Chem. Theory Comp.* **2012**, *8*, 1037-1047.

32. Cimas, Á.; Tielens, F.; Sulpizi, M.; Gaigeot, M.-P.; Costa, D., The Amorphous Silica–Liquid Water Interface Studied by Ab Initio Molecular Dynamics (AimD): Local Organization in Global Disorder. *J. Phys. Condens. Mat.* **2014**, *26*, 244106.
33. Leung, K.; Nielsen, I. M. B.; Criscenti, L. J., Elucidating the Bimodal Acid–Base Behavior of the Water–Silica Interface from First Principles. *J. Am. Chem. Soc.* **2009**, *131*, 18358–18365.
34. Marie-Pierre, G.; Michiel, S.; Marialore, S., Oxide/Water Interfaces: How the Surface Chemistry Modifies Interfacial Water Properties. *J. Phys. Condens. Matt.* **2012**, *24*, 124106.
35. Du, Q.; Freysz, E.; Shen, Y. R., Vibrational Spectra of Water Molecules at Quartz/Water Interfaces. *Phys. Rev. Lett.* **1994**, *72*, 238–241.
36. Ostroverkhov, V.; Waychunas, G. A.; Shen, Y. R., Vibrational Spectra of Water at Water/A-Quartz (0001) Interface. *Chem. Phys. Lett.* **2004**, *386*, 144–148.
37. Sung, J.; Zhang, L.; Tian, C.; Shen, Y. R.; Waychunas, G. A., Effect of Ph on the Water/A-Al<sub>2</sub>O<sub>3</sub> (11̄02) Interface Structure Studied by Sum-Frequency Vibrational Spectroscopy. *J. Phys. Chem. C* **2011**, *115*, 13887–13893.
38. Yeganeh, M. S.; Dougal, S. M.; Pink, H. S., Vibrational Spectroscopy of Water at Liquid/Solid Interfaces: Crossing the Isoelectric Point of a Solid Surface. *Phys. Rev. Lett.* **1999**, *83*, 1179–1182.

39. Kataoka, S.; Gurau, M. C.; Albertorio, F.; Holden, M. A.; Lim, S.-M.; Yang, R. D.; Cremer, P. S., Investigation of Water Structure at the TiO<sub>2</sub>/Aqueous Interface. *Langmuir* **2004**, *20*, 1662-1666.
40. Kim, J.; Kim, G.; Cremer, P. S., Investigations of Polyelectrolyte Adsorption at the Solid/Liquid Interface by Sum Frequency Spectroscopy: Evidence for Long-Range Macromolecular Alignment at Highly Charged Quartz/Water Interfaces. *J. Am. Chem. Soc.* **2002**, *124*, 8751-8756.
41. Becroft, K. A.; Richmond, G. L., In Situ Vibrational Spectroscopic Studies of the CaF<sub>2</sub>/H<sub>2</sub>O Interface. *Langmuir* **2001**, *17*, 7721-7724.
42. Hua, W.; Chen, X.; Allen, H. C., Phase-Sensitive Sum Frequency Revealing Accommodation of Bicarbonate Ions, and Charge Separation of Sodium and Carbonate Ions within the Air/Water Interface. *J. Chem. Phys. A* **2011**, *115*, 6233-6238.
43. Tyrode, E.; Liljeblad, J. F. D., Water Structure Next to Ordered and Disordered Hydrophobic Silane Monolayers: A Vibrational Sum Frequency Spectroscopy Study. *J. Phys. Chem. C* **2013**, *117*, 1780-1790.
44. Nihonyanagi, S.; Yamaguchi, S.; Tahara, T., Direct Evidence for Orientational Flip-Flop of Water Molecules at Charged Interfaces: A Heterodyne-Detected Vibrational Sum Frequency Generation Study. *J. Chem. Phys.* **2009**, *130*, 204704.
45. Sovago, M.; Campen, R. K.; Wurpel, G. W. H.; Müller, M.; Bakker, H. J.; Bonn, M., Vibrational Response of Hydrogen-Bonded Interfacial Water Is Dominated by Intramolecular Coupling. *Phys. Rev. Lett.* **2008**, *100*, 173901.

46. Li, I.; Bandara, J.; Shultz, M. J., Time Evolution Studies of the H<sub>2</sub>O/Quartz Interface Using Sum Frequency Generation, Atomic Force Microscopy, and Molecular Dynamics. *Langmuir* **2004**, *20*, 10474-10480.
47. Jena, K. C.; Hore, D. K., Variation of Ionic Strength Reveals the Interfacial Water Structure at a Charged Mineral Surface. *J. Phys. Chem. C* **2009**, *113*, 15364-15372.
48. Liljeblad, J. F. D.; Tyrode, E., Vibrational Sum Frequency Spectroscopy Studies at Solid/Liquid Interfaces: Influence of the Experimental Geometry in the Spectral Shape and Enhancement. *J. Phys. Chem. C* **2012**, *116*, 22893-22903.
49. Dewan, S.; Yeganeh, M. S.; Borguet, E., Experimental Correlation between Interfacial Water Structure and Mineral Reactivity. *J. Phys. Chem. Lett.* **2013**, *4*, 1977-1982.
50. Jena, K. C.; Covert, P. A.; Hore, D. K., The Effect of Salt on the Water Structure at a Charged Solid Surface: Differentiating Second- and Third-Order Nonlinear Contributions. *J. Phys. Chem. Lett.* **2011**, *2*, 1056-1061.
51. Dove, P. M., The Dissolution Kinetics of Quartz in Aqueous Mixed Cation Solutions. *Geochim. Cosmochim. Acta* **1999**, *63*, 3715-3727.
52. Dove, P. M.; Craven, C. M., Surface Charge Density on Silica in Alkali and Alkaline Earth Chloride Electrolyte Solutions. *Geochim. Cosmochim. Acta* **2005**, *69*, 4963-4970.
53. Yang, Z.; Li, Q.; Chou, K. C., Structures of Water Molecules at the Interfaces of Aqueous Salt Solutions and Silica: Cation Effects. *J. Phys. Chem. C* **2009**, *113*, 8201-8205.

54. Covert, P. A.; Jena, K. C.; Hore, D. K., Throwing Salt into the Mix: Altering Interfacial Water Structure by Electrolyte Addition. *J. Phys. Chem. Lett.* **2013**, *5*, 143-148.
55. Liu, D.; Ma, G.; Xu, M.; Allen, H. C., Adsorption of Ethylene Glycol Vapor on A-Al<sub>2</sub>O<sub>3</sub> (0001) and Amorphous SiO<sub>2</sub> Surfaces: Observation of Molecular Orientation and Surface Hydroxyl Groups as Sorption Sites. *Environ. Sci. Technol.* **2005**, *39*, 206-212.
56. Isaienko, O.; Borguet, E., Hydrophobicity of Hydroxylated Amorphous Fused Silica Surfaces. *Langmuir* **2013**, *29*, 7885-7895.
57. Malati, M. A.; Estefan, S. F., The Role of Hydration in the Adsorption of Alkaline Earth Ions onto Quartz. *J. Coll. Interf. Sci.* **1966**, *22*, 306-307.
58. Allen, L. H.; Matijević, E., Stability of Colloidal Silica. *J. Coll. Interf. Sci.* **1969**, *31*, 287-296.
59. Abendroth, R. P., Behavior of a Pyrogenic Silica in Simple Electrolytes. *J. Coll. Interf. Sci.* **1970**, *34*, 591-596.
60. Tadros, T. F.; Lyklema, J., Adsorption of Potential-Determining Ions at the Silica-Aqueous Electrolyte Interface and the Role of Some Cations. *J. Electroanal. Chem. Interf. Electrochem.* **1968**, *17*, 267-275.
61. Salis, A.; Parsons, D. F.; Boström, M.; Medda, L.; Barse, B.; Ninham, B. W.; Monduzzi, M., Ion Specific Surface Charge Density of Sba-15 Mesoporous Silica. *Langmuir* **2010**, *26*, 2484-2490.

62. Icenhower, J. P.; Dove, P. M., The Dissolution Kinetics of Amorphous Silica into Sodium Chloride Solutions: Effects of Temperature and Ionic Strength. *Geochim. Cosmochim. Acta.* **2000**, *64*, 4193-4203.
63. Karlsson, M.; Craven, C.; Dove, P.; Casey, W., Surface Charge Concentrations on Silica in Different 1.0 M Metal-Chloride Background Electrolytes and Implications for Dissolution Rates. *Aquat. Geochem.* **2001**, *7*, 13-32.
64. Besteman, K.; Zevenbergen, M. A. G.; Heering, H. A.; Lemay, S. G., Direct Observation of Charge Inversion by Multivalent Ions as a Universal Electrostatic Phenomenon. *Phys. Rev. Lett.* **2004**, *93*, 170802.
65. van der Heyden, F. H. J.; Stein, D.; Besteman, K.; Lemay, S. G.; Dekker, C., Charge Inversion at High Ionic Strength Studied by Streaming Currents. *Phys. Rev. Lett.* **2006**, *96*, 224502.
66. Lyklema, J., Overcharging, Charge Reversal: Chemistry or Physics? *Colloid. Surface. A.* **2006**, *291*, 3-12.
67. Labbez, C.; Jönsson, B.; Skarba, M.; Borkovec, M., Ion–Ion Correlation and Charge Reversal at Titrating Solid Interfaces. *Langmuir* **2009**, *25*, 7209-7213.
68. Pashley, R. M., Forces between Mica Surfaces in La<sup>3+</sup> and Cr<sup>3+</sup> Electrolyte Solutions. *J. Colloid Interf. Sci.* **1984**, *102*, 23-35.
69. Rashchi, F.; Xu, Z.; Finch, J. A., Adsorption on Silica in Pb and Caso<sub>4</sub> Co<sub>3</sub> Systems. *Colloid. Surf. A* **1998**, *132*, 159-171.

70. Dishon, M.; Zohar, O.; Sivan, U., From Repulsion to Attraction and Back to Repulsion: The Effect of Nacl, Kcl, and Cscl on the Force between Silica Surfaces in Aqueous Solution. *Langmuir* **2009**, *25*, 2831-2836.
71. Franks, G. V., Zeta Potentials and Yield Stresses of Silica Suspensions in Concentrated Monovalent Electrolytes: Isoelectric Point Shift and Additional Attraction. *J. Coll. Interf. Sci.* **2002**, *249*, 44-51.
72. Jordan, D. S.; Malin, J. N.; Geiger, F. M., Interactions of Al (III), La (III), Gd (III), and Lu (III) with the Fused Silica/Water Interface Studied by Second Harmonic Generation. *Environ. Sci. Technol.* **2010**, *44*, 5862-5867.
73. Mifflin, A. L.; Gerth, K. A.; Weiss, B. M.; Geiger, F. M., Surface Studies of Chromate Binding to Fused Quartz/Water Interfaces. *J. Phys. Chem. A* **2003**, *107*, 6212-6217.
74. Al-Abadleh, H. A.; Mifflin, A. L.; Bertin, P. A.; Nguyen, S. T.; Geiger, F. M., Control of Carboxylic Acid and Ester Groups on Chromium (VI) Binding to Functionalized Silica/Water Interfaces Studied by Second Harmonic Generation. *J. Phys. Chem. B* **2005**, *109*, 9691-9702.
75. Azam, M. S.; Weeraman, C. N.; Gibbs-Davis, J. M., Specific Cation Effects on the Bimodal Acid–Base Behavior of the Silica/Water Interface. *J. Phys. Chem. Lett.* **2012**, *3*, 1269-1274.
76. Azam, M. S.; Weeraman, C. N.; Gibbs-Davis, J. M., Halide-Induced Cooperative Acid–Base Behavior at a Negatively Charged Interface. *J. Phys. Chem. C* **2013**, *117*, 8840-8850.

77. Azam, M. S.; Darlington, A.; Gibbs-Davis, J. M., The Influence of Concentration on Specific Ion Effects at the Silica/Water Interface. *J. Phys. Condens. Mat.* **2014**, *26*, 244107.
78. Dewan, S.; Carnevale, V.; Bankura, A.; Eftekhari-Bafrooei, A.; Fiorin, G.; Klein, M. L.; Borguet, E., Structure of Water at Charged Interfaces: A Molecular Dynamics Study. *Langmuir* **2014**, *30*, 8056-8065.
79. Flores, S. C.; Kherb, J.; Konelick, N.; Chen, X.; Cremer, P. S., The Effects of Hofmeister Cations at Negatively Charged Hydrophilic Surfaces. *J. Phys. Chem. C* **2012**, *116*, 5730-5734.
80. Gmür, T. A.; Goel, A.; Brown, M. A., Quantifying Specific Ion Effects on the Surface Potential and Charge Density at Silica Nanoparticle–Aqueous Electrolyte Interfaces. *J. Phys. Chem. C* **2016**, *120*, 16617-16625.
81. Flores, S. C.; Kherb, J.; Cremer, P. S., Direct and Reverse Hofmeister Effects on Interfacial Water Structure. *J. Phys. Chem. C* **2012**, *116*, 14408-14413.
82. Gibbs-Davis, J. M.; Kruk, J. J.; Konek, C. T.; Scheidt, K. A.; Geiger, F. M., Jammed Acid–Base Reactions at Interfaces. *J. Am. Chem. Soc.* **2008**, *130*, 15444-15447.
83. Lis, D.; Backus, E. H. G.; Hunger, J.; Parekh, S. H.; Bonn, M., Liquid Flow Along a Solid Surface Reversibly Alters Interfacial Chemistry. *Science* **2014**, *344*, 1138-1142.
84. Kosmulski, M., Ph-Dependent Surface Charging and Points of Zero Charge: Iii. Update. *J. Coll. Interf. Sci.* **2006**, *298*, 730-741.
85. Iler, R. K., *The Chemistry of Silica* John Wiley & Sons, Inc.: United States of America, 1979.

86. Guo, Z.; Guilfoyle, R. A.; Thiel, A. J.; Wang, R.; Smith, L. M., Direct Fluorescence Analysis of Genetic Polymorphisms by Hybridization with Oligonucleotide Arrays on Glass Supports. *Nucleic Acids Res.* **1994**, *22*, 5456-5465.
87. Hellmann, R.; Wirth, R.; Daval, D.; Barnes, J.-P.; Penisson, J.-M.; Tisserand, D.; Epicier, T.; Florin, B.; Hervig, R. L., Unifying Natural and Laboratory Chemical Weathering with Interfacial Dissolution–Reprecipitation: A Study Based on the Nanometer-Scale Chemistry of Fluid–Silicate Interfaces. *Chem. Geol.* **2012**, *294–295*, 203-216.
88. Daval, D.; Hellmann, R.; Saldi, G. D.; Wirth, R.; Knauss, K. G., Linking Nm-Scale Measurements of the Anisotropy of Silicate Surface Reactivity to Macroscopic Dissolution Rate Laws: New Insights Based on Diopside. *Geochim. Cosmochim. Acta.* **2013**, *107*, 121-134.
89. Brown, M. A.; Beloqui Redondo, A.; Sterrer, M.; Winter, B.; Pacchioni, G.; Abbas, Z.; van Bokhoven, J. A., Measure of Surface Potential at the Aqueous–Oxide Nanoparticle Interface by Xps from a Liquid Microjet. *Nano Lett.* **2013**, *13*, 5403-5407.
90. Campen, R. K.; Pymer, A. K.; Nihonyanagi, S.; Borguet, E., Linking Surface Potential and Deprotonation in Nanoporous Silica: Second Harmonic Generation and Acid/Base Titration. *J. Phys. Chem. C* **2010**, *114*, 18465-18473.
91. Konek, C. T.; Musorrafiti, M. J.; Al-Abadleh, H. A.; Bertin, P. A.; Nguyen, S. T.; Geiger, F. M., Interfacial Acidities, Charge Densities, Potentials, and Energies of Carboxylic Acid-Functionalized Silica/Water Interfaces Determined by Second Harmonic Generation. *J. Am. Chem. Soc.* **2004**, *126*, 11754-11755.

92. Lambert, W. J.; Middleton, D. L., Ph Hysteresis Effect with Silica Capillaries in Capillary Zone Electrophoresis. *Anal. Chem.* **1990**, *62*, 1585-1587.
93. Huang, T. L., On the Ph Hysteresis of Electroosmotic Mobility with Capillary Zone Electrophoresis in Silica Capillary. *Chromatographia* **1993**, *35*, 395-398.
94. Koopal, L. K., Mineral Hydroxides: From Homogeneous to Heterogeneous Modelling. *Electrochim. Acta* **1996**, *41*, 2293-2305.
95. Davis, J. A.; James, R. O.; Leckie, J. O., Surface Ionization and Complexation at the Oxide/Water Interface: I. Computation of Electrical Double Layer Properties in Simple Electrolytes. *J. Colloid Interf. Sci.* **1978**, *63*, 480-499.
96. Woods, B. L.; Walker, R. A., Ph Effects on Molecular Adsorption and Solvation of P-Nitrophenol at Silica/Aqueous Interfaces. *J. Phys. Chem. A* **2013**, *117*, 6224-6233.
97. Lagström, T.; Gmür, T. A.; Quaroni, L.; Goel, A.; Brown, M. A., Surface Vibrational Structure of Colloidal Silica and Its Direct Correlation with Surface Charge Density. *Langmuir* **2015**, *31*, 3621-3626.
98. Shapovalov, V. L.; Brezesinski, G., Breakdown of the Gouy-Chapman Model for Highly Charged Langmuir Monolayers: Counterion Size Effect. *J. Phys. Chem. B* **2006**, *110*, 10032-10040.
99. Brezonik, P. L., Arnold, W. A., *Water Chemistry: An Introduction to the Chemistry of Natural and Engineered Aquatic Systems*; Oxford University Press, 2011.

100. Logan, C. A., A Review of Ocean Acidification and America's Response. *BioScience* **2010**, *60*, 819-828.
101. Martin, W.; Baross, J.; Kelley, D.; Russell, M. J., Hydrothermal Vents and the Origin of Life. *Nat Rev Micro* **2008**, *6*, 805-814.
102. Kosmulski, M., Positive Electrokinetic Charge of Silica in the Presence of Chlorides. *J. Coll. Interf. Sci.* **1998**, *208*, 543-545.
103. Ding, F.; Hu, Z.; Zhong, Q.; Manfred, K.; Gattass, R. R.; Brindza, M. R.; Fourkas, J. T.; Walker, R. A.; Weeks, J. D., Interfacial Organization of Acetonitrile: Simulation and Experiment. *J. Phys. Chem. C* **2010**, *114*, 17651-17659.
104. Stack, A. G.; Higgins, S. R.; Eggleston, C. M., Point of Zero Charge of a Corundum-Water Interface Probed with Optical Second Harmonic Generation (Shg) and Atomic Force Microscopy (Afm): New Approaches to Oxide Surface Charge. *Geochim. Cosmochim. Acta*. **2001**, *65*, 3055-3063.
105. Fitts, J. P.; Machesky, M. L.; Wesolowski, D. J.; Shang, X.; Kubicki, J. D.; Flynn, G. W.; Heinz, T. F.; Eisenthal, K. B., Second-Harmonic Generation and Theoretical Studies of Protonation at the Water/A-TiO<sub>2</sub> (1 1 0) Interface. *Chem. Phys. Lett.* **2005**, *411*, 399-403.
106. Becroft, K. A.; Moore, F. G.; Richmond, G. L., Charge Reversal Behavior at the CaF<sub>2</sub>/H<sub>2</sub>O/Sds Interface as Studied by Vibrational Sum Frequency Spectroscopy. *J. Phys. Chem. B* **2003**, *107*, 3675-3678.

107. Brown, M. A.; Abbas, Z.; Kleibert, A.; Green, R. G.; Goel, A.; May, S.; Squires, T. M., Determination of Surface Potential and Electrical Double-Layer Structure at the Aqueous Electrolyte-Nanoparticle Interface. *Phys. Rev. X* **2016**, *6*, 011007.
108. Darlington, A. M.; Gibbs-Davis, J. M., Bimodal or Trimodal? The Influence of Starting Ph on Site Identity and Distribution at the Low Salt Aqueous/Silica Interface. *J. Phys. Chem. C* **2015**, *119*, 16560-16567.
109. Agmon, N., Infrared Spectroscopy: The Acid Test for Water Structure. *Nat. Chem.* **2016**, *8*, 206-207.
110. Okumura, M.; Yeh, L. I.; Myers, J. D.; Lee, Y. T., Infrared Spectra of the Solvated Hydronium Ion: Vibrational Predissociation Spectroscopy of Mass-Selected  $\text{H}_3\text{o}^+ \cdot (\text{H}_2\text{o})_N(\text{H}_2)_M$ . *J. Phys. Chem.* **1990**, *94*, 3416-3427.
111. Tarbuck, T. L.; Ota, S. T.; Richmond, G. L., Spectroscopic Studies of Solvated Hydrogen and Hydroxide Ions at Aqueous Surfaces. *J. Am. Chem. Soc.* **2006**, *128*, 14519-14527.
112. Fega, K. R.; Wilcox, A. S.; Ben-Amotz, D., Application of Raman Multivariate Curve Resolution to Solvation-Shell Spectroscopy. *Appl. Spectrosc.* **2012**, *66*, 282-288.
113. Wang, J., From DNA Biosensors to Gene Chips. *Nucleic Acids Res.* **2000**, *28*, 3011-3016.
114. Hayes, P. L.; Malin, J. N.; Konek, C. T.; Geiger, F. M., Interaction of Nitrate, Barium, Strontium and Cadmium Ions with Fused Quartz/Water Interfaces Studied by Second Harmonic Generation. *J. Phys. Chem. A* **2008**, *112*, 660-668.

115. Allen, L. H.; Matijević, E.; Meites, L., Exchange of  $\text{Na}^+$  for the Silanolic Protons of Silica. *J. Inorg. Nucl. Chem.* **1971**, *33*, 1293-1299.
116. Eisenthal, K. B., Liquid Interfaces Probed by Second-Harmonic and Sum-Frequency Spectroscopy. *Chem. Rev.* **1996**, *96*, 1343-1360.
117. Janusz, W.; Matysek, M., Coadsorption of Cd(II) and Oxalate Ions at the  $\text{TiO}_2$ /Electrolyte Solution Interface. *J. Coll. Interf. Sci.* **2006**, *296*, 22-29.
118. Rezwan, K.; Meier, L. P.; Gauckler, L. J., A Prediction Method for the Isoelectric Point of Binary Protein Mixtures of Bovine Serum Albumin and Lysozyme Adsorbed on Colloidal Titania and Alumina Particles. *Langmuir* **2005**, *21*, 3493-3497.
119. Fitts, J. P.; Shang, X.; Flynn, G. W.; Heinz, T. F.; Eisenthal, K. B., Electrostatic Surface Charge at Aqueous/ $\text{Al}_2\text{O}_3$  Single-Crystal Interfaces as Probed by Optical Second-Harmonic Generation. *J. Phys. Chem. B* **2005**, *109*, 7981-7986.
120. Levine, B. F.; Bethea, C. G., Effects on Hyperpolarizabilities of Molecular Interactions in Associating Liquid Mixtures. *J. Chem. Phys.* **1976**, *65*, 2429-2438.
121. Gubskaya, A. V.; Kusalik, P. G., The Multipole Polarizabilities and Hyperpolarizabilities of the Water Molecule in Liquid State: An Ab Initio Study. *Mol. Phys.* **2001**, *99*, 1107-1120.
122. Gubskaya, A. V.; Kusalik, P. G., The Total Molecular Dipole Moment for Liquid Water. *J. Chem. Phys.* **2002**, *117*, 5290-5302.

123. Torii, H., Time-Domain Calculations of the Polarized Raman Spectra, the Transient Infrared Absorption Anisotropy, and the Extent of Delocalization of the OH Stretching Mode of Liquid Water. *J. Phys. Chem. A* **2006**, *110*, 9469-9477.
124. Moad, A. J.; Moad, C. W.; Perry, J. M.; Wampler, R. D.; Goeken, G. S.; Begue, N. J.; Shen, T.; Heiland, R.; Simpson, G. J., Nlopredict: Visualization and Data Analysis Software for Nonlinear Optics. *J. Comput. Chem.* **2007**, *28*, 1996-2002.
125. Morita, A.; Hynes, J. T., A Theoretical Analysis of the Sum Frequency Generation Spectrum of the Water Surface. *Chem. Phys.* **2000**, *258*, 371-390.
126. Walrafen, G. E., Raman Spectral Studies of the Effects of Temperature on Water Structure. *J. Chem. Phys.* **1967**, *47*, 114-126.
127. Nihonyanagi, S.; Yamaguchi, S.; Tahara, T., Water Hydrogen Bond Structure near Highly Charged Interfaces Is Not Like Ice. *J. Am. Chem. Soc.* **2010**, *132*, 6867-6869.
128. Singh, P. C.; Nihonyanagi, S.; Yamaguchi, S.; Tahara, T., Ultrafast Vibrational Dynamics of Water at a Charged Interface Revealed by Two-Dimensional Heterodyne-Detected Vibrational Sum Frequency Generation. *J. Chem. Phys.* **2012**, *137*, 094706.
129. Verreault, D.; Hua, W.; Allen, H. C., From Conventional to Phase-Sensitive Vibrational Sum Frequency Generation Spectroscopy: Probing Water Organization at Aqueous Interfaces. *J. Phys. Chem. Lett.* **2012**, *3*, 3012-3028.
130. Petersen, P. B.; Saykally, R. J., On the Nature of Ions at the Liquid Water Surface. *Annu. Rev. Phys. Chem.* **2006**, *57*, 333-364.

131. Kékicheff, P.; Marčelja, S.; Senden, T. J.; Shubin, V. E., Charge Reversal Seen in Electrical Double Layer Interaction of Surfaces Immersed in 2:1 Calcium Electrolyte. *J. Chem. Phys.* **1993**, *99*, 6098-6113.
132. Liu, J.; Xu, Z.; Masliyah, J., Studies on Bitumen–Silica Interaction in Aqueous Solutions by Atomic Force Microscopy. *Langmuir* **2003**, *19*, 3911-3920.
133. Lorenz, C. D.; Travesset, A., Charge Inversion of Divalent Ionic Solutions in Silica Channels. *Phys. Rev. E* **2007**, *75*, 061202.
134. Hayes, P. L.; Malin, J. N.; Jordan, D. S.; Geiger, F. M., Get Charged Up: Nonlinear Optical Voltammetry for Quantifying the Thermodynamics and Electrostatics of Metal Cations at Aqueous/Oxide Interfaces. *Chem. Phys. Lett.* **2010**, *499*, 183-192.
135. Martin S. Silberberg, D. R., *Chemistry: The Molecular Nature of Matter and Change*, 6th ed.; McGraw Hill: New York, N.Y., 2002.
136. Lovering, K. A.; Bertram, A. K.; Chou, K. C., New Information on the Ion-Identity-Dependent Structure of Stern Layer Revealed by Sum Frequency Generation Vibrational Spectroscopy. *J. Phys. Chem. C* **2016**, *120*, 18099-18104.
137. Khatib, R.; Backus, E. H. G.; Bonn, M.; Perez-Haro, M.-J.; Gaigeot, M.-P.; Sulpizi, M., Water Orientation and Hydrogen-Bond Structure at the Fluorite/Water Interface. *Sci. Report.* **2016**, *6*, 24287.